Master's thesis

NTNU
Norwegian University of Science and Technology
Faculty of Engineering
Department of Geoscience and Petroleum

Lisa Henrika Henriksen

Mineralogical assessment of rocks of hydropower tunnels subjected to swelling

Master's thesis in Geology
Supervisor: Krishna Kanta Panthi
Co-supervisor: Bjørn Eske Sørensen, Jessica Ka Yi Chiu
May 2022

NTNU
Norwegian University of
Science and Technology

Lisa Henrika Henriksen

Mineralogical assessment of rocks of hydropower tunnels subjected to swelling

Master's thesis in Geology
Supervisor: Krishna Kanta Panthi
Co-supervisor: Bjørn Eske Sørensen, Jessica Ka Yi Chiu
May 2022

Norwegian University of Science and Technology
Faculty of Engineering
Department of Geoscience and Petroleum

NTNU
Norwegian University of
Science and Technology

NTNU
Norwegian University of Science and Technology

Department of Geoscience and Petroleum

Your ref.: MS/N40T61/IGP/LHHKP Date: 20.09.2021

GEOL3090 Master Thesis
for
GeoReal student Lisa Henrika Henriksen

Mineralogical assessment of rocks of hydropower tunnels subjected to swelling

Background

In waterway tunnels of hydropower project passing through weak and swelling rocks, there exists risk of failures caused by developed plastic deformation due to schistocity and swelling during powerplant operation. Especially, the clay-bearing rocks consisting swelling minerals like montmorillonite (smectite) are sensitive to degradation once exposed to water, which may lead to expansion of the tunnel wall leading to additional support pressure. Statkraft has experienced problems of tunnel collapses in some of the international projects built in Andes Mountains and elsewhere. Hence, Statkraft through HydroCen is directly involved in the research on potential swelling and slaking extent of weak rocks such as flysch, serpentinite, andesite, and clay rich sedimentary rocks. A PhD research that addresses slake durability and swelling behavior of some such rocks was completed, giving a qualitative link to the mineralogy of the samples. Statkraft is further supporting to continue research in this area with main focus on the quantitative mineralogical investigation technique.

MSc thesis task

This MSc thesis is the continuation of the PhD research completed in November 2020 and will have following main tasks:

- Review on swelling mechanism of some minerals, problem associated to swelling rocks for hydropower tunnels.
- Review on the principle of traditional methods of assessing swelling minerals consisting of XRay Diffraction (XRD), X-Ray fluorescene (XRF), Differential thermal analysis (DTA), Petrographic thin sections and SEM analysis.
- Testing of XRD perpping methods for analysis of “soft rocks”, that until now has been giving ambiguous results on the XRD at the department of geoscience and petroleum. Test will compare standard method using crushing and grinding using disc mill with careful sieving and micronizing in ethanol using the Mcrone micronizer mill.

- Review on the potential alternative methods such as Automatic Mineralogy System (AMS) and Hyperspectral imaging (HSI) in the laboratory
- Review and assess geological condition along the headrace tunnel of Moglicë HPP in Albania including sample locations
- Collect and synthesize laboratory test results of swelling rocks made at NTNU for both Moglicë and other projects
- Carry out laboratory assessment using both traditional (XRD, optical microscopy and SEM on thin sections) and using AMS and HIS on the collected samples.
- Carry out field scanning using HSI and sampling both in Albania and Norway (if possible).
- Analyse and discuss on how the identification of minerals using alternative laboratory and field methods can contribute to improve the understanding in the swelling behaviour and engineering geological challenges associated to hydropower tunnels passing through weak and swelling rocks.
- Compare and discuss different methods for identifying swelling minerals with focus on feasibility and degree of confidence in identifying minerals of interest, especially minerals contributing to swelling.

Relevant computer software packages

Candidate shall use relevant computer software for the master study.

Background information for the study

- Relevant information about the project such as reports, maps, information and data received from the supervisors and collected by the candidate.
- The information provided by the professor about rock engineering and hydropower.
- Previous MSc and PhD theses, scientific papers and books related to tunnelling in weak rocks.
- Literatures in rock engineering, rock support principles, rock mechanics and tunnelling.

Cooperating partner

Statkraft International is the cooperating partner. Dr. Siri Stokseth and MSc Thomas Schönborn are the contact persons from the Statkraft. Associate Professor Bjørn Eske Sørensen and PhD fellwo Jessica Ka Yi Chiu at IGP are the co-supervisors of this MSc thesis.

The thesis work is to start on 23rd August 2021 and to be completed by 15th May 2021.

The Norwegian University of Science and Technology (NTNU)
Department of Geoscience and Petroleum

20th September 2021

Krishna Panthi

Dr. Krishna K. Panthi
Professor of geological engineering, main supervisor

Abstract

Hydropower tunnels located in weak and swelling rock masses are prone to stability problems and failures. Co-operating partner Statkraft is supporting further research for the assessment of swelling minerals through mineralogical investigation techniques. This master thesis has aimed to evaluate traditional investigation techniques as well as potential alternative methods for assessing swelling minerals in the laboratory. In addition, it was aimed to evaluate the modified preparation method and whether this can be an established method for soft rocks. The tested rock samples were collected from the Moglicë hydropower plant in Albania.

A swelling potential was found in all tested samples through the oedometer swelling pressure test. Low swelling was classified in most samples, and medium swelling was found in the fault gouge rock. The swelling was likely caused by the presence of smectite clay and zeolite minerals in the rock specimens. It is interpreted that the zeolite minerals caused the increased swelling in the fault gouge material.

The study implied that mineralogical assessment should depend on various laboratory methods, rather than the reliance on one method. Mineral identification errors were observed in all the tested laboratory methods to a varying degree. The X-Ray Diffraction (XRD) method showed the best results related to the detection of swelling minerals with a good correlation to the measured swelling pressure [MPa]. The findings of the two alternative methods, Automated Mineralogy System (AMS) and Hyperspectral Imaging (HSI), were ambiguous. In contrast to XRD, both methods provide beneficial visualization of the sample mineralogy. Limitations were discovered in the mineralogical composition and quantification, thus making the methods unsuitable as sole assessment methods.

The study uncovered the potential of the modified crushing method and recommends this to be an established preparation method for soft and weak rocks at the Department of Geoscience and Petroleum at NTNU. Compared with the standard samples, it appears that the modified samples preserved soft minerals better, and also reduced the disintegration of rock material. A large loss of material was discovered in both crushing methods. This was assumed to be due to the loss of hard silicate minerals and soft clay material. For future projects, alterations should be made to the modified method to make the crushing procedure less time-consuming, more automated, and reduce the loss of material.

The rock mass quality of the samples is mainly weak and disintegrated, making it difficult to perform adequate rock mechanical tests. Three samples of varying lithological character were tested by the Uniaxial Compressive Strength test (UCS), the results were strongly influenced by weak minerals and fractures, and thus not reliable. The mean tensile strength of the rock mass was 2.35 MPa, obtained from Brazil tensile strength test. The number of samples is below the ISRM recommended amount for both tests.

Continued investigation is necessary to fully assess the potential of the different mineralogic and rock mechanical laboratory methods. Additional testing using a larger number of samples is recommended as this may reduce uncertainty. The modified preparation method should be adjusted and applied to soft rocks in future projects. Both AMS and HSI have shown potential with mineralogical classification along with XRD. It would be beneficial to improve post-processing and machine learning approaches for the laboratory data as mineral quantification has revealed limitations.

Sammendrag

Vannkraft tunneler lokalisert i svakt og svellende bergmasse er utsatt for stabilitets problemer og kollaps. Samarbeidspartneren Statkraft ønsker å støtte videre forskning som skal identifisere og vurdere svellende mineraler ved utførelse av mineralogiske undersøkelsesmetoder. Formålet med denne masteroppgaven er å vurdere tradisjonelle undersøkelsesmetoder, i tillegg til potensialet for alternative undersøkelsesmetoder, for å avdekke svellende mineraler i laboratoriet. Videre var hensikten å vurdere den modifisert knusemetode og anslå om den kan bli en etablert metode for svake bergarter. Bergartsprøvene som ble testet er hentet fra Moglicë vannkraftverk i Albania.

Et svellepotensiale er funnet i alle bergartsprøvene ved hjelp av ødometer svelletest. De fleste prøver var klassifisert som lav svelling, mens medium svelling var målt i fault gouge (forkastningsmel) materialet. Svelling var trolig forårsaket av smektitt leire og zeolitt mineraler i bergartsprøvene. Det er tolket at zeolitt mineraler førte til høy svelletrykk i fault gouge prøven.

Studien antydet at mineralogisk vurdering burde avhenge av ulike laboratoriemetoder, enn å avhenge av én metode. Feilestimering av mineraler er oppdaget i alle laboratorietestene i ulik grad. X-ray diffraksjon (XRD) viste best resultat i forhold til identifisering av svellende mineraler med en god korrelasjon til målt svelletrykk [MPa]. Resultatene i de to alternative metodene, Automated Mineralogy System (AMS) og Hyperspectral Imaging (HSI), var noe uklar. I motsetning til XRD gir begge disse metodene god visualisering av mineralogien i prøvene. Det ble oppdaget begrensninger relatert til mineral sammensetning og kvantifisering, noe som gjør metodene uegnet som eneste vurderingsmetode.

Studien avdekket potensialet til den modifiserte knusemetoden og anbefaler at den blir en etablert prepareringsmetode for myke og svake bergarter ved Institutt for Geovitenskap og Petroleum ved NTNU. Sammenlignet med standardprøvene ser det ut til at de modifiserte prøvene bevarte myke mineraler bedre, og reduserte også desintegrasjonen av bergartsmateriale. Det ble oppdaget et stort massetap i begge knusemetodene. Dette er antatt å skyldes tap av harde silikatmineraler og mykt leirematerialе. For fremtidige prosjekter bør det gjøres endringer i den modifiserte metoden for å gjøre knuseprosedyren mindre tidkrevende, mer automatisert og redusere tap av materiale.

Bergmassekvaliteten på prøvene er hovedsakelig av svake og oppknust berg, noe som gjør det vanskelig å utføre tilstrekkelige bergmekaniske tester. Tre prøver av varierende litologisk karakter ble testet med enaksial trykkfasthet test (UCS), resultatene var sterkt påvirket av svake mineraler og sprekker, og er dermed ikke pålitelige. Den gjennomsnittlige strekkfastheten til bergmassen var 2,35 MPa, målt fra Brasiltest. Antall prøver er lavere enn ISRM anbefalinger for begge testene.

Videre undersøkelser er nødvendig for å grundig vurdere potensialet til de ulike mineralogiske og bergmekaniske laboratoriemetodene. Ytterligere testing med et større antall prøver anbefales da dette kan redusere usikkerheten. Den modifiserte prepareringsmetoden bør forbedres og bli tatt i bruk på myke bergarter i fremtidige prosjekter. Både AMS og HSI har vist potensiale ved mineralogisk klassifisering sammen med XRD. Det ville være fordelaktig å forbedre tilnærminger til etterbehandling og maskinlæring for laboratoriedataene, ettersom det er vist begrensninger i mineralkvantifisering.

Acknowledgments

This master thesis has been carried out as part of my master's degree in geology at the Norwegian University of Science and Technology (NTNU). This thesis has been in co-operation with Statkraft AS. I am thankful for the encouragement of the project and the financial support provided by Statkraft for my thesis work.

Professor Krishna Kanta Panthi has been my main supervisor for this thesis. I am thankful for his guidance and feedback throughout this thesis. Associate professor Bjørn Eske Sørensen has been the co-supervisor and I am thankful for his advice and contribution to the project. Principle engineering geology and geotechnics Thomas Schönborn have been the contact person at Statkraft. I am grateful for the help he has given with relevant project information, providing samples, and organization of a field trip to Moglicë, Albania. I would also like to thank PhD fellow Jessica Ka Yi Chui for joining me in the field and for helping with hyperspectral imaging and providing data.

I am grateful for all the help I have received through all the laboratory work from the employees at the Department of Geoscience and Petroleum. This includes Laurentius Tijhuis, Torill Sørlokk, Jon Runar Drotninghaug, Gunnar Vistnes, Stefanie Lode, Kjetil Eriksen, Jostein Røstad. Also, Friederike Koerting at the HySpex by NEO laboratory in Oslo. Additionally, I am thankful to my summer internship co-worker Karoline Arctander for the fun we had building a DYI photo booth for the rock core boxes.

When I first started this master thesis, I did not expect it to come with so many complications. From smashed rock cores, preparation fiascos in the lab, software complications, unfinished results, and countless delays. I was strongly considering changing the thesis title to "Anything that can go wrong will go wrong." (Murphy's law). With that said, everything did work out in the end.

I would like to give special thanks to my parents who have always supported me and pushed me to perform my best. To my partner, thank you for always believing in me. I also want to thank my aunt and uncle who have been like my bonus parents these five years in Trondheim and nonetheless for all the dinners they have served me. And of course, I show gratitude to the rest of my beloved family.

At last, I would like to thank my friends and fellow students for five amazing years together in Trondheim, from long days of studying at the campus to cold and rainy weather in the field.

Lisa Henrika Henriksen

May 2022

Table of Contents

1 Introduction

1.1 Background

The rock samples used in this master thesis are delivered by co-operating partner Statkraft from the Moglicë hydropower plant located in Albania. Statkraft is a Norwegian power company working both nationally and internationally. Statkraft has several hydropower plants (HPP) abroad, many of which are located in weak and weathered rock masses differing from the typical Norwegian rocks. There have been an increasing number of stability problem cases within the hydropower industry, many of which are associated with swelling problems and degraded rocks (Selen, 2020). For instance, in the La Higuera hydropower plant located in the Chilean Andes mountains. Water tunnels in hydropower plants are exposed to cyclic wetting and drying. Weak and weathered rocks are sensitive to changes in moisture content, with the clay-bearing rocks consisting of swelling minerals being an important factor (Selen et al., 2021a). Because of these conditions, a hydropower tunnel is especially venerable to clay-bearing rocks consisting of swellable minerals with the existing risk of failure and stability problems. Engineering geological projects abroad do not show the same rock mass characteristics as local, Norwegian projects. However, suggested methods for testing and assessment of swelling potential are based on Norwegian rock characteristics.

1.2 Objectives of the study

The objectives of this thesis is to assess geological conditions along the Moglicë headrace tunnel in Albania with a focus on swelling minerals. This master thesis aims to test and compare different laboratory methods, along with field methods, for assessing swellable and difficult minerals in hydropower water tunnels. Another aspect of this master thesis is to evaluate a new, modified preparation method that will be more suitable for weak and weathered rocks. This new method will be reviewed and compared to the standard methods used in present laboratory testing. Based on these aims, the following questions will be addressed:

- Is there a swelling potential in the rock mass, and what causes the swelling?
- Can the Automated Mineralogy System (AMS) and Hyperspectral Imaging (HSI) be used to assess mineralogy at the same level as X-Ray Diffraction (XRD)?
- Does the modified crushing and preparation method show an improvement in preserving minerals in soft and weak rock compared to the standard preparation method?
- Is the modified XRD sample better than the standard XRD samples considering swelling mineral identification?
- How is the geological condition and rock mass quality along the Moglicë headrace tunnel?

To accomplish the goals for this master thesis, the following methods and reviews have been used. The laboratory investigation will be performed, analyzed, and critically reviewed.

- Literature study to review swelling mechanisms and problems associated with swelling minerals.
- Traditional laboratory testing for assessing swelling minerals, including:
    - X-ray diffraction (XRD)
    - X-ray fluorescence (XRF)
    - Oedometer swelling pressure test
    - Optical thin-section microscopy
- Perform Automated Mineralogy System (AMS) analysis.
- Perform Hyperspectral imaging (HSI) in the laboratory and the field.
- Compare the standard preparation method against a new modified preparation method using the laboratory testing results.
- Evaluate geological conditions by carrying out engineering geology rock mass testing, including:
    - Uniaxial compressive strength test (UCS)
    - E-modulus and Poisson ratio
    - Brazil test
    - Density and velocity measurements

1.3 Limitations

The rock samples provided from the Moglicë headrace tunnel area are the specimens that have been used during this thesis work. The rock samples are drilled from an area close to the Shemsit adit along the headrace tunnel, therefore not fully representative of the conditions of the actual headrace tunnel. Moreover, during transportation from Albania to Norway in the summer of 2021 the samples were heavily shuffled and broken up, with even one core box being dropped to the ground (this box was not used for this thesis). The samples had to be rearranged to their original position as best as possible using older photos. With this in mind, the placement of each sample piece might not be fully correct and the samples are more disintegrated than in the in-situ conditions, hence influencing the test result and core logging.

During the laboratory work, it was discovered that the number of samples would be limited, this was based on the state of the rock mass and also the time limitations of this study. Factors related to sample preparation, storage, and limitations of laboratory techniques will also be influential. It was discovered a somewhat large loss of material during sample preparation. The results gained from the laboratory testing have limited reliability as the number of samples tested is limited. Further, several of the laboratory analysis rely on only a small representative area for the entire rock mass. This is something to take into consideration.

1.4 Synthesize previous work

There have been performed several studies at NTNU related to swelling rocks in hydropower projects, many of which have been in cooperation with Statkraft. The field of research has been for both Moglicë hydropower plant, but also in other Statkraft

hydropower projects abroad such as in Chile and the Philippines. Only some of the aspects of these previous studies will be presented as they are the most associated with this thesis.

A master thesis and doctoral thesis performed by Lena Selen (Selen, 2017; 2020) aimed to study the rock properties of rocks from the Alimit HPP in the Philippines and the Moglicë HPP in Albania. The aim of the theses was, among other things, to review and discuss the existing test methodologies uses at NTNU and also to compare the different laboratory approaches at two different institutes, this being NTNU (Norwegian University of Science and Technology) and KiT (Karlsruhe Institute of Technology). Two other master thesis's by Skrede (2017) and Frengen (2020) performed stability and mineralogical analysis, as well as numerical analysis, of weak and swellable rock masses in the Portillo tunnel in Chile and Moglicë headrace tunnel in Albania, respectively.

The presence of swelling minerals was confirmed through XRD and/or swelling tests in the studies mentioned. Selen (2017) discovered a swelling potential linked to the presence of zeolite (laumontite) minerals in the andesitic rock types, where the rock samples containing the highest amount of laumontite correspondingly showed the largest swelling pressure. The author also uncovered differences between the two associated institutes. Even though both NTNU and KiT use the same ISRM suggested standard method for the oedometer swelling test there were discovered differences making it difficult to compare the test results. Selen (2017) proposes that equal standards should be made between institutes to make them more comparable, also that general improvements to the oedometer swelling test should be made at NTNU.

Mineral detection and classification were performed by XRD and DTA laboratory test methods. The use of SEM analysis as an additional mineral classification was recommended by several of the studies (e.g. Selen, 2017; 2020; Skrede, 2017), also referring to the use of optical thin section methods. The study by Skrede (2017) concluded that normal light microscopy makes it hard to identify clay minerals and therefore recommends the use of SEM. The author further argues that XRD, as well as light microscopy, is a task for experienced mineralogists and does not provide enough information.

The studies mentioned experienced that the samples did not withstand the preparation, especially for rock mechanical tests. It was suggested by Selen (2017; 2020) that there should be implemented a standardized preparation method for weak rocks that is more gentle and fitted for the weak rock conditions. As presented in Frengen (2020) the rock material had poor quality and it was hard to find satisfactory specimens to be tested. The author brought up that prepping and storage of the samples may also cause damage to the rocks. The conglomerate and sandstone flysch from Moglicë was classified as high strength from UCS of 137 ± 22 MPa, whereas the clay flysch had a lack of intact material. The point load test of the flysch clay had a low strength of 8 ± 3 MPa. The swelling potential in the Moglicë samples had an average of 0.18 ± 0.06 MPa. The long-term stability of the tunnel and tunnel support appears to be good, however, the deformation from swelling should be monitored during inspections and further analysis is required (Frengen, 2020).

2 Theory about difficult minerals

2.1 Definition of difficult minerals

During an underground excavation of hydropower water tunnels, weak and altered rock masses can cause serious problems effecting the stability and safety of the project. The main reason for this is that weak rocks such as shale, serpentinites, flysch, or claystone contain swelling, slaking and/or disintegrating minerals (Selen & Panthi, 2018). Rock masses in water tunnels also experience problems associated with non-swelling minerals, for example, from minerals such as talc (weak, low internal friction), micas (weak, low friction), brucite (possible corrosion), or calcite (solvable). Low friction minerals are particularly problematic in contact with water as the friction can be reduced (Nilsen, 2016).

Alterations of previously competent rocks have proven to be one of the most challenging problems in water tunnels. A reduction of grain size is common, with some minerals being altered to clay size particles. A reduced competency in the altered material can cause the material to either behave plastically under pressure or swell in contact with water (Wahlstrom, 1973). As hydropower tunnels experience cycles of drying and wetting, rock types containing swelling clay encounter volume changes, thus leading to deterioration, weakening and breakdown of rocks, also called slaking (Goodman, 1993). As explained in the article by Selen et al. (2020), a hydropower water tunnel experience dry conditions during the construction period, the tunnels are then filled with water over a long period after it is complete. During the operational lifetime, the hydropower water tunnel is exposed to cyclic wetting and drying as a result of periodical inspections and repair.

Weathering of rock is a physical and chemical process that causes alterations in the form of mineralogical and lithological changes in rock or soil material. The process takes place at or near the earth's surface (Vivoda Prodan & Arbanas, 2016). The stability of minerals on the earth's surface varies. Minerals such as quartz and calcite are stable, while other minerals such as olivine or plagioclase which are formed in deep environments and later exposed to the surface are less stable (Wahlstrom, 1973). From an engineering point of view, weathered rocks are less competent as the properties of the rock have been changed (Wahlstrom, 1973). When excavating a hydropower water tunnel through a weathered zone or weathered rock this must be taken into consideration. The extent of the weathered mineral aggregates will depend on erosion.

Hydrothermal alteration is a process in rocks leading to the formation of new minerals based on the instability of the original mineral phases. This is caused by physico-chemical conditions in circulating high-temperature water (100-500°C) in major or minor channel ways, mostly in faults or joints. The alterations also occur along grain boundaries on small scale (Fulignati, 2020; Wahlstrom, 1973). The geological processes are highly influenced by the physical and chemical properties of the hydrothermal fluids which exist over a range of temperature and pressure differences. The various near-surface geological fluids include meteoric water, seawater, basinal/connate water, metamorphic fluids and magmatic fluids, also deep earth fluids (Steele-MacInnis & Manning, 2020). The interaction of the fluids and the rock mass changes the mineralogical, chemical and textural properties of the rock as the fluids attack the minerals, clay minerals are the most significant product of this

alteration (Fulignati, 2020). There are several types of hydrothermal alteration. Rocks containing clay mineral aggregates, such as chlorite, smectite or illite have normally a connection with hydrothermal alteration. Clay minerals, for example chlorite or montmorillonite, replace other silicate minerals in the rock mass and thus alter and change the character of the rock mass. Hydrothermal alteration of mafic/ultramafic rock can lead to serpentinization or chloritization and is also associated with epidotes, carbonates and various clay minerals. Evidence of hydrothermal alteration is associated with the presence of pyrite crystals, or framboidal pyrites (S. Lode, personal communication, 2022; Wahlstrom, 1973). An overview of typical clay minerals and which minerals they are altered from is presented in Table 2-1 along with fluid, pH, temperature and alteration facies.

Table 2-1: Clay minerals that are typically caused by hydrothermal alteration with the altered mineral, fluid, pH, temperature and alteration facies. Table modified from Fulignati (2020).

Clay mineral	Altered mineral	Fluid	pH	Temperature	Hydrothermal Alteration Facies
Smectite	Silicates (plagioclase, feldspar, pyroxene, olivine, volcanic glass)	Aqueous	5.5-7	<160 °C	Argillic
Kaolinite	Aluminosilicate minerals,	Aqueous	4.5-6	<200 °C	Intermediate argillic
Illite-smectite (I/S)	Smectite	Aqueous	5.5-7	150-220 °C	Phyllic
Illite	K-feldspar, plagioclase	Aqueous	5.5-7	220-350 °C	Propylitic
Chlorite	Mafic/ultramafic minerals (pyroxene, olivine)	Aqueous	5.5-7	220-350 °C	Propylitic
Talc	Mafic/ultramafic minerals (olivine)	Aqueous	5.5-7	250-350 °C	Propylitic
Serpentine	Mafic/ultramafic minerals	Aqueous, Seawater	5.5-7	250-350 °C	Propylitic

2.2 Slaking

Slaking is defined by Goodman (1993) as the deterioration, weakening and breakdown of rock material as a result of cyclic wetting and drying. After excavation the tunnel is exposed to wetting and drying conditions, thus leading to slaking and time-dependent changes in the rock mass properties. The effects of slaking can lead to stability problems in hydropower water tunnels, particularly in weak and altered rocks with the presence of swelling clay minerals (Panthi, 2006; Selen, 2020; Selen et al., 2021b). Slaking is most common in rocks containing swelling clay. Continual volume change in the rock mass results in shearing and loss of material. Not only will excavation of slaking rock be troublesome, but also the installment of rock support (Goodman, 1993; Panthi, 2006; Skrede, 2017).

2.3 Swelling

According to the International Society for Rock Mechanics (ISRM, 1983) swelling of rock is a time-dependent volume increase that involves a physico-chemical reaction with water. The swelling mechanism is a combination involving water and stress relief, as swelling can only take place simultaneously with or following stress relief. The ability to swell is limited to rocks containing minerals such as smectites, mixed-layered clays, anhydrite and zeolites (Selmer-Olsen et al., 1989). For swelling to take place access to water is crucial, in addition to other factors which are further discussed in the following chapter.

There are some differences in the swelling of rock in national and international projects. In Norway, swelling minerals are often associated as a gouge material in weakness zones, typically in faults, joints, veins, crushing zones or minerals in altered rocks. The latter is less usual in Norwegian geological conditions as the material has been removed by glaciation processes. By contrast, swelling minerals encountered in international projects are mostly found as hydrothermally altered or weathered rocks. Tunnel collapses or cave-in from swelling minerals have resulted in increased costs, delays, and financial loss of projects, some even resulting in project abandonment (Selmer-Olsen et al., 1989).

Swelling causes a deformation around the tunnel periphery and is often confused with squeezing ground, the terms are often used interchangeably (ISRM, 1983). As stated, swelling includes volume increase in the presence of water and will displace into the tunnel as a result of this. It may take time before the effect of swelling is active or noticeable in the tunnel. Squeezing on the other hand is related to time and stress. The effect of squeezing is evident immediately after excavation and may continue over a long period or only during the construction period. Weak and plastic rock material is displaced in the tunnel periphery from a stress gradient which causes the material to move into the tunnel opening (Carter et al., 2010; Stefanussen, 2017). The squeezing effect and phenomena is explained further in Chapter 3.2. Several tunneling cases indicate that tunnel squeezing and swelling operate at the same time. With this in mind, it can be difficult to separate the two phenomena when operating an engineering geological project (Stefanussen, 2017).

2.3.1 Swelling mechanisms

To understand how swelling of rocks can take place the underlying mechanisms have to be examined. There are two types of swelling observed in clays; osmotic swelling and intracrystalline swelling (Einstein, 1996).

Osmotic swelling is a result of large ion concentration differences between the clay surface and the pore water. This type of swelling occurs in clays or clayey rocks, typically during tunnel excavations when rocks are unloaded and capable of taking up water. Osmotic swelling is related to the double layer effect and external applied stress. When pressure is released the equilibrium inside the rock is lost and a new equilibrium has to be obtained. As illustrated in Figure 2-1 water intrudes between the double layer and pushes them apart. Swelling will continue until equilibrium is reached. Osmotic swelling can act over a larger distance, however, the theoretical maximum swelling pressure is approximately 2 MPa (Einstein, 1996; Madsen & Müller-Vonmoos, 1989).

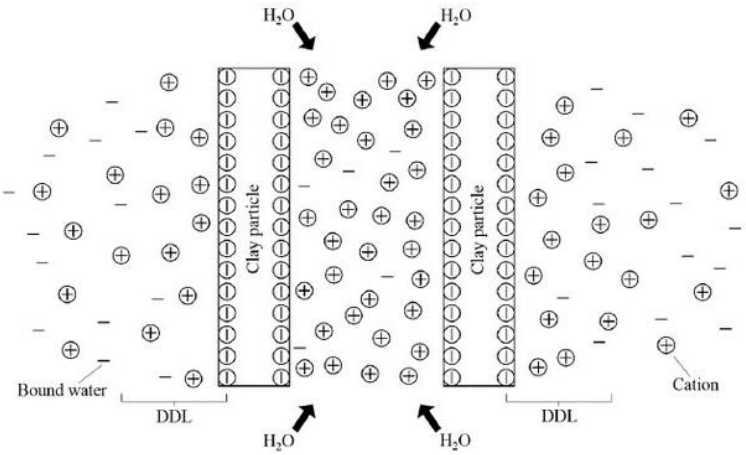

Figure 2-1: Osmotic swelling of clay minerals (Ikpe et al., 2018).

Intracrystalline swelling occurs in smectites, for instance, montmorillonite and mixed layer clays, as well as anhydrite and pyrite (Einstein, 1996). The structure of the clay minerals is important for the swelling mechanism, as the exchangeable interlayer cation is hydrated in contact with water. The cations are rearranged between the clay layers and thus widening the spacing between the layers, as seen in Figure 2-2. This leads to a volume increase of the crystal. This type of swelling acts over small distances. The theoretical maximum swelling pressure for intracrystalline clay is 100 MPa (Einstein, 1996; Madsen & Müller-Vonmoos, 1989).

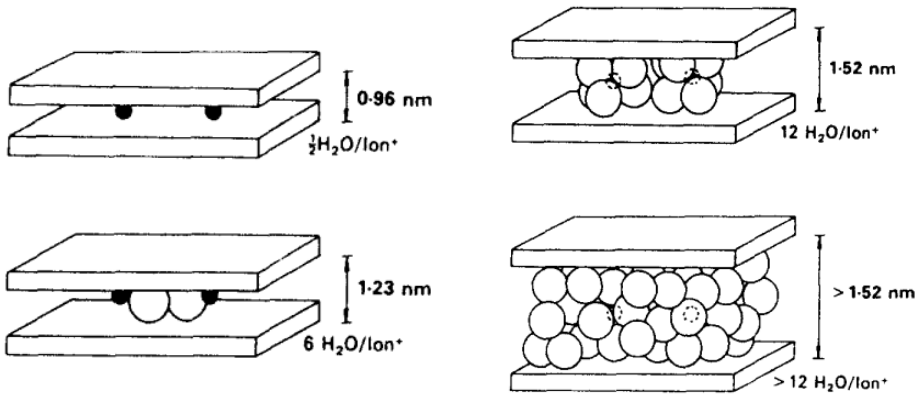

Figure 2-2: Intracrystalline swelling of sodium montmorillonite (Madsen & Müller-Vonmoos, 1989).

In reality, several swelling mechanisms interact at the same time. Prediction of the actual volume increase and swelling pressure is therefore difficult even with a theoretical value (Einstein, 1996). A variety of factors will also contribute to the degree of swelling. According to Selmer-Olsen et al. (1989), these are the amount and type of swelling minerals; the amount and type of mobile cations; the degree of consolidation of the material in the zone; the access to water; and the degree of unloading after excavation.

2.4 Swelling and difficult minerals

2.4.1 Smectite

Smectites are a group of clay minerals consisting of minerals such as montmorillonite, beidellite and nontronite. They are composed of sheets of octahedral (O) and tetrahedral

(T) layers in a 2:1 structure. As illustrated in Figure 2-3, the smectite minerals have the ability to absorb water (H_2O molecules) between the structural layers, resulting in swelling and volume increase (Deer et al., 2013; Frengen, 2020; Nelson, 2014; Selmer-Olsen et al., 1989).

Montmorillonite is the most common smectite mineral. This clay mineral is a result of weathering and alteration of eruptive ingenious rocks, typically from tuffs and volcanic ashes, at the expense of silicate minerals (plagioclase, feldspar, pyroxene and olivine). Alteration usually occurs in-situ in marine environments. Montmorillonite is associated with other minerals such as cristobalite, zeolites, biotite, quartz, feldspar and zircon (Deer et al., 2013; Fulignati, 2020; Nelson, 2014). In contact with water, montmorillonite can expand to several times its original volume, making it very dangerous in hydropower tunnels (Nelson, 2014).

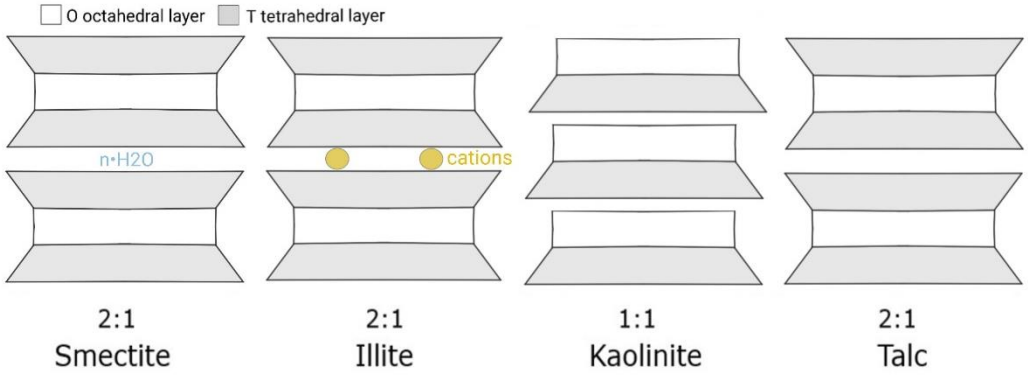

Figure 2-3: Mineral structure of smectite, illite, kaolinite and talc with octahedral and tetrahedral layers. Modified from Frengen (2020).

2.4.2 Illite

Illites are a group of non-swelling clay minerals that closely resemble micas, particularly muscovites. The structures of the two minerals have a 2:1 layer structure with cations sandwiched between the two sheets, as can be seen in Figure 2-3. The interlayered cations prevent water from entering the structure and thus prevent swelling. Illites are formed by weathering and hydrothermal alterations of K and Al-rich rocks, commonly from mudrocks and shales (Deer et al., 2013; Nelson, 2014). Likewise, the illitization of smectite minerals is common in clay-rich sediments and shales (Lanson et al., 2009). Illites may have interlayered smectite units in the structure forming illite-smectite mix-layer aggregates. The characteristics can to some degree resemble smectites, for example through swelling (Deer et al., 2013).

Because of the close resemblance to muscovites, there have been difficult to distinguish illites using X-Ray Diffraction (XRD). The use of other techniques has been recommended to distinguish the two minerals (Sari, 2018). Further, the extremely fine-grained clay minerals have been hard to identify with optical methods. The muscovite can be differed from illite in optical methods by being larger than the clay size (<2 μm) particles. Chemically illite differs from muscovite by having more silica and less potassium (Deer et al., 2013).

2.4.3 Kaolinite

Kaolinite is the most common mineral in the kaolinite group. The structure of kaolinite is in a T-O structure (1:1 layer) with weak van der Waals bonding between the layers, see Figure 2-3. The structure hinders the absorption of water into the mineral. In other words, the mineral does not expand. Kaolinite is formed by weathering and hydrothermal alterations. Kaolinite derives from rocks rich in feldspar, muscovite, and other Al-rich silicates, typically granites, rhyolites and quartz diorites (Deer et al., 2013; Nelson, 2014). Even though kaolinite is a non-swelling mineral, it is a secondary mineral that may be associated with swelling clay minerals in weakness zones or weak rock masses (Selmer-Olsen et al., 1989).

2.4.4 Talc

Talc is a weak and soft mineral occurring in mainly metamorphosed ultrabasic rocks from hydrothermal alterations. It can be easily spotted as it often has a characteristic light green/white color, greasy feeling, and a pearly luster. The mineral is known for its very low hardness, and it can be easily removed by a nail on the rock surface. As illustrated in Figure 2-3, the structure of talc is 2:1 of sheets of octahedral (O) and tetrahedral (T) layers where the octahedral layers are composed of magnesium. In comparison to the smectite minerals, the constituent layers are uncharged resulting in no interlaying cations. Whereas the smectite minerals absorb water into the structure, the talc minerals do not because of this (Deer et al., 2013; Nelson, 2015). Talc is a low friction mineral often occurring in weakness zones along tunnel alignments. A low friction mineral can enhance gravitational load failures caused by swelling material. The presence of talc can in some cases be an indicator of swelling minerals present in the rock mass (Nilsen, 2016; Selmer-Olsen et al., 1989).

2.4.5 Zeolite

Zeolites are a group of aluminosilicate minerals with laumontite and mordenite being part of this group. Zeolites are structured in a framework of linked tetrahedra, forming rings. The open cavities in the structure are usually occupied by water molecules and extra cations with freedom of movement, allowing an exchange of ions and water molecules (Deer et al., 2013). This gives zeolites the ability to both swell and contract when hydrated or dehydrated, without damaging the structure. If such rocks are constrained it can possibly cause a significant stress development during both states of hydration and dehydration (Kranz et al., 1989). Laumontite occurs in altered volcanoclastic sediments and deep-sea sediments at slightly elevated temperatures, as they are sensitive to changes in temperature and pressure, and in presence of water. They have been found in tuff rocks and basaltic rocks (Deer et al., 2013).

2.4.6 Serpentine

Serpentines are a group of phyllosilicate minerals consisting of three main forms, namely lizardite, antigorite and chrysotile. Serpentine minerals are formed by hydrothermal alteration, also called serpentinization, of mafic or ultramafic rocks (Deer et al., 2013; Fulignati, 2020). A chemical reaction with ferromagnesian silicate minerals such as pyroxene and olivine can form serpentine minerals. Magnetite may also be a result in these conditions when the iron is present. Other typical minerals associated with serpentines are the green-colored talc and chlorite alteration minerals (Marinos et al., 2006; Selen & Panthi, 2018).

3 Problems associated with difficult minerals in water tunnels

Difficult minerals, as presented in the previous chapter, can lead to swelling, squeezing or cause low friction. When these minerals are present in hydropower water tunnels there can arise dangerous situations with severe consequences of tunnel failure or collapses. Waterway tunnels of hydropower projects are exposed to cycles of wetting and drying due to construction (typical draining case), water filling (typical wetting case) and tunnel drawdown (emptying) during the operation phase. Hence, the rock mass will be exposed to large moisture changes throughout the lifetime of a hydropower plant.

In addition, construction delays and high costs are often associated with the types of problems related to difficult minerals. Having that said, it is possible to reduce the effects through good planning and investigation in the pre-construction phase of hydropower projects. The investigation results will give an estimation of the final cost and construction time, as well as help to estimate the required tunnel support. It is also an important step for evaluating the technical and economic feasibility of the project. Due to the complexity of the rock mass and the fact that every project is different, there will always be some kind of deviation between the predicted and actual rock mass quality. This deviation should be within an acceptable limit (Brox, 2019; Panthi & Nilsen, 2007).

There have been several tunnel failures in the hydropower tunnels through the years. Many of the failures occurred shortly after the operational start, many which were from the presence of weak minerals and fault zones that was not detected in adequate time. Additionally, there have been cases where estimated tunnel support has been insufficient (Brox, 2019). To highlight the potential consequences of difficult and swelling minerals in hydropower tunnels, two case examples are presented. The cases are from La Higuera hydropower plant in Chile and Kaligandaki 'A' hydropower project in Nepal.

3.1 Case I: La Higuera HPP, Chile

The La Higuera hydropower plant in Chile experienced a case of tunnel collapse caused by swelling minerals. The geology of South America and especially Chile has had several incidents with swelling minerals, as well as squeezing rocks, over the last years. This has been seen in cases like the Esti hydropower project in Panama, Los Chacayes Hydropower Plant and Hornitos Hydropower Plant in Chile (Carter et al., 2010; Stefanussen, 2017).

The La Higuera HPP is located in the Tinquirica valley in the central part of the country, about 160 km from the capital Santiago. Along with the La Confluencia HPP, it makes up a twin hydropower plant (Figure 3-1) with an installed capacity of 155 MW and 158 MW, respectively. Both hydropower plants are co-owned by Statkraft and Pacific Hydro. The tunnels were constructed by drill and blast method from 2006 to 2008 with operational start in 2010 (Carter et al., 2010; Statkraft, 2021b).

Figure 3-1: La Higuera and La Confluencia hydropower plants located in Chile. Modified from Google Earth (2021).

This part of the Chilean geology is in the Coya-Machalí Formation composed of volcanoclastic rocks, mainly of finely bedded reddish brown and dark brown siltstones, shales, sandy siltstones, sandstones, breccia, conglomerates and tuffs (Carter et al., 2010). According to Charrier *et al.* (1996), the formation is formed from the alteration of basaltic lavas, detrital sediments and pyroclastic flow/ash. The rocks in this formation are found to have a large swelling potential, with the appearance of smectite and zeolite being significant (Riemer, 2009, as cited in Selen, 2017). The Coya-Machalí Formation is overlain by volcanic and continental volcanic rocks. Further, the formation is intruded by granodioritic and dioritic rocks (Carter et al., 2010). The intrusions have been affected by hydrothermal alterations, resulting in swelling potential (Riemer, 2009, as cited in Selen, 2017).

An observation made by Carter et al. (2010) indicates that the more reddish-colored rocks in the Chilean tunnels are more likely to swell compared to the greyish and brownish rocks. This has not been confirmed but could be related to the physico-chemical and mineralogic state of the rocks. XRD and rock chemistry evaluation conducted on the reddish rocks from the Coya-Machalí Formation indicates a significant amount of smectite clays. Yet, testing of solid rock samples shows no considerable swelling or expansion of the rocks. In comparison, when the samples were powdered to <150 µm a significant swelling could be detected by testing procedures with an expansion of 20%, even up to 60-70%. Swelling pressure up to 1 MPa was also detected. The observations consider that a mechanical disturbance of the intact rock will induce swelling behavior in the rock mass (Carter et al., 2010). With this in mind, faults or weakness zones in the rock mass along the tunnel periphery could lead to severe swelling, as well as time-dependent alterations of the intact rock mass in tunnel sections.

A collapse with a rock volume of 12 000 m^3 (Figure 3-2) occurred in 2011, only about 9 months after production started. The collapse appeared in highly weathered rocks associated with swelling minerals and zeolite veins. It has been concluded that the tunnel, which was excavated through a reddish volcanic rock (tuff), passed a large fault consisting of minerals with a severe swelling potential. This prominent feature was though not detected and nominal tunnel support such as rock bolts, mesh and shotcrete was used as the final rock support (Broch & Palmström, 2017; Brox, 2019).

Figure 3-2: Collapse of weathered rock in the La Higuera headrace tunnel. Photo from Brox (2019).

Broch and Palmström (2017) point out several measures which could have prevented the extent of the tunnel collapse. Firstly, the application of shotcrete immediately after blast makes it difficult for engineering geologists to evaluate the state of the rock mass and also observe a possible change over time. Secondly, the dewatering of the tunnel for inspection should have happened at an earlier time. It took a whole year before the inspection was done after the increase in head loss was registered. Thirdly, preliminary watering could have revealed the behavior of the fault zone. As well as regular inspections and repair work. Brox (2019) further criticizes the inadequate tunnel support used in most hydropower tunnels and states this as a root cause of failures. A detailed description of geotechnical information and suspected weakness zones should be made, and a final tunnel support designed based on this.

The cost of repair and production downtime, which took two years, could have been cut down considerably if these preventions were accomplished. An example of this is from the La Confluencia hydropower plant. Because of the similar rock conditions in both areas, the experiences from La Higuera were used to avoid rock failures. The La Confluencia hydropower plant was constructed at the time of the La Higuera tunnel collapse. Measurement was taken to locate the areas where swelling could occur, such as preliminary watering and rapid checking using ethylene glycol. In the subjected areas additional rock support was added. So far the measurement that were taken have been successful, as there have been no problems during the operational drift of the plant (Broch & Palmström, 2017).

3.2 Case II: Kaligandaki 'A' hydropower project (KGA)

The headrace tunnel of the Kaligandaki 'A' hydropower project in Nepal experienced severe stability problems which were associated with squeezing (Figure 3-3), as well as small-scale tunnel collapses due to weak rocks. Tunnel squeezing often occurs in weak rocks and weakness/fault zones, thus is very common in the lesser Himalayan schistose rocks (Panthi, 2006).

Swelling, squeezing and a combination of both are some of the most challenging instability situations which may occur during tunnel excavation as well as during operation and can result in tunnel collapses. As explained in Chapter 2.3, there are similarities between the two phenomena, and the terms are often used interchangeably. While swelling of rock is dependent on the access and reaction with water which causes a volume increase, squeezing is related to time and stress conditions (Stefanussen, 2017). The International Society of Rock Mechanics (ISRM) defines the squeezing of rocks as a time-dependent large deformation that occurs around tunnels and is associated with creep caused by exceeding limiting shear stress. During an excavation of a tunnel, the stresses will be re-distributed on the periphery of the tunnel and there will occur a deformation in the rock surrounding mass. In weak and schistose rocks, such as shale, phyllite and mudstone, rock squeezing will take place if the strength of the rock mass is less than the re-distributed stress. The rock material will have a time-dependent inward movement towards the tunnel, also called plastic deformation (Barla, 2002; Panthi, 2012).

Figure 3-3: Squeezing in the Kaligandaki headrace tunnel. Photo from Impregilo SpA (1989) in Panthi (2006).

The Kaligandaki 'A' hydropower plant is located in the western part of Nepal in the Lesser Himalaya, approximately 200 km west of Kathmandu. Hydropower generation has a large potential in Nepal considering the topography and the snow-covered mountains of the Himalayas. The Kaligandaki project has an installed capacity of 144 MW with an annual energy generation of 842 GWh. The project was completed in 2002 and is owned by Nepal Electricity Authority (NEA). As shown in Figure 3-4, a 5950 m long headrace tunnel

transfers the water from the Kaligandaki river. The headrace tunnel was excavated primarily by drill and blast method. Installed tunnel support was dependent on the rock mass quality along the tunnel alignment (Panthi, 2006; 2012). Based on this the rock support primarily consisted of steel ribs in a spacing interval of 0.6 to 1.5 m, steel fiber reinforced shotcrete with thickness from 15 to 60 cm, fully grouted rock bolts and full concrete lining as final support (Panthi & Shrestha, 2018).

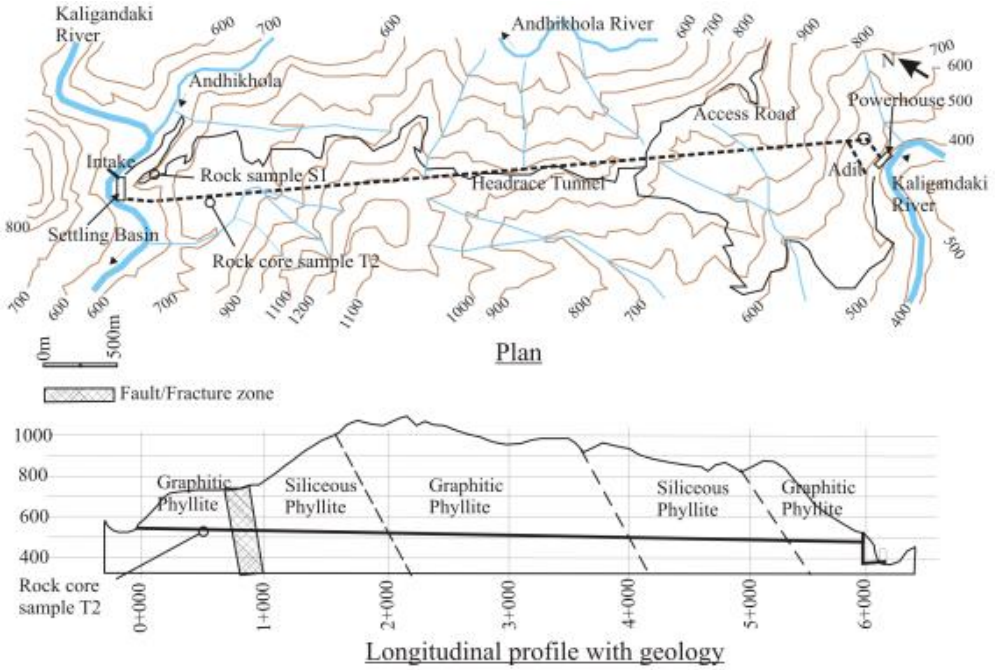

Figure 3-4: Longitudinal profile and topography of the headrace tunnel in the Kaligandaki 'A' hydropower project (Panthi, 2006).

Himalayan geology is very complex and is influenced by active tectonic movement, climatic and topographic conditions. A high degree of weathering, weak rock mass quality, rock stresses and effects from groundwater are characteristics that all cause stability problems in engineering geological projects (Panthi, 2006). The geology of the project area consists of highly deformed rocks, mainly siliceous and graphitic phyllites and dolomite. A longitudinal profile of the geology along the headrace tunnel is illustrated in Figure 3-4. Most of the tunnel section has a large rock cover (80% of the tunnel exceeding 200 m), and the maximum overburden is approximately 620 m. The rocks are formed from Precambrian to lower Paleozoic shallow marine sediments and are slightly to highly weathered, thinly foliated and fractured. Additionally, several close-laying faults are found along the headrace tunnel (Panthi, 2006; Panthi and Nilsen, 2007; Panthi and Shrestha, 2018). According to the Q-system, the overall quality of the rock mass is in the category of poor to extremely poor (Panthi & Shrestha, 2018).

Several sections of the headrace tunnel experienced stability problems and failure during excavation, two of these incidents are shown in Figure 3-5. As previously stated, the tunnel passes through sheared and metamorphosed weak rocks which are particularly prone to squeezing. Panthi (2006) identifies two factors to be significant for the stability problems. Firstly, the rock mass consisted of weak and foliated phyllites with a low self-supporting capability that resulted in several small to medium scale tunnel collapses. Secondly, a high overburden and large stress concentration resulted in that the phyllite rock mass was squeezed frequently.

Figure 3-5: a) Tunnel collapse due to stress and strength anisotropy. b) Instability and cracks caused by tunnel squeezing. Photo by Impregilo SpA (1999) as cited in Panthi (2006).

During the excavation of the Kaligandaki 'A' headrace tunnel the rock mass quality was found to be poorer than predicted during the feasibility and detailed design phases. This case gives a good example of why adequate planning and investigations in tunneling projects are important. As the estimated construction time was from January 1997 to July 2000 and the project was not completed until the summer of 2002, this deviation led to a two-year delay and further an increase in cost for the project. The final rock support cost was approximately two times the estimated cost. Hence, when planning a tunneling project the pre-construction investigation should be adjusted to the complexity and type of project, simply to avoid additional time and cost expenses (Panthi & Nilsen, 2007).

4 Moglicë Hydropower Plant

The rock tested in this thesis is collected from the Moglicë HPP owned by Statkraft. This chapter will give a brief introduction to the Moglicë HPP and the Devoll hydropower project with the geological conditions of the project area.

4.1 Brief about Moglicë HPP

The Moglicë hydropower plant (HPP) is a part of the Devoll Hydropower Project which is owned and operated by Statkraft along the Devoll river and catchment area (Statkraft, 2021c). The Devoll valley is located in the south-eastern part of Albania between the town Maliqi (Korcë district) and the village Banjë (Elbasan district). This is about 100 km south of the capital Tirana (Devoll HPP, 2011a). The location of the Devoll catchment area and the Moglicë hydropower plant is shown in Figure 4-1. Additional to the Moglicë hydropower plant the Devoll Hydropower project also includes the Banjë hydropower plant. Construction of Banjë HPP lasted from 2013 to 2016, while Moglicë HPP was constructed from 2015 to operational start in 2020. Together the two hydropower plants have an installed capacity of approximately 269 MW and energy generation of approximately 700 GWh/year (Statkraft, 2021a).

An overview of the Moglicë hydropower plant is found in Figure 4-2. The project area is built up with a 167 m asphalt core dam. The dam has a storage capacity of approximately 380 million cubic meters and utilized a 300 m water head from the reservoir (Selen, 2020; Statkraft, 2021c). Water transport is done through 28 tunnel-section of approximately 11,8 km to an underground powerhouse cavern (Devoll HPP, 2011a).

Figure 4-1: Location of the Devoll basin and Moglicë Hydropower plant within Albanian borders. Modified after Frengen (2020); Statkraft (2021a).

Figure 4-2: Overview of the Moglicë hydropower plant. Modified from Selen (2020).

4.2 Geological conditions along the headrace tunnel

4.2.1 Regional geology

Albania has a rugged topography that originates from the Albanides mountain range and is prominent in the easternmost part of the country. The mountains are divided into the Internal Albanides in the east and External Albanides in the west (Nieuwland et al., 2001). Moglicë hydropower plant lies within the Internal Albanides consisting of ophiolites and various sedimentary rocks, mainly flysch. (Aasen et al., 2013; Nieuwland et al., 2001). The area is primarily divided into the Krasta flysch zone (pink), Mirdita mélange zone (light blue) and Devoll ophiolite nappe (green) (Devoll HPP, 2011a), as shown in Figure 4-3.

The Krasta zone is dominated by flysch series in the uppermost part of the headrace tunnel, and in the dam and intake area. The rock mass varies between sandstone and siltstone dominated flysch with alternating layers. Claystone and conglomerates are also present in some areas. The strength and mechanical characteristics of the flysch are dependent on the individual layers. However, the extreme heterogeneousness of flysch gives the rock a very poor rock mass quality (Aasen et al., 2013; Devoll HPP, 2011a).

The Mirdata mélange zone is a transition zone between the flysch series and the ophiolitic nappe and consists of a reworked mixture from both origins. The rock types found in the Mélange zone include sheared serpentinites, ophiolitic breccias, flysch and volcanic rocks (Rusi & Hoxha, 2013). The zone is extended in an E-W direction of approximately 400 m to 1 km. Mélanges are typically very chaotic and in a tectonic disorder. The Mirdita mélange zone, for instance, has several distinct N-S striking fault zones with varying blocks of the sedimentary and volcanic rocks in a sheared soil-like mass (Devoll HPP, 2011a; Marinos et al., 2006).

The Devoll ophiolite nappe is located in the downstream part of the tunnel section and belongs to the western ophiolite belt consisting of mafic and ultramafic rocks. Sedimentary rocks are also found deposited in between the lava flows in the ophiolite nappe. The ophiolites are part of the oceanic crust of an ancient ocean which is trusted up on the continental crust. The rocks have been altered and metamorphosed or serpentinized to a varying degree. In contact with water, typically in fractures, ferromagnesian minerals such

as pyroxene and olivine can transform to serpentinite. This can also be called autometamorphism where ophiolitic rocks are serpentinized. The altered minerals get a reduction in strength, thus making them more prone to tectonic shearing and faults (Devoll HPP, 2011a; Marinos et al., 2006). The ophiolites in the project area are of homogenous and sound quality, with the exception of localized serpentinization of peridotite (Aasen et al., 2013).

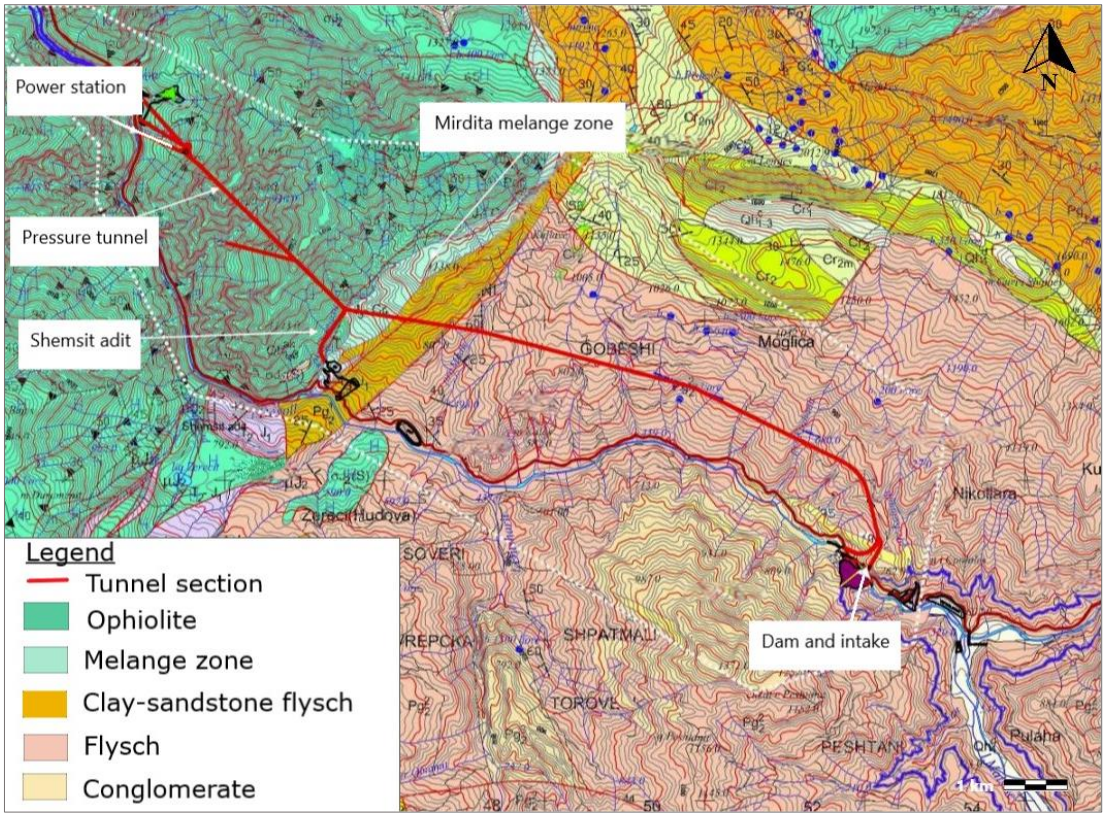

Figure 4-3: Geological map and tunnel section of the Moglicë hydropower project area. Modified from Devoll HPP (2011a).

4.2.2 Ground investigation

A large number of geological investigations of the ground and rock mass quality need to be performed in any hydropower project. Investigations done for the Moglicë hydropower project includes desk studies, field mapping and ground investigations including rotary core drilling and refraction seismic measurements. Stress measurements and groundwater investigations were performed in all investigation boreholes. Rock cores obtained from the drilling were used for geological mapping and further laboratory testing. The following tests were performed (Aasen et al., 2013).

- Uniaxial compressive strength, UCS
- E-modulus, E
- Point load, I_{s50}
- Brazilian tensile strength, BTS
- Sound velocity, v_p
- Petrographic analysis/thin section
- Drilling rate index/Cutter life index (DRI/CLI)
- Cerchar scratch test
- Slake durability

4.2.3 Rock mass classification

The varying nature of the rock mass properties makes it hard to use solely one classification system. Investigations in the Devoll HPP (2011) report used the Marinos & Hoek (2001) modified GSI-value in the flysch series in Appendix A. The flysch rock types alternated with sandstone and siltstone in varying thicknesses. The Flysch rocks are classified from A to H based on their quality from good to very poor rock. As illustrated in Figure 4-4, flysch of E, F and H quality was the most common in the Moglicë hydropower plant area, with sections of B, C and D quality also present in the rock mass (Devoll HPP, 2011b). Class E is defined as "Weak siltstone or clayey shale with sandstone layers" and class F is defined as tectonically deformed, faulted/folded, sheared siltstone or clayey shale in a chaotic structure (Marinos & Hoek, 2001). The flysch rocks have a large variation in uniaxial compressive strength (UCS) with values ranging from 5 MPa to 100 MPa. Most of the rock mass seems to be within the UCS range of 20-50 MPa, representing a medium strong rock (Brevig et al., 2011).

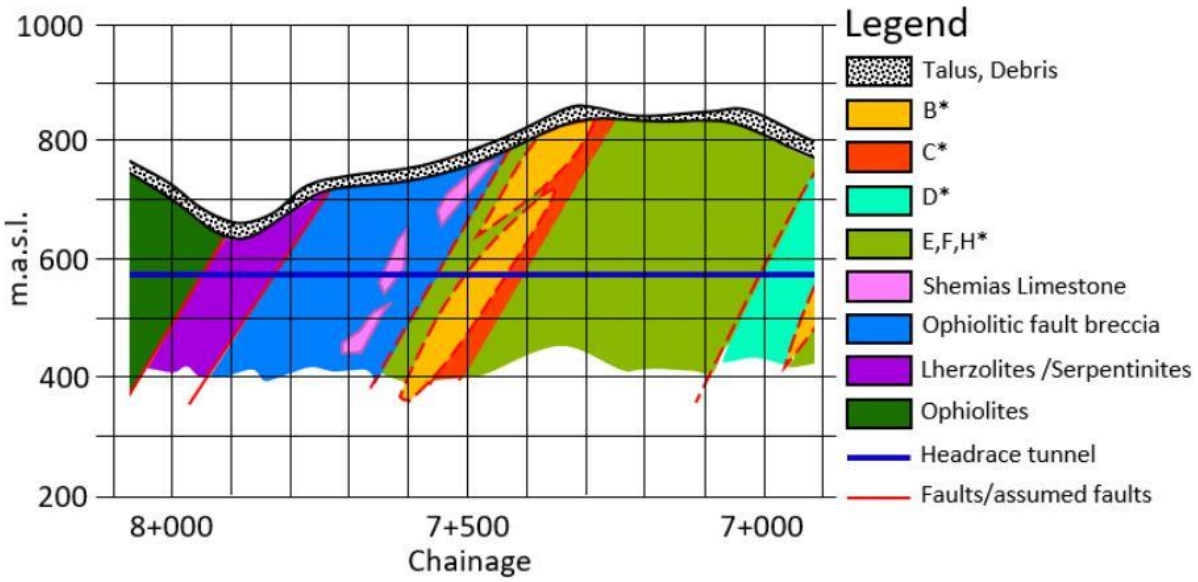

Figure 4-4: Longitudinal profile of the Moglicë headrace tunnel with geological conditions. Flysch rocks are annotated based on quality classes. Figure from Frengen (2020).

The geological condition between chainage 7500 to 8000 has a large variation in rock mass quality and lithology, as seen in Figure 4-4. This zone represents the transition zone between the flysch series and the Devoll ophiolite, in other words, the Mélange zone. An overview of the rock mass classification of each rock type is given in Table 4-1 with GSI and UCS values. According to the obtained UCS-values, the rock mass varies from very strong rock in the ophiolitic clasts, to strong in the limestone/sandstone, volcanic/pillow breccia, moderate in the serpentines and weak rock in the matrix and sheared serpentinite. The uniaxial compressive strength classification is according to ISRM (1978b) in Appendix B.

Table 4-1: Rock mass classification between areas 7510 - 7950 in GSI and UCS. From Brevig et al. (2011).

From - to	Rock type	UCS (MPa)	GSI
7510 - 7550	Sandstone	20 – 40	15 - 30
	Siltstone/clayey shale	25 – 50	
7550 - 7830	Ophiolitic clasts	100 – 250	10 - 25
	Matrix	1 – 25	
	Limestone lenses	50 – 100	50 - 80
	Sandstone layers	50 - 100	25 - 50
	Volcanic/pillow breccia		
7830 - 7950	Serpentinite/Lherzolite	40 – 45	25 - 40
	Schistose serpentinite	30 – 35	
	Sheared serpentinite	1 - 25	10 - 20

The Devoll ophiolite nappe was classified according to the "little q" system. This includes the Shemsit access tunnel and the power cavern, which had a q-classification (%) as presented in Table 4-2. The rock mass quality is grouped into five classes, q1 to q5. The classes represent very good (q1), good (q2), fair (q3), poor (q4) and extremely poor (q5) rock conditions (Brevig et al., 2011). The little q classification system is a modification of the Q system to incorporate the swelling characteristics to the rock mass quality, the description is found in Appendix B. A poorer rock classification indicates, among others, a higher amount of swelling clay present in the rock mass. The required rock support is based on the rock mass quality (q-classification), the size of the opening and the usage. The rock support for the different q classes are presented in the reports (Brevig et al., 2011; Devoll HPP, 2011a).

Table 4-2: Rock mass quality along the Shemsit access tunnel and power cavern according to the little q classification system (%). From Devoll HPP (2011a).

	q1	q2	q3	q4	q5
Shemsit access tunnel (%)	0-5	10-30	40-60	10-20	0-10
Power cavern (%)	0-5	10-30	55-80	5-15	0-5

4.3 Fieldwork

A field trip to the Moglicë hydropower plant in Albania was completed from 5.-8. April 2022 along with Statkraft representant Thomas Schönborn and co-supervisor Jessica Ka Yi Chiu. The goal of the fieldwork was to carry out field scanning using hyperspectral imaging. During the visit, two roadside outcrops along the Moglicë headrace tunnel were visited. Both outcrops were located within a 2 km radius of the Shemsit adit (Figure 4-3). A more descriptive explanation is given in Chapter 5.7.4.

5 Methodology

To answer the research questions of this study many methods were applied. The methods include laboratory work performed mainly at the Department of Geoscience and Petroleum. In addition to visits to the HySpex laboratory in Oslo and fieldwork performed in Moglicë, Albania. A range of laboratory testing was performed, including traditional methods for assessing swelling minerals, such as X-Ray Diffraction (XRD), X-Ray Fluorescence (XRF) and petrographic thin sections. Alternative assessment of mineralogy using Automatic Mineralogy System (AMS) and Hyperspectral imaging (HSI) was also applied. The latter was performed at the HySpex laboratory in Oslo, as well as by field scanning performed on-site in Moglicë. Other laboratory methods include ISRM suggested oedometer swelling pressure test. Additionally, a review of the modified preparation method has been performed and compared to the standard preparation method.

5.1 Material description

The rock material is collected from an area along the Moglicë headrace tunnel, more precisely, close to the Shemsit access tunnel. The Shemsit access tunnel is located in the Mirdita mélange zone and the Devoll ophiolite complex of the project area, as seen in Figure 4-3. The investigated cores were drilled in the summer of 2021, whereas the section from depth 68-80m was used in this thesis. During the initial core logging completed on-site, the rock cores were classified as a flysch type rock and described as "siltstone with thinly layers of sandstone and limestone". An improved logging performed during this thesis work resulted in a complete revision of the earlier logging, verifying a mixture of several rock types, namely fault gouge, serpentinite, chlorite rich shale with carbonates, altered basalt, shale, and a shale-marble-mixture, displayed in Figure 5-1.

During transportation from Albania to Norway the rock cores were exposed to severe shuffling and further disintegration. The rock cores were rearranged with old photos of the core boxes in an attempt to put all the pieces back in their original position. Considering this there might be deviations in the rock core boxes which can impact the results of this thesis.

Figure 5-1: Core samples from the Shemsit adit in Moglicë HPP with rock classification. Photo by Lisa Henrika Henriksen and Karoline Arctander, summer 2021.

5.1.1 Fault gouge

Fault gouge is an extremely fractured and crushed rock with several broken up, porous rock pieces of varying size from clay size up to ca. 5 cm. The rock is characterized by a fine-grained rock mass that is highly composed of clay minerals. The matrix is of a dark grey mineral with small-scale white veins (1 mm) throughout. The rock mass is shale-dominated with a mixture of several of the other rock types from the area. Some of the larger serpentinite pieces have a talc covered surface. The fault gouge material is located from depth 68.00-68.80m in the core sample. The fault gouge is shown as Sample 1 in Figure 5-3.

5.1.2 Serpentinite

The serpentinite rock type is located from depths 68.80-71.20m and is characterized as partly disintegrated with pieces of varying sizes (Figure 5-1). The rock groundmass is aphanitic and consists of mainly dark green to black minerals with a few white calcite veins throughout the rock specimen. A talc mineral coating appears on the surface of the rock pieces. The rock has a fatty feeling to the touch on the fracture surface. A black, shiny, and slippery surface also appears on the fractures. The rock mass appears as homogenous in terms of color and fabric. Sample 2 in Figure 5-3 shows a close-up piece of serpentinite.

5.1.3 Chloritic shale with carbonate fragments

The rock core section from 71.20-72.00m is a inhomogenous, chlorite rich shale with incorporated carbonate fragments. The rock is characterized by light green chlorite dominated groundmass with large inclusions of grey/white carbonate minerals (Sample 3 in Figure 5-3). Large sections of marble are twisted into the chlorite rich matrix. Additionally, calcite veins with a thickness of 0.5-2 cm run through both rock masses. A transitional zone from serpentinite to the chlorite rich rock type is located at depths 70.80-71.20m.

5.1.4 Altered basalt

The altered basalt is found in several meter thick sections from depth 72.00-80.00m with interlaying shale and shale-marble-mix, as can be seen in Figure 5-1. A close up of the rock is seen as sample 5 in Figure 5-3. The basalt is a black or dark grey, massive, fine-grained rock. There is a varying amount of white calcite or quartz veins and clasts throughout the rock, mostly with 1-2 mm thickness. However, clasts can be up to 1 cm thick. In some sections, for instance, the depths of 77.72 to 78.14 m, the white carbonate fragments are particularly large (several cm). Thus, varies slightly from the other sections of altered basalt.

5.1.5 Shale

Two areas of clayey silty shale are found interlaying between the altered basalt at sections 72.30-72.49 and 75.38-76.00 m (Figure 5-1). The shale consists of dark grey to black fine-grained matrix with several white quartz and calcite sigma clasts of size 1-5 mm. The rock is smooth to the touch. Additionally, small-scale veins (1-2 mm) with a white mineral filling are observed. The rock is layered (laminated) and breaks apart easily into thin layers. On the surface of the fracture planes, there is found spots of a black and slippery mineral filling with a pearly luster. Evidence of tectonic activity is present as carbonate sigmaclasts are incorporated into the shale, as shown in Sample 4 in Figure 5-3.

5.1.6 Shale-marble-mix

The shale-marble-mix is characterized with a dark grey rock matrix with several carbonate veins and fragments incorporated in a messy mix. The rock is less layered with more randomly oriented calcite veins compared to the shale. The veins have a thickness varying from approximately 1 mm to 1 cm. Small-scale tectonic faulting is observed in the rock mass, as shown in Figure 5-2.

Figure 5-2: Small-scale tectonic faulting in a shale-marble-mix rock type.

5.1.7 Rock samples

The rock samples investigated during this thesis work are presented in Table 5-1. In total nine samples were chosen, seven of which are the main samples used for both thin section and crushing, this will be explained in the following section. Samples 8 and 9 are additional samples only used during optical thin section, Automated Mineralogy System (AMS) and hyperspectral imaging (HSI). The samples are of varying rock types as displayed in the table. Photos of the rock samples are shown in Figure 5-3. Placement of the different sample specimens from the rock core boxes are displayed in Appendix C.

Table 5-1: Overview of tested rock samples with depth [m] and rock type classification.

Sample nr.	Thin section area	Depth [m]	Rock type
Sample 1	TS1	68.00 – 68.15	Fault gouge
Sample 2	TS2	70.28 – 70.40	Serpentinite
Sample 3	TS3	71.80 – 72.00	Chlorite rich shale with carbonate
Sample 4	TS4	72.47 – 72.51	Shale
Sample 5	TS5	72.51 – 72.60	Altered basalt
Sample 6	TS6	75.40 – 75.50	Shale
Sample 7	TS7	77.80 – 78.00	Altered basalt
Sample 8*	TS8	73.90 – 74.00	Altered basalt
Sample 9*	TS9	77.20 – 77.30	Shale-marble-mix

*Samples only used in thin section scanner, AMS and HSI.

Figure 5-3: Photo of the nine rock samples used during this master thesis.

5.2 Crushing

Recent studies (e.g. Selen, 2020) have recognized the lack of suitable preparation techniques applied to weaker rock types. The author has suggested replacing the current techniques with more gentle methods to avoid destruction and preserve the mineral composition of the rock specimen. This also includes avoiding high temperatures and the inclusion of water for clay rich rocks. One of the aims of this study has been to further evaluate a modified preparation method applied to weak rocks, and simultaneously compare this with the standard preparation method used at the Department of Geoscience and Petroleum. Considering the Norwegian standard methods are adapted to strong rocks, a modified preparation method could be beneficial for weaker rock types. The purpose of the modified crushing method is to preserve weak minerals and simultaneously prevent forming of amorphous material. This method is tested on samples 1-7 presented in Table 5-1. The modified method is developed alongside supervisors Krishna Kanta Panthi, Bjørn Eske Sørensen and laboratory employee Laurentius Tijhuis.

An overview of the preparation method and laboratory testing procedure is shown in Figure 5-4. The initial core sample was coarsely crushed and split into two sections; standard and modified. The modified sample was further split into two fractions (100–300 µm and <100 µm) during crushing and sieving, thus creating three duplicate sample sets. The splits are presumed to be identical in mineral composition. Each of the three splits would further be crushed and prepared for XRD, XRF, powder thin-section and swelling test. XRD and XRF were taken from the same bulk material. Seven core samples were used in this study. Additionally, there was made polished thin sections of the seven rock samples which is evaluated optically in microscope and in the Automated Mineralogy System (AMS).

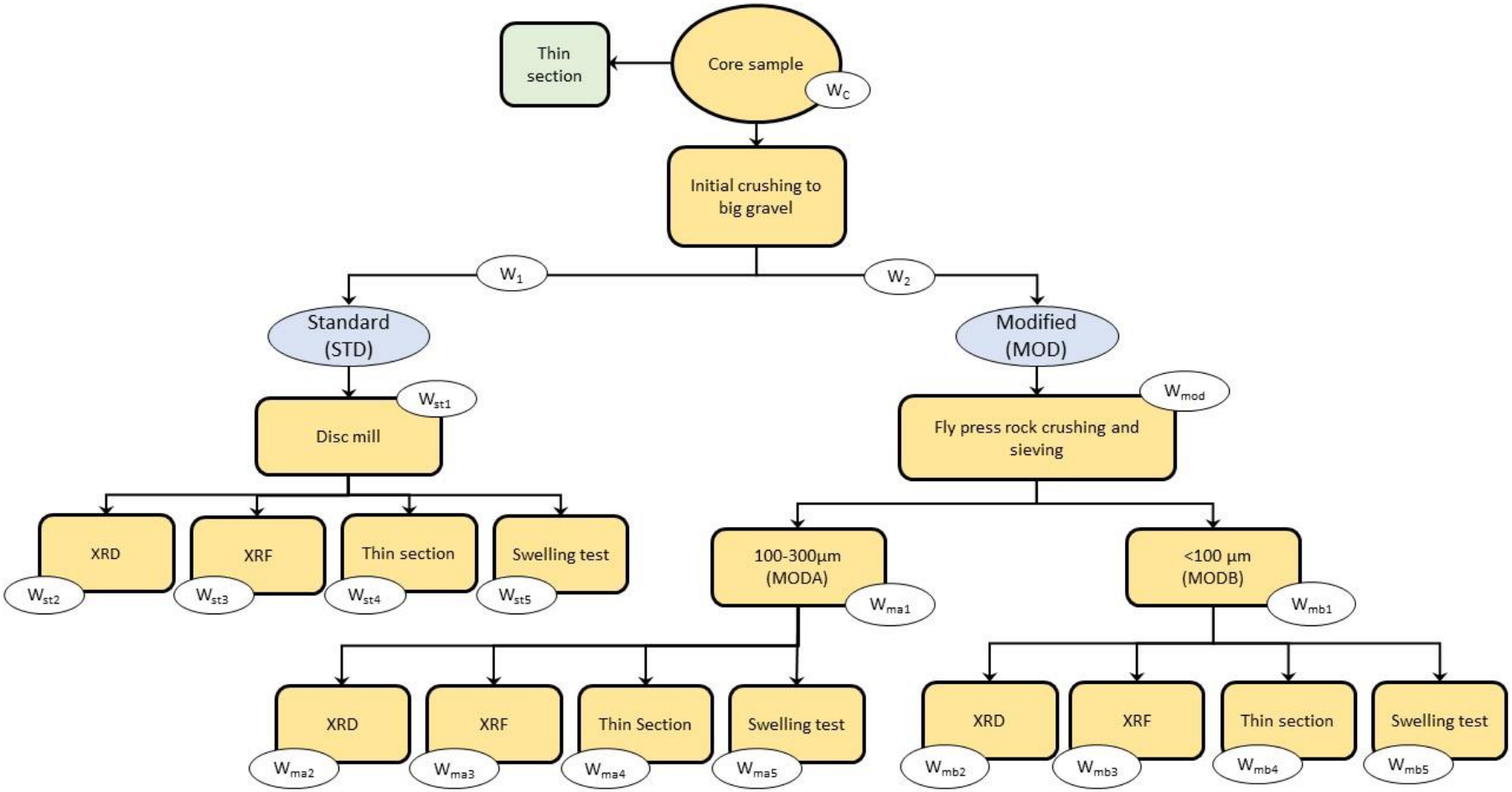

Figure 5-4: Flowchart for the laboratory testing procedure. W_x - sample weight presented in Appendix D.

5.2.1 Standard crushing method

The standard crushing and preparation method is as follows. The Fly Press Rock Crusher (Figure 5-5) is used to crush the sample material coarsely. The sample material is placed in the machine and crushed between two metal plates to gravel size material. Further, the gravel-sized material is grinded to a fine-fraction material (approximately <10µm) in the Retsch Vibratory Disc Mill RS 200 (Figure 5-5) where friction between the disc and material inside the jar causes the material to get milled down. Note that the jar is limited to approximately 20-30 g material (for a 50 ml grinding jar) in each run to assure maximum friction generation. Run time is set to 1.5 minutes. The equipment is cleaned between each sample to avoid contamination. The milled material is split into three parts using a splitter. The splits are meant for the continued laboratory testing (XRD/XRF, oedometer swelling test and powder thin sections) to assure identical mineral composition.

The standard crushing method is an automated and fairly simple preparation method. Still, it was discovered several 1-2 mm large grains in samples STD3-STD6. Because of this the selected samples (STD3-STD6) were crushed an additional time, thus causing risk for over-crushed material and add to differences between samples as some materials were only crushed one time. The additional crushing also resulted in a larger material loss. Loss of material can lead to misrepresentation of the minerals and thus affect the overall interpretation of the rock mass.

5.2.2 Modified crushing method

To reduce the exposure to high temperatures and rough mechanical crushing the modified preparation method includes manual labor through the Fly Press Rock Crusher, a mortar and pestle, and a set of sieves. The sieves have a grid opening of 315 µm and 100 µm. Resulting in two fractions: 100-315 µm and <100 µm. The former is referred to as 100-300µm in this thesis.

The procedure of the modified crushing method is as follows. The intact sample is placed in the Fly Press Rock Crusher between two steel discs. Manual force is used to bring the discs together by swinging a long arm and thus crushing the sample material. The arm is swung back and forth to crush the sample material. The material is regularly sieved with small particles being removed to prevent being overly crushed. A mortar and pestle are used correspondingly to the Fly Press Rock Crusher. The mortar and pestle were mostly used when the Fly Press Rock Crusher had problems crushing the last remaining rock material. The whole procedure is repeated until all material has passed through the sieve. The equipment is displayed in Figure 5-5. It is also important to reduce the risk of contamination by cleaning all the equipment thoroughly between each sample.

By using this method there is a high risk of material loss as neither the Fly Press Rock crusher bowl nor the mortar is located in a closed space. Particles can easily get flung out if the procedure is not done with care. During crushing and sieving the material loss was evident as particles were scattered around the equipment. As shown in Figure 5-5, a sheet of paper is used to catch flying particles and thus try to minimize the loss of material. However, some material loss is inevitable. The impact of this can be evaluated from the laboratory test results.

The seven samples that were crushed by the modified method had an initial weight that varied from approximately 90 to 182 g where all the material had to pass through the sieves to get the correct representation of the mineral composition. The modified crushing

method took approximately 4 to 5 hours per sample. This corresponds to five working days to complete the crushing of seven samples.

Figure 5-5: Instruments used for standard and modified crushing methods.

5.3 X-Ray Diffraction (XRD)

5.3.1 Background

X-ray diffraction (XRD) is an analytical method to identify and determine the mineralogical composition of a rock sample. During the procedure, the sample gives a characteristic x-ray diffraction pattern for each mineral. This "fingerprint" can be matched against a database by comparing relative peak heights of the crystalline phases and thus identifying the mineral composition of the rock sample (Dutrow & Clark, 2021; Selen et al., 2020). The samples are grinded to a fine powder (approximately <10 µm) in a fluid to minimize the preferred orientation of particles. This is a measurement to simulate the random orientation of grains of bulk material and thus get a more representative quantification of minerals (Dutrow & Clark, 2021; Holder & Schaak, 2019).

Figure 5-6 illustrates the basic concept of the XRD analysis. The prepared samples are placed in the x-ray diffractometer where the x-rays are transmitted through a cathode ray tube. On the surface of the sample, the x-ray will interact with the crystals and the reflected x-ray will give information about the lattice structure of the crystal. This is related to Braggs law ($n\lambda=2d\sin\theta$) where the unique d-spacing can be used for the identification of minerals. To scan every part of the crystal lattice the scanning is done at varying 2θ angles (Dutrow & Clark, 2021).

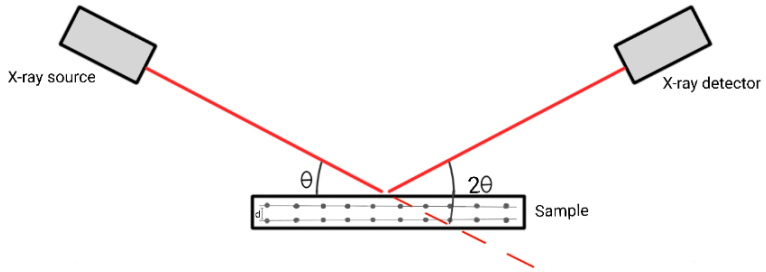

Figure 5-6: X-ray diffraction from Braggs law.

5.3.2 Laboratory procedure

The XRD tests were performed in the chemical/mineralogical laboratory at NTNU and was conducted on the seven standard and modified sample material as previously explained.

The XRD analysis is prepared by the standardized method at NTNU. Firstly, approximately 2 g of the pulverized sample material is milled in the McCrone Micronizing Mill (Figure 5-7a) with 10 ml ethanol (98%) for 2 minutes. Secondly, the material is washed off with ethanol and placed in a petri dish. The petri dish is dried in a drying cabinet at 60°C for the standard samples. The modified samples have a lowered temperature at approximately 40°C. Thirdly, the dried sample material is placed into a powder specimen holder that is further analyzed in the D8 ADVANCE X-Ray Diffractometer shown in Figure 5-7. For identification and quantification of the diffraction patterns the DIFFRAC.EVA (identification) and DIFFRAC.TOPAS (quantification) software was used in combination with the PDF-4+ database.

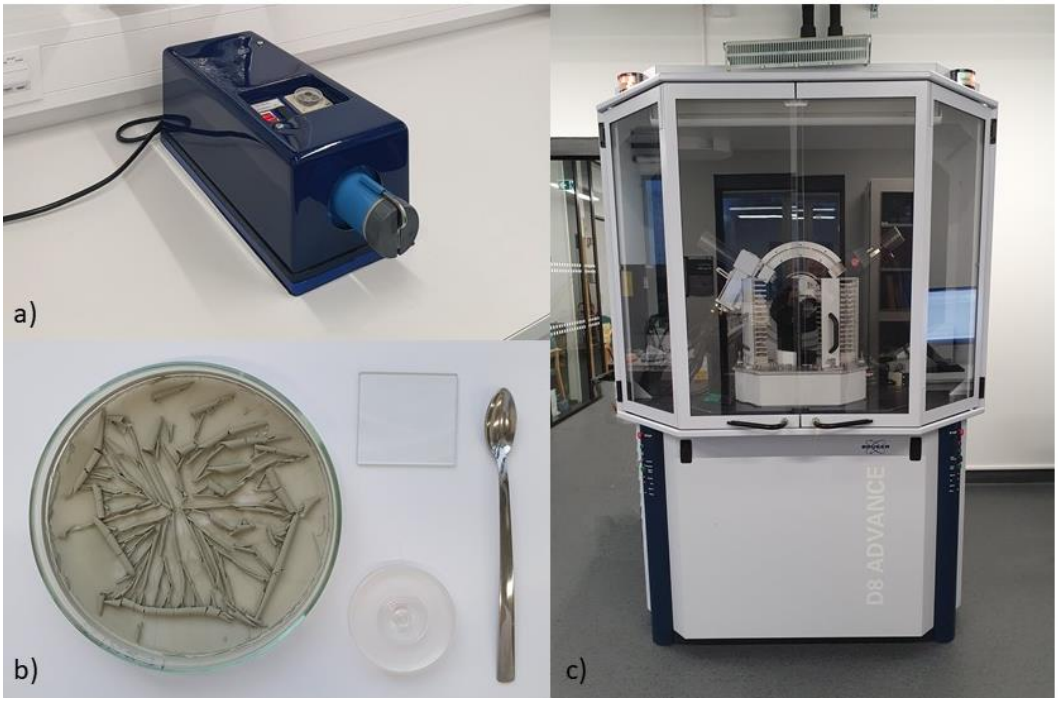

Figure 5-7: a) McCrone Micronizing Mill. b) Petri dish with dried sample material, powder specimen holder and tools to help fill the holder. c) D8 ADVANCE X-Ray Diffractometer.

5.4 X-Ray Fluorescence (XRF)

X-Ray Fluorescence (XRF) is a method for quantifying the elements in an intact material, such as a rock mass. Both major elements (>0,5 %) and trace elements (<0,5 %) can be detected using XRF. In this thesis, only the major elements were quantified. The method is often used in geological investigations to classify and characterize differences in rock types. Each element has a characteristic fluorescence ray that will be emitted when the x-ray is in contact with the sample. The wavelength of this fluorescence ray will be registered by a detector (NGU, 2020).

The analyses are done on powdered rock samples in a bulk material milled down to approximately <10 µm. A total of 21 samples were analyzed using the x-ray fluorescence. The samples were split into three sets with seven samples in each set. As explained in Chapter 5.2 both modified and standard samples were tested. Considering the XRF analysis demands an extremely fine-fractioned powder for analysis the modified fraction of 100-300 µm was milled in the Retsch vibratory disc mill RS 200. The fraction <100 µm was evaluated to be fine enough and was thus not further milled.

The preparation procedure is as follows. Approximately 2.5 g of the bulk sample is weighed into a porcelain crucible (Figure 5-8a) and heated in the Nabertherm B180 furnace for one hour at 1000 °C. The loss on ignition (LOI) can be calculated from this process and is an important factor in the characterization of the geochemistry. The water contained in the mineral structure will be removed at high temperatures, as well as other organic materials. The sample is weighed before and after ignition as the sample mass is most likely to decrease (ALS, 2021). A mixture of 5,0 g lithium tetraborate and 0,5 g of the previously glowed sample material is mixed in a platinum crucible. As shown in Figure 5-8, the mixture is melted in the Claisse TheOx Advanced fusion instrument and formed into a glass bead. The glass bead is analyzed in the XRF spectrometer (PANalytical ZETIUM minerals edition) at the NTNU chemical/mineralogical laboratory. The software SuperQ 6 (WROXI method) is used as it is commonly used to cover rocks and geological materials (Malvern Panalytical, 2022).

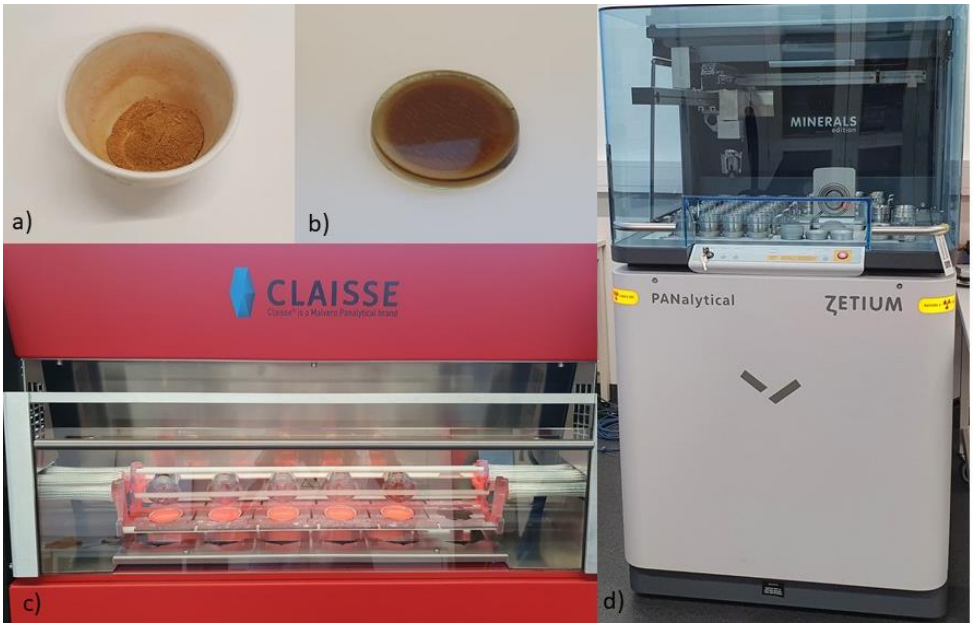

Figure 5-8: a) Porcelain crucible with the sample material. b) Glass bead. c) Claisse TheOx Advanced fusion instrument for XRF. d) PANalytical ZETIUM minerals edition XRF spectrometer.

5.5 Optical microscopy of thin section

Eight polished thin sections were prepared at the thin section laboratory located at the Department of Geoscience and Petroleum. The eight thin sections were chosen according to areas of interest in the rock cores to perform optical light microscopy and AMS analysis, five of the samples had already been scanned using hyperspectral imaging (Table 5-2). The idea was to get the exact surface for comparison between the HSI and AMS methods. TS2 and TS4/TS5 have some deviations from the exact surface. Further, 3 additional thin sections (TS6, TS7 and TS1) were prepared for corresponding core samples chosen for crushing and testing.

Table 5-2: Overview of sample nr, thin section nr, AMS, crushing and hyperspectral surface analysis.

Sample nr.	Thin section nr.	AMS	Crushing	Hyperspectral surface
TS1	39110	Yes	yes	no
TS2	39081	Yes	yes	yes
TS3	39082	Yes	yes	yes
TS4	39083*	Yes	yes	yes
TS5		Yes	Yes	no
TS6	39111	Yes	yes	no
TS7	39112	Yes	yes	no
TS8	39084	Yes	no	yes
TS9	39085	Yes	no	yes

*TS4 and TS5 are located in the same thin section specimen.

Petrographic thin section analysis is used to identify and classify the mineralogy of the rock sample. A microscope is used to view the microtextures in the rock with higher resolution. The use of textural characteristics will provide information about the formation and chemical composition of the mineral (Raith et al., 2012). The Olympus BX51 Thin Section Scanner with the Märzhäuser Wetzlar SCAN motorized microscope stage (Figure 5-9) located at the microscopy laboratory was used to scan the eight thin sections with the Olympus Stream Motion software. All thin sections were scanned with four light setups, plane-polarized light (PPL), cross-polarized light (XPL), fluorescence light (FL) and reflectance light (RL). Plane- and cross-polarized light was used to determine optical properties such as color, cleavage, relief, and interference color. Fluorescence light was used to observe the fracture distribution and reflectance light was used to highlight opaque minerals.

Figure 5-9: Olympus BX51 Thin Section Scanner and SCAN motorized microscope stage.

5.6 Automated Mineralogy System (AMS)

Mineralogical analyses were performed using scanning electron microscopy (SEM), including backscatter electron (BSE) imaging, energy dispersive X-ray spectroscopy (EDS), and the automated mineralogy system (AMS) (Graham, 2017). The analysis was performed at the Electron Microscope Laboratory at the Department of Geoscience and Petroleum of the Norwegian University of Science and Technology (NTNU). The EM Laboratory at NTNU hosts a ZEISS Sigma 300VP Field Emission SEM (Figure 5-10) that is equipped with two Bruker Xflash 6|30 129 eV EDS detectors and ZEISS Mineralogic Software.

Figure 5-10: ZEISS Sigma 300VP Field Emission SEM. Photo from FELMI-ZFE (2022).

Automated mineralogy is a way of classifying the mineralogy of the sample by combining the capability of different techniques, thus creating an efficient and seamless analysis to gain information (Graham et al., 2015). The AMS technique collects unquantified EDS

spectra with a high-resolution grid covering the analyzed mineral grains. The mineral phase is identified based on the contained element weight percent (Wt%). The EDS spectrum is matched to a list of known reference EDS spectra for the minerals and thus classified (Graham & Keulen, 2019).

Eight polished thin sections were coated with a thin carbon layer (~20 nm) and investigated with AMS. All thin sections were evaluated in the optical microscope (thin section scanner) beforehand to determine the mineral composition and find a representative area of interest to do the scans. A mineral list was created beforehand from this and XRD analysis results. Additionally, 15 powder thin section samples obtained from the crushing procedures were analyzed using the Automated mineralogy system. Only 15 of 21 powder samples were analyzed due to time pressure.

Scanning electron microscopy applied to fine-grained material (submicrometer scale) has previously been challenging because of the differences between grain size and electron beam diameter, resulting in mixed signals of the chemistry of individual grains (Graham & Keulen, 2019). However, the authors further explain how fine-grained samples can be mapped with the automatic mineralogy system using a considerably smaller step size than the diameter of the electron beam and at a very high resolution. Considering the fine grain size of the samples in this thesis, it was chosen to use a step size of 0.6 µm, a 1500x magnification and an acceleration voltage of 15 kV. For the powder thin section, a step size of 3 µm was chosen, along with 290x magnification and acceleration voltage of 15 kV. During the post-processing stage, the samples were checked using the post-processing software for quality control. The mineral list was updated to optimize quality.

5.7 Hyperspectral Imaging (HSI)

5.7.1 Background information

Hyperspectral imaging, also called imaging spectroscopy, is a method for remote mapping and analysis of geology that is based on the reflectance properties of minerals. This method can be used in the laboratory, in the field (terrestrial and airborne), from aircraft, and satellites. The potential of using close-range hyperspectral imagining to map mineralogy on the tunnel face has been further studied in the latest years (Clark, 1999; Kurz et al., 2017).

Identification and mapping are done under infrared lights as most minerals give a unique spectral signature in the infrared spectral range (Kurz et al., 2017). Photons are emitted towards the rock sample and enter a mineral where they can be reflected, scattered, or absorbed by the grain surface. The spectrometer can measure the wavelengths from these processes and thus give information about the mineralogy (Clark, 1999). A spectrometer can measure a broader spectrum of wavelengths than what is visible to the human eye. Visible light has a wavelength range from 0.4 to 0.7 µm. In remote sensing, the wavelength range from 0.4 to 1.0 µm is known as VNIR (visible-near-infrared) and the interval from 1.0 to 2.5 µm is referred to as SWIR (short-wave infrared) (Clark, 1999).

5.7.2 Usage in hydropower tunnels

As mapping and investigation of the tunnel face geology is an important part of engineering geological projects it is essential to find new, more efficient, and better methods to do so. Close-range hyperspectral imaging can provide a more safe and time-efficient way of analyzing the in situ geological conditions of the tunnel, as well as being a digital archive

(Kurz et al., 2017). Hyperspectral imaging is done at a distance from the tunnel face to collect mineralogical data in a remote, non-contact way. The use of this method in the tunneling industry has some limitations as there is no direct sunlight to illuminate the tunnel face, as the entire tunnel wall is required to be illuminated during the procedure. The use of artificial lights has been proven to give good quality hyperspectral data. There is also a space issue, considering the setup of the equipment is limited to the tunnel space (Kurz et al., 2017).

The present-day methods for the identification of swelling and difficult minerals involve several time-consuming and expensive tests. This includes mineralogical and engineering geological tests such as XRD and swelling tests, respectively. A large number of studies (Chabrillat et al., 2002; He & Barton, 2021; Kurz et al., 2017) have tried to evaluate whether the approach of using imaging spectroscopy can detect swelling clay, and have found positive results where the detection of clay minerals such as montmorillonite (smectite), kaolinite and illite. The fact that hyperspectral imagining can map the lithology of the tunnel face, including those minerals which may be difficult to identify by the eye, can be a huge resource in the future.

5.7.3 Laboratory procedure

Hyperspectral imaging in the laboratory was performed in the HySpex laboratory in Oslo by PhD fellow Jessica Ka Yi Chiu and myself. In the HySpex laboratory, we were well received by Dr. Friederike Körting, who helped and guided us throughout our visit. The equipment and setup utilized at the HySpex laboratory are shown in Figure 5-11. During scanning, the samples were placed on a moving stand where it was possible to set up the start and end positions. The scans were performed with a Hyspex SWIR 384 Pushbroom spectrometer and Hyspex VNIR 1800 Pushbroom spectrometer accompanied by a halogen light source and a variation of two lenses, 30 cm and 1 m, respectively. Reflectance panels are used for calibration to remove image artifacts. These white reflectance panels can have variating reflectance standards (Koerting, 2021) and the ones used for the samples are 5% and 20%. The HySpex laboratory uses the HySpex ground software.

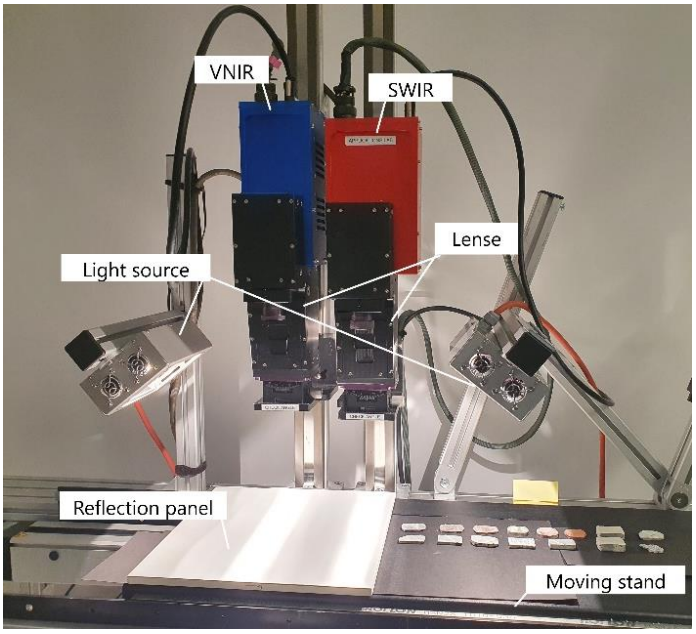

Figure 5-11: Hyperspectral imaging setup at HySpex laboratory. The rock chip samples scanned in this photo will not be used in this thesis.

During the visit to the HySpex laboratory in Oslo, all three rock core boxes obtained from Moglicë were scanned. This was done by placing the boxes on the moving stand and scanning the top surface of the rock cores. There were doubts if the moving stand was too small compared to the core sample boxes and if the measurement would be performed. In the end, with some adjustments, it was made possible to scan all the cores. However, the last approximately 20 cm of the cores had to be cut out of the scan. The reflectance panel also had to be scanned separately because of this issue. The reflectance panel was placed at the same height as the highest part of the rock core. Additionally, some rock sample pieces of the rock cores were further analyzed by scanning the surface. The reflectance panel is at the same distance from the lens as the scanned surface of the samples. Table 5-3 indicates which lenses were used for each sample specimen.

Table 5-3: Overview of lenses chosen for each rock sample.

Samples	Lenses
Rock core boxes	1 m
Sample 2	30 cm
Sample 3	30 cm
Sample 4	30 cm
Sample 8	30 cm
Sample 9	30 cm

5.7.4 Field procedure

A field trip to Moglicë, Albania took place in April 2022 with the intention to perform hyperspectral imaging in the field. The field trip was taken alongside PhD fellow Jessica Ka Yi Chiu and Statkraft associate Thomas Schönborn. The hyperspectral scanning was performed on two roadside outcrops along the Moglicë headrace tunnel (Figure 5-12). The outcrops were chosen as they were accessible and the lithology has known swelling minerals. Information about the setup of the two outcrops is given in The results from the field scans are not processed at the time of submission, thus not included in the results.

Table 5-4. The hyperspectral imaging scans was performed by Jessica Ka Yi Chiu, whereas I helped with the setup of equipment. The results from the field scans are not processed at the time of submission, thus not included in the results.

Table 5-4: Moglicë 1 and Moglicë 2 field information.

Location	Distance	Lenses	Field-of-view	Rock type
Moglicë 1	Ca. 15 m	VNIR: 13-23m, SWIR: 9-50m	16° (vertical), 80° (horizontal)	Flysch
Moglicë 2	Ca. 12 m	VNIR: 13-23m, SWIR: 9-50m	16° (vertical), 90° (horizontal)	Serpentinite

Figure 5-12: a) Moglicë 1 outcrop with reflectance panel and ground control points (red circles) oriented towards NW. Reflectance panel (50x50x2cm) for scale. Photo by Lisa Henrika Henriksen. b) Moglicë 2 outcrop with reflectance panel and ground control points (red circles) oriented towards NE. Reflectance panel (50x50x2cm) for scale. Photo by Jessica Ka Yi Chiu.

The equipment taken into the field is provided by the Hyspex laboratory in Oslo. This includes a rotary tripod, Hyspex VNIR 1800 Pushbroom spectrometer, Hyspex SWIR 384 Pushbroom spectrometer, lenses, field computer and 50% reflection panel (50x50cm). The setup of the equipment is shown in Figure 5-13. As the procedure was done outside, sunlight was used as the illumination source. A GPS was also used in the field for georeferencing of the photogrammetry model.

In the field, the two cameras were mounted to the rotary tripod and connected to the field computer. An aggregator was used to provide power to the cameras and rotary tripod. The outcrop was marked with ground control points and the reflection panel was placed in the center of the chosen scan area with an orientation parallel to the outcrop surface (Figure 5-12). The scans were done horizontally along the outcrop by rotating the cameras placed

on the tripod. HySpex ground is the software used for scan in the field. HySpex rad software is used for radiometric calibration and the radiance is corrected and transferred to relative reflectance by empirical line calibration using ENVI software (J. K. Y. Chiu, personal communication, April 2022; Koerting, 2021).

The integration time is adjusted in the field to achieve approximately 70-80% saturation on the reflectance panel. By doing this it is ensured that the saturation from the rock mass is adequate. The field raw data indicates that the rock shows about 30-40% saturation. Too low saturation will induce too much noise compared to the signal. Oversaturated pixels in hyperspectral images cannot be analyzed (J. K. Y. Chiu, personal communication, April 2022).

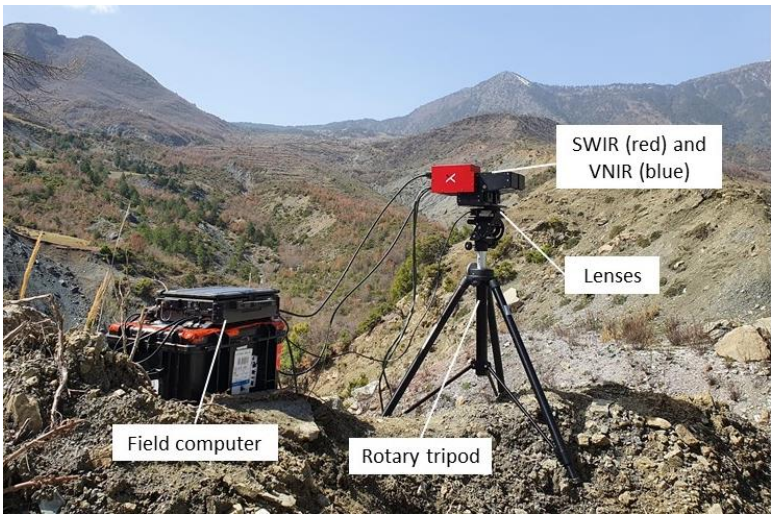

Figure 5-13: Hyperspectral imaging setup at Moglicë 1 with field computer, rotary tripod and cameras. Note that the blue VNIR camera is located behind the red SWIR camera. The lenses are not mounted in this photo.

5.8 Oedometer swelling test

The oedometer swelling test is performed to estimate the magnitude of swelling and swelling pressure [MPa] in the rock samples. Classification of swelling pressure is given in Table 5-5.

Table 5-5: Classification of swelling pressure. Table after NTNU standard (Mao et al., 2011).

Classification	Swelling Pressure [MPa]
Low	<0.1
Moderate	0.1 – 0.3
High	0.3 – 0.75
Very high	>0.75

This test is notably an index test, meaning it should only be used for comparing and classification, and not interpreted as an actual in situ condition (ISRM, 1983). The in-situ conditions are difficult to represent in the laboratory and the initial moisture state and stress situation are ignored at NTNU. The advantage of this is that it gives a quick, uniform and reproducible way to test samples. It will also indicate the potential stability and swelling problems during excavation.

A study by Selen & Panthi (2021) highlighted the differences between the preparation and testing methods conducted at different institutes. The test was performed on duplicate samples. The obtained swelling pressure during testing indicated a difference where samples that fell into the category of "inactive" in one institute showed considerable swelling potential in another institute. While there exist some explanations for the differences, there is a level of uncertainty in the oedometer test.

5.8.1 Pulverized Oedometer Swelling Test

At NTNU/SINTEF the standard approach for swelling test is the ISRM suggested oedometer swelling test. The oedometer apparatus is used to find the maximum swelling pressure [MPa] under the condition of zero volume change. The measured pressure will indicate the pressure needed for constraining the rock under circumstances of an undisturbed specimen and constant volume when immersed in water (ISRM, 1979b).

To conduct a swelling test on pulverized material the oedometer cell has to be prepared, compacted, and put to swelling. For each sample, 20 g of material is used in a 20 cm^2 test cell. The sample is placed between a porous glass bottom-filter and a brass top-filter. A locking ring, cylinder and cylinder liner are used to hold the material in place, while a piston is added on top of the top filter. All parts used to prepare the oedometer cell can be viewed in Figure 5-14. The oedometer cell is placed in the apparatus for compaction for 24 hours with a load of 400 N and discharging for additional 2 hours.

Figure 5-14: Parts for constructing the test cell for the oedometer apparatus.

The material is put to swelling by adding distilled water to the test cell. The water will access the sample material through the porous filters at the top and bottom. The height transduces register the change in height as water enters. The swelling pressure is measured for 24 hours by applying pressure equivalent to the swelling to maintain zero volume change, this is done by the automated step-motor (ISRM, 1979b). Figure 5-15 shows the oedometer setup for the swelling stage of the test. All tests are performed in laboratory conditions.

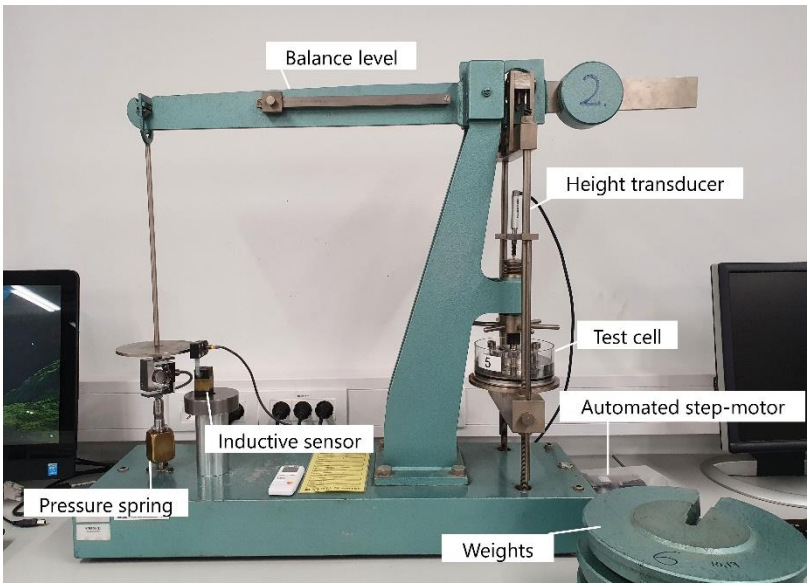

Figure 5-15: Setup of oedometer swelling test apparatus for pulverized samples.

6 Laboratory test results

6.1 Sample overview

Seven core samples were collected from the rock cores for analysis. The samples were split into a crushing stage and a thin section, as shown in Figure 6-1. In one of the cases, two rock units are displayed in one single thin section, TS4 and TS5. Figure 6-1 shows an overview of the samples and how they are related when it comes to laboratory testing and numbering. Note that there are some variations in the steps from sample to sample. The crushed part of the samples is split into standard and modified preparation methods for evaluation of the procedures. Each of them is tested by X-ray diffraction (XRD), X-ray fluorescence (XRF), oedometer swelling test and automated mineralogy system (AMS) through powder thin sections. The intact thin sections (TS) are exposed to optical light microscopy and AMS. Two additional samples, TS8 and TS9, are only prepared as thin sections from optical light microscopy and AMS analysis. The sample numbering with corresponding thin sections is displayed in Table 6-1.

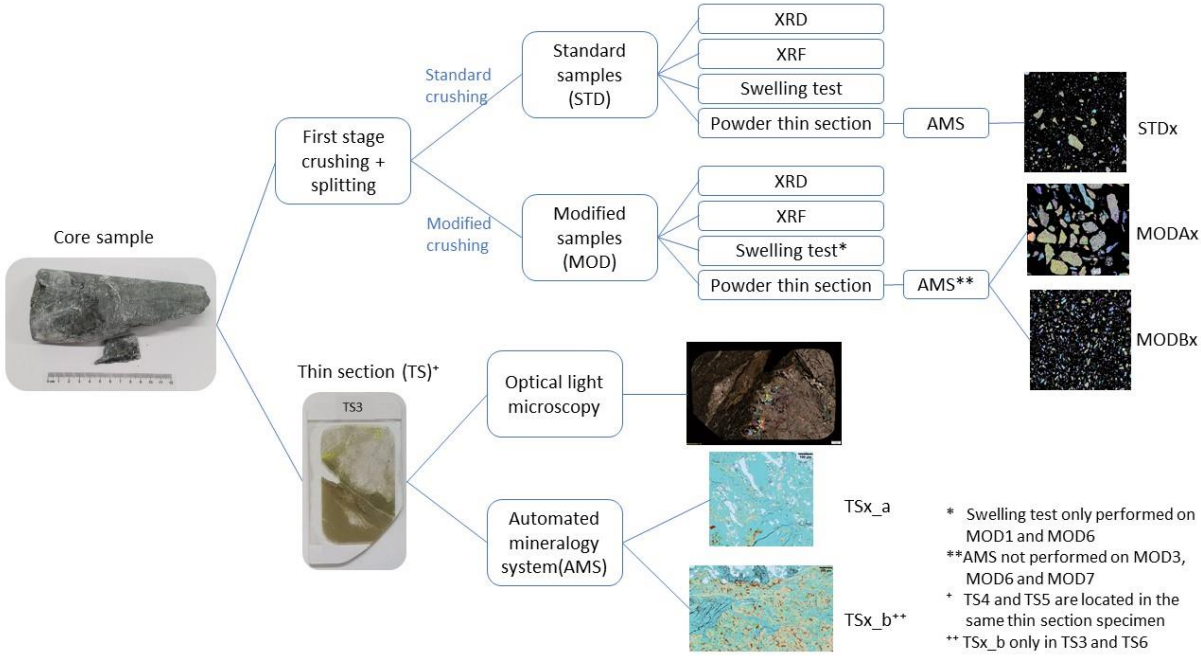

Figure 6-1: Flowchart illustrating the sample preparation, laboratory procedure and sample numbering.

Table 6-1: Overview of sample nr, thin section area, thin section nr and AMS scan area of the nine samples. Only related to intact thin section (TS) specimens.

Sample nr.	Thin section area	Thin section nr.	AMS area
S1	TS1	39110	TS1
S2	TS2	39081	TS2
S3	TS3	39082	TS3_a, TS3_b
S4	TS4	39083	TS4
S5	TS5		TS5

S6	TS6	39111	TS6_a, TS6_b
S7	TS7	39112	TS7
S8*	TS8	39084	TS8
S9*	TS9	39085	TS9

*Only used for thin sections and AMS

6.2 Crushing

A comparison of the sample weights before and after crushing are shown in Table 6-2. The material loss given in percent is calculated based on the weighed material before and after crushing. Sample MOD1 was used as demo material for the modified crushing method, the weight is therefore not accessible. In both the standard and modified versions, the loss of material is different between samples. Samples 3, 4 and 5 have a higher percentage compared to the other samples in both cases. Samples 2 and 7 have a lower loss of material. The modified crushing has an overall higher loss of material compared to the standard crushing, except for MOD5. Be aware that standard and modified crushing weight does not add up to the core sample weight as some material is split and removed from this particular study. An overview of the crushing material weight is displayed in Appendix D.

Table 6-2: Material weight before and after crushing and material loss (%).

	1	2	3	4	5	6	7
Core sample							
Before crushing (g)	253.05	523.6	496.5	509.1	522.5	540.7	396.5
Standard (STD)							
Before crushing (g)	63.6	55.5	124.3	120.2	144.5	131.8	88.7
After crushing (g)	60.8	54.9	114.8	112	130.2	129	87.1
Material loss (%)	4.4	1.1	7.6	6.8	9.9	2.1	1.8
Modified (MOD)							
Before crushing (g)	-	133.3	182	92.7	90.9	100.1	108.1
After crushing (g)	83.8	124.6	163.2	84.6	83.3	93.3	102.1
Material loss (%)	-	6.5	10.3	8.7	8.4	6.8	5.6

6.3 X-Ray Diffraction (XRD)

The mineralogy of the standard and modified samples obtained from XRD analysis is displayed in Table 6-3 and Table 6-4, respectively. The main constituents of most samples are quartz, plagioclase, chlorite and calcite with varying quantification. Samples STD2 and MOD2 differ with serpentine being the main mineral, there is also a high amount of chlorite in the sample. The remaining rock samples have a smaller amount of serpentine compared to sample 2. The mineral composition of the samples is differing, as seen in the tables below. In terms of swelling minerals, smectite was detected in 12 out of 14 samples. Smectite was not identified in STD6 and STD7, this will be further described below. Other potential swelling minerals detected are from the zeolite group, which are only found in STD1 and MOD1.

A comparison chart was made for all seven samples to display the differences between the standard and modified mineral quantification, this is displayed in Figure 6-2. The correlation between standard and modified mineral phases are varying in the samples. Samples 5 and 6 have a fairly good correlation, samples 2 and 3 show a moderately good correlation, and samples 1, 4 and 7 have a poor correlation.

- *Sample 1*: shows a poor correlation where approximately half of the minerals are higher in MOD1 and the other half is higher in STD1. There does not appear to be a link between the mineral either through hard or soft minerals. Smectite and muscovite show the best correlation of the mineral phases. K feldspar is only present in the modified sample.
- *Sample 2*: shows a moderately good correlation where chlorite and talc have a higher percentage in STD2 while serpentine, quartz, cpx (clinopyroxene) and smectite show the opposite. Magnetite and calcite have a good correlation.
- *Sample 3*: shows a poor correlation where, same as sample 1, approximately half of the identified minerals are higher in either STD3 or MOD3. It appears to be detected more hard minerals in the STD3 and more soft minerals in MOD3.
- *Sample 4*: has a poor correlation where most minerals have a higher quantification in STD4, except for serpentinite, smectite and muscovite. A few minerals do however show a good relationship between standard and modified (e.g., pyrrhotite, spessartine, chlorite).
- *Sample 5*: shows a somewhat good correlation in most identified minerals. The most noticeable exceptions are from plagioclase (standard) and smectite (modified), while cpx, chlorite, calcite, serpentine and titanite have some smaller differences in the relationship.
- *Sample 6*: shows a good correlation in all detected minerals except quartz, smectite and chlorite. A lot of minerals are concentrated around zero percent with low differences.
- *Sample 7*: hard minerals such as quartz, plagioclase and cpx show a poor correlation in the sample, however, they do not show a particular trend. Soft minerals such as calcite, serpentine and smectite also have a poor correlation. The remaining minerals have a moderate relationship between modified and standard samples.

Table 6-3: XRD results for standard preparation method in weight%.

	Standard (STD) [Wt%]						
Mineral	1	2	3	4	5	6	7
Quartz	27	9	3	16	2	35	10
Plagioclase	11	-	25	19	43	18	29
Chlorite	6	34	25	8	11	7	4
K Feldspar	-	-	-	-	-	-	-
Amphibole	-	-	-	-	1	-	-
CPX	-	3	16	4	14	-	5
Calcite	10	2	7	29	5	1	29
Datolite	-	-	-	-	-	-	12
Talc	22	13	2	-	-	-	-
Serpentine	3	38	12	0	5	0	0
Smectite	1	0	1	1	0	-	-
Zeolite	5	-	-	-	-	-	-
Titanite	-	-	9	-	8	5	3
Pyrite	-	-	-	0	0	0	0
Pyrrhotite	-	-	0	0	1	1	-
Muscovite	13	-	-	18	7	33	8
Kaolinite	3	-	-	4	-	-	-
Magnetite	-	1	1	-	-	-	-
Spessartine	-	-	-	1	3	1	-

Table 6-4: XRD results for modified preparation method in weight%. Original values in Appendix E.

	Modified (MOD) [Wt%]						
Mineral	1	2	3	4	5	6	7
Quartz	22	10	3	15	2	34	9
Plagioclase	8	-	22	16	37	17	26
Chlorite	5	29	26	9	12	8	4
K Feldspar	4	-	-	-	-	-	-
Amphibole	-	-	-	-	1	-	-
CPX	-	5	15	3	15	-	4
Calcite	15	2	7	27	7	1	33
Datolite	-	-	-	-	-	-	11
Talc	15	12	2	-	-	-	-
Serpentine	4	40	13	2	6	0	2
Smectite	1	2	3	4	3	1	1
Zeolite	8	-	-	-	-	-	-
Titanite	-	-	8	-	7	5	2
Pyrite	-	-	-	0	0	0	0
Pyrrhotite	-	-	0	0	0	1	-
Muscovite	12	-	-	22	6	33	7
Kaolinite	6	-	-	1	-	-	-
Magnetite	-	1	1	-	-	-	-
Spessartine	-	-	-	1	2	0	-

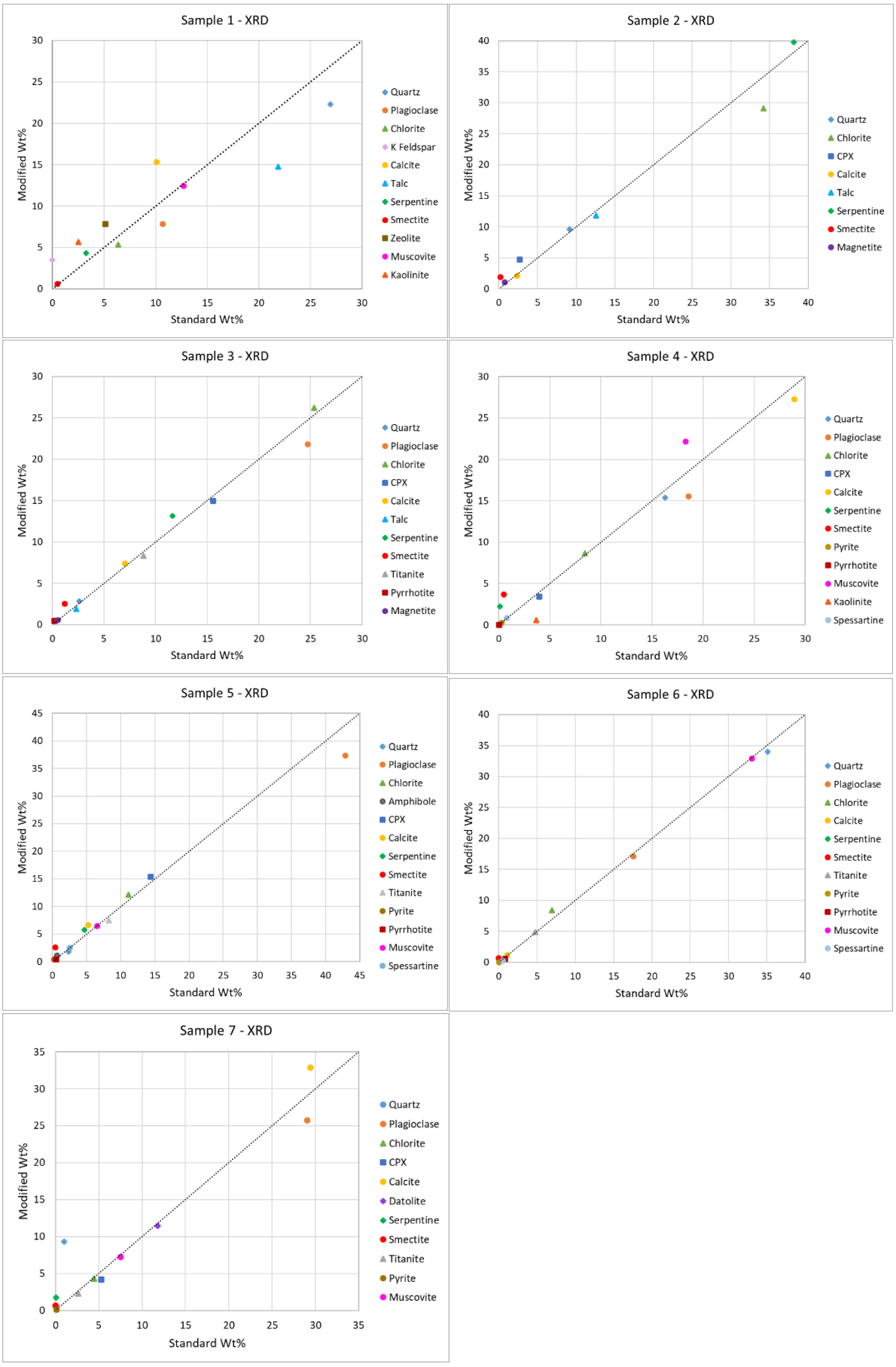

Figure 6-2: Comparison chart of standard (x-axis) and modified (y-axis) XRD results of sample 1-7.

The figures below are based on the values of smectite identified from XRD. In Figure 6-3a, the blue color indicates the weight percent of smectite found in the standard samples while the orange color indicates the amount of smectite in the modified samples. There was detected swelling clay (smectite) in all seven samples with a varying amount. The standard samples STD3, as well as STD1 and STD4, had the highest detection of smectite. In both STD6 and STD7, the smectite minerals were nonexistent. On the other hand, the smectite minerals emerge in MOD6 and MOD7. Sample MOD4, as well as MOD3 and MOD5, revealed the highest smectite amount of the modified samples.

The identified smectite is higher in the modified samples compared to the standard samples, as seen in Figure 6-3a. The green points represent the deviation between the modified and standard samples. The mean is set to the standard values when calculating the deviation, as shown in Equation 6.1. The higher or lower the deviation, the further from this mean value the data is. All samples have a positive deviation in this case indicating an increase in smectite detection in the modified samples. The relative deviation of the samples is highly varying, with a range from 19% in sample 1 to 100% in sample 6 and 7. From the results in Figure 6-3a, the modified and standard smectite is closely related in sample 1. On the other hand, samples 2, 4, 5, 6 and 7 have a high smectite increase in the modified samples. Sample 3 shows a moderate increase. Figure 6-3b illustrates the relation of standard Wt% and modified Wt% of the smectite mineral group of the seven samples. From the figure it is clear that all seven samples have an increase in the quantified amount of smectite in the modified samples.

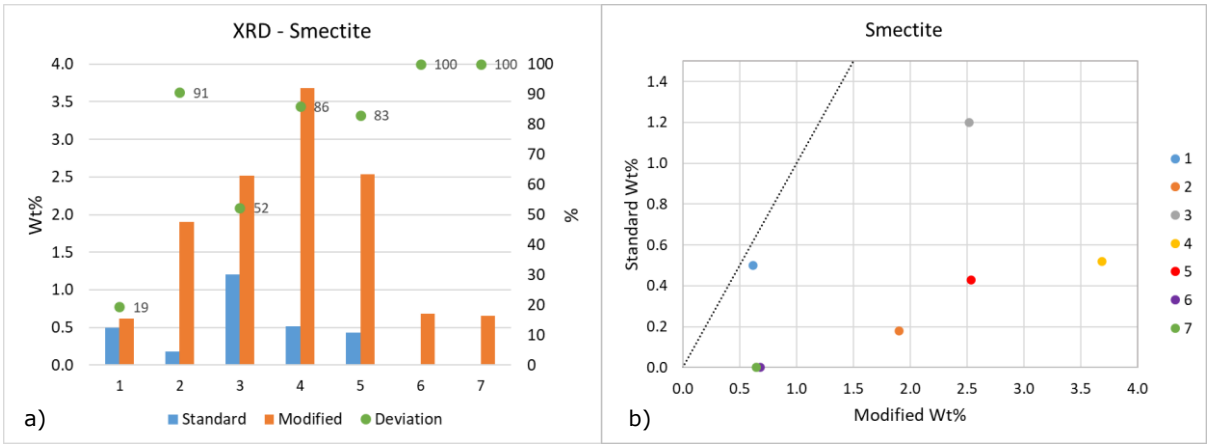

Figure 6-3: a) Correlation of the content of smectite clay mineral (Wt%). b) Comparison chart of quantified smectite clay mineral in standard (x-axis) and modified (y-axis) samples.

Table 6-5 presents the total amount of hard and soft minerals identified in the standard and modified samples. The grouping is based on the Mohs hardness scale. Hard minerals include quartz, plagioclase, feldspar, amphibolite, clinopyroxene (cpx), datolite, titanite, pyrite, pyrrhotite, magnetite and spessartine. Soft minerals include chlorite, calcite, talc, serpentine, smectite, zeolite, muscovite (mica) and kaolinite. A relative deviation of hard (blue) and soft (orange) minerals is calculated from Equation 6.1 and presented in Figure 6-4. The relative deviation is split between the hard and soft minerals to compare the differences between the standard (STD) and modified (MOD) samples.

$$Relative\ deviation\ (\%) = \frac{MOD - STD}{MOD} * 100 \tag{6.1}$$

The closer the relative deviation is to zero, the more similar the modified values are to the standard values. A positive increase in relative deviation indicated a higher amount of mineral detection in the modified samples. An increase in the negative values indicated a

higher amount of mineral detected in the standard samples. Based on this all samples in Figure 6-4 show an increase in soft minerals and a decrease of hard minerals in the modified samples, except for sample 2 which shows the opposite.

Table 6-5: Total hard and soft minerals grouped from the standard and modified crushing XRD results.

		1	2	3	4	5	6	7
Total hard	Standard	38	13	52	40	72	59	59
	Modified	34	15	49	35	66	57	53
Total soft	Standard	62	87	48	60	28	41	41
	Modified	66	85	51	65	34	43	47

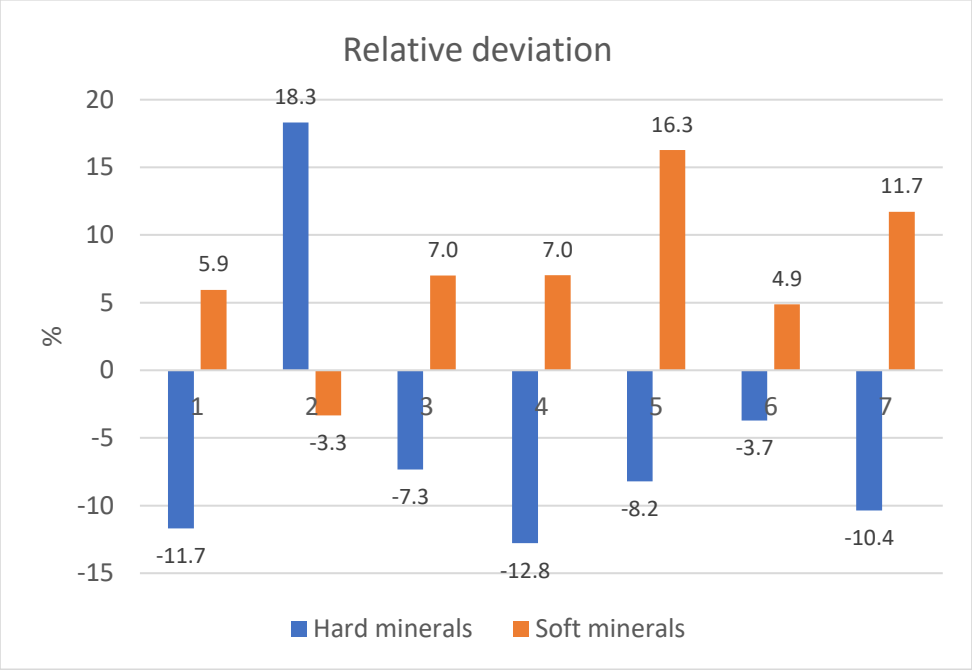

Figure 6-4: Relative deviation of hard and soft minerals obtained from XRD.

6.4 X-Ray Fluorescence (XRF)

The results achieved from X-Ray Fluorescence (XRF) in both standard and modified versions are presented in Table 6-7. All results are main elements. The samples show a relatively similar total sum, except sample 7 which was lower in percentage (96.19% and 96.86%). The loss of ignition (LOI) for the samples varied from 4.56 to 15.63%. The chemical distribution show similarities in all samples, for example, there is a large presence of SiO_2 in all samples. There are also some larger differences, for instance, the MgO content is much higher in samples 1 and 2 compared to samples 6 and 7.

A calculated sum of squares and standard deviation (SD) was used to evaluate the differences between the two crushing methods. The sum of squares formula is shown in Equation 6.2. In this study, the standard value is used as the mean value when calculating the sum of squares, the result from the calculation is presented in Table 6-6 and Table 6-8.

The more the sum of square and standard deviation differs from zero, the larger is the deviation between the standard and modified samples. A deviation indicates a possible loss of material as there has been a change in the chemical composition of the rock samples. The ideal situation would show no deviations. As seen in Table 6-6 all samples have somewhat low values, except for sample 5 (SD=1.37) and sample 7 (SD=2.40). From Table 6-8 it can be seen that the elements SiO_2, CaO and Al_2O_3 have the largest deviation in almost all samples, thus indicating some material loss connected to this elements.

$$Sum\ of\ squares = \sum_{i=0}^{n} (mod_i - std_i)^2 \tag{6.2}$$

Table 6-6: Sum of squares and standard deviation for the seven samples.

	1	2	3	4	5	6	7
Sum of squares	0.75	0.38	0.10	0.97	1.86	0.33	5.76
Standard deviation (SD)	0.87	0.62	0.31	0.98	1.37	0.58	2.40

Table 6-7: XRF results [%] from standard and modified bulk material. Original modified (MODA and MODB) values in Appendix F.

	Modified [%]							Standard [%]						
	1	2	3	4	5	6	7	1	2	3	4	5	6	7
K_2O	0.36	0.01	0.16	2.78	0.31	4.05	0.97	0.36	0.01	0.14	2.68	0.31	4.03	1.03
MgO	22.28	32.84	13.41	5.19	7.65	3.56	2.89	22.35	32.74	13.33	5.08	7.81	3.53	3.01
Mn_3O_4	0.15	0.18	0.21	0.13	0.20	0.09	0.15	0.15	0.17	0.21	0.14	0.20	0.09	0.14
Na_2O	1.23	0.30	2.49	1.69	3.20	1.62	2.63	1.15	0.32	2.49	1.74	3.31	1.57	2.67
P_2O_5	0.06	<0.003	0.16	0.10	0.18	0.12	0.09	0.05	<0.003	0.16	0.10	0.19	0.11	0.09
SiO_2	44.82	40.21	38.10	40.59	42.06	55.71	37.74	44.35	39.89	38.21	40.17	42.63	55.79	39.22
TiO_2	0.47	0.04	1.92	0.74	2.02	0.72	0.51	0.44	0.04	1.91	0.80	2.14	0.73	0.56
Al_2O_3	7.30	2.49	11.21	12.88	12.20	14.77	9.27	7.03	2.50	11.15	12.65	12.62	14.70	9.66
CaO	3.16	1.16	8.08	11.88	9.85	1.85	20.83	3.50	1.27	8.09	12.43	8.79	1.91	19.42
Fe_2O_3	7.01	8.50	12.42	8.95	12.23	10.42	5.86	6.95	8.48	12.34	8.72	12.48	10.39	6.04
NiO	0.11	0.28	0.004	0.004	0.006	0.003	0.003	0.12	0.27	0.004	0.003	0.01	0.002	0.003
PbO	<0.007	<0.007	<0.007	<0.007	<0.007	<0.007	<0.007	<0.007	<0.007	<0.007	<0.007	<0.007	<0.007	<0.007
SO_3	0.34	0.21	0.06	0.45	0.005	0.75	0.20	0.32	0.16	0.06	0.42	0.005	0.57	0.13
SrO	0.02	0.02	0.03	0.02	0.03	0.02	0.02	0.02	0.02	0.04	0.03	0.03	0.01	0.02
V_2O_5	0.02	0.01	0.07	0.03	0.07	0.02	0.02	0.02	0.01	0.07	0.02	0.08	0.02	0.02
ZnO	0.01	0.005	0.013	0.02	0.01	0.01	0.01	0.007	0.004	0.01	0.01	0.01	0.02	0.01
ZrO_2	0.01	<0.003	0.01	0.02	0.01	0.02	0.01	0.00	<0.003	0.01	0.01	0.02	0.02	0.01
BaO	<0.004	<0.004	0.01	0.04	0.01	0.04	0.02	0.01	<0.004	0.01	0.04	0.01	0.04	0.02
Cr_2O_3	0.16	0.37	0.01	0.01	0.01	0.01	0.01	0.17	0.38	0.02	0.01	0.01	0.01	0.01
CuO	0.004	<0.002	0.006	0.007	0.007	0.007	0.005	0.004	<0.002	0.007	0.006	0.006	0.008	0.006
HfO_2	<0.004	<0.004	<0.004	<0.004	<0.004	<0.004	<0.004	<0.004	<0.004	<0.004	<0.004	<0.004	<0.004	<0.004
LOI 1000°C	12.25	12.75	10.23	13.17	7.40	4.56	15.63	12.17	13.25	10.49	13.75	7.29	5.06	14.68
Sum	99.75	99.37	98.61	98.69	97.47	98.35	96.86	99.18	99.42	98.61	98.63	97.80	98.55	96.19

Table 6-8: Difference and difference squared of XRF results.

	Difference = $mod_i - std_i$							Difference squared						
	1	2	3	4	5	6	7	1	2	3	4	5	6	7
K_2O	0.00	0.00	0.02	0.10	-0.01	0.01	-0.06	0.00	0.00	0.00	0.01	0.00	0.00	0.00
MgO	0.06	0.10	0.08	0.11	-0.16	0.03	-0.12	0.00	0.01	0.01	0.01	0.03	0.00	0.01
Mn_3O_4	0.01	0.00	0.00	-0.01	-0.01	0.00	0.01	0.00	0.00	0.00	0.00	0.00	0.00	0.00
Na_2O	-0.08	-0.02	0.00	-0.05	-0.11	0.05	-0.04	0.01	0.00	0.00	0.00	0.01	0.00	0.00
P_2O_5	0.00	0.00	0.00	-0.01	-0.01	0.01	-0.01	0.00	0.00	0.00	0.00	0.00	0.00	0.00
SiO_2	-0.47	0.32	-0.11	0.42	-0.57	-0.08	-1.48	0.22	0.10	0.01	0.18	0.33	0.01	2.18
TiO_2	-0.02	0.00	0.01	-0.05	-0.13	0.00	-0.05	0.00	0.00	0.00	0.00	0.02	0.00	0.00
Al_2O_3	-0.27	-0.02	0.06	0.23	-0.42	0.07	-0.40	0.07	0.00	0.00	0.05	0.18	0.01	0.16
CaO	0.35	-0.11	-0.01	-0.55	1.07	-0.07	1.41	0.12	0.01	0.00	0.30	1.14	0.00	1.99
Fe_2O_3	-0.06	0.03	0.09	0.23	-0.24	0.03	-0.19	0.00	0.00	0.01	0.05	0.06	0.00	0.03
NiO	0.01	0.00	0.00	0.00	0.00	0.00	0.00	0.00	0.00	0.00	0.00	0.00	0.00	0.00
PbO	0.00	0.00	0.00	0.00	0.00	0.00	0.00	0.00	0.00	0.00	0.00	0.00	0.00	0.00
SO_3	-0.01	0.04	0.00	0.03	0.00	0.18	0.07	0.00	0.00	0.00	0.00	0.00	0.03	0.01
SrO	0.00	0.00	0.00	-0.01	-0.01	0.01	0.00	0.00	0.00	0.00	0.00	0.00	0.00	0.00
V_2O_5	0.00	0.00	0.00	0.00	-0.01	0.00	0.00	0.00	0.00	0.00	0.00	0.00	0.00	0.00
ZnO	0.00	0.00	0.00	0.00	0.00	0.00	0.00	0.00	0.00	0.00	0.00	0.00	0.00	0.00
ZrO_2	0.00	0.00	0.00	0.01	0.00	0.00	0.00	0.00	0.00	0.00	0.00	0.00	0.00	0.00
BaO	0.00	0.00	0.00	0.00	0.00	0.00	0.00	0.00	0.00	0.00	0.00	0.00	0.00	0.00
Cr_2O_3	0.01	-0.01	0.00	0.00	0.00	0.00	0.00	0.00	0.00	0.00	0.00	0.00	0.00	0.00
CuO	0.00	0.00	0.00	0.00	0.00	0.00	0.00	0.00	0.00	0.00	0.00	0.00	0.00	0.00
HfO_2	0.00	0.00	0.00	0.00	0.00	0.00	0.00	0.00	0.00	0.00	0.00	0.00	0.00	0.00
LOI 1000°C	-0.08	-0.50	-0.26	-0.58	0.11	-0.50	0.95	0.01	0.25	0.07	0.34	0.01	0.25	0.91
Sum	-0.55	-0.03	0.01	0.07	-0.32	-0.18	0.68	0.31	0.00	0.00	0.01	0.10	0.03	0.46

6.5 Results from SEM-based automated mineralogy and optical microscopy on intact samples

This section presents the results obtained from the Automated Mineralogy System (AMS) performed on the intact thin sections and a rock description based on the images from the thin section scanner. Nine thin section samples were investigated (Figure 6-5). One of the thin sections was prepared into two thin sections as the sample was inhomogeneous, the sample referred to is displayed as TS4/TS5.

The main features and lithology of each thin section is evaluated by optical light microscopy. All thin sections are displayed as cross-polarized (XPL) images in this chapter. All plane polarized (PPL), cross-polarized (XPL), fluorescence light (FL) and reflectance light (RL) images of the thin sections are shown in Appendix G.

A chosen representable area of each thin section is scanned and analyzed by AMS. The result from the AMS includes a table with quantified minerals (Table 6-9), false-colored mineral maps and backscatter electron micrograph (BSE). The results are also presented in Appendix H and Appendix I. Table 6-9 gives an overview of the main mineralogy uncovered during the Automated Mineralogy System (AMS) analysis. The values are given in Wt% and the minerals are grouped. Note that the detected minerals with an extremely low percentage have been removed from the table and can be viewed in Appendix H. Also, a false-colored mineral map created from the AMS is compared to the corresponding XPL thin section scans. In two of the samples, TS3 and TS6, two AMS scans were performed to give a better mineral representation of the rock. These are referred to as TSx_a and TSx_b, respectively.

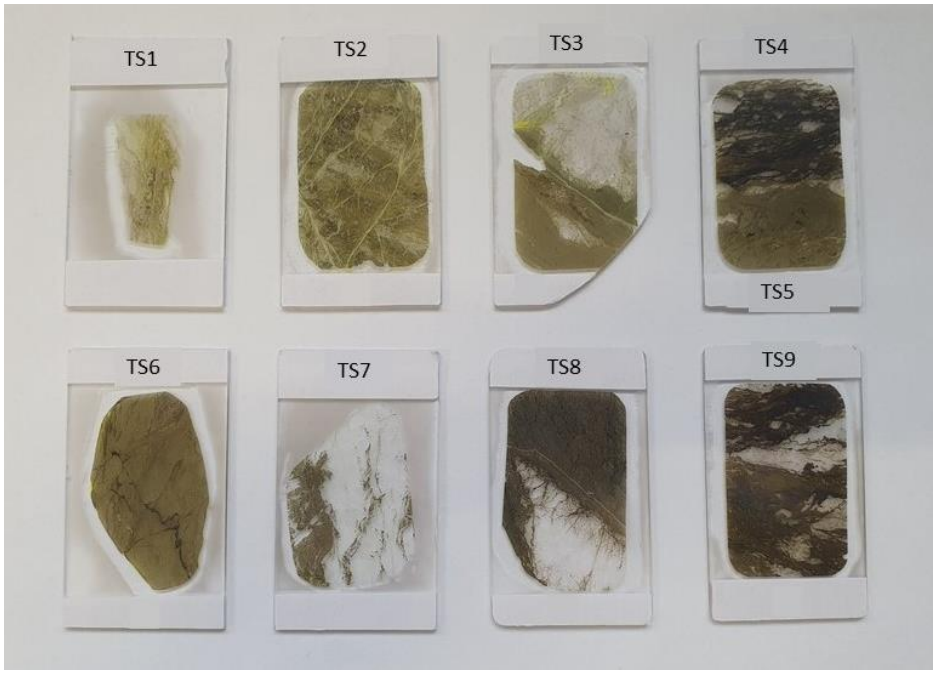

Figure 6-5: Thin section samples from TS1 to TS9. Note that TS4 and TS5 are located in the same polished thin section.

Table 6-9: AMS results [Wt%] from thin sections (TS).

	[Wt %]										
Mineral	TS1	TS2	TS3_a	TS3_b	TS4	TS5	TS6_a	TS6_b	TS7	TS8	TS9
Quartz	13.37	1.593	0.151	2.446	4.087	2.524	41.07	15.28	1.032	4.670	5.098
Plagioclase	18.61	0.013	1.508	8.502	9.286	36.49	6.077	7.046	22.04	25.87	21.83
Plag-chlor-mix	7.814	0.000	1.259	13.53	9.814	19.20	1.364	1.367	3.018	5.877	12.48
Chlorite	26.61	2.370	79.16	52.01	9.153	21.16	4.248	8.404	22.84	34.67	22.85
K Feldspar	0.061	-	0.015	0.053	0.264	0.129	4.977	2.657	0.008	0.069	0.824
Amphibole	0.048	0.048	0.199	0.126	0.055	0.976	0.005	0.008	1.302	0.658	0.059
CPX	1.001	20.571	0.554	1.402	0.306	7.699	0.037	0.024	14.45	15.83	0.382
Calcite	3.579	-	12.76	4.101	18.85	0.069	0.359	0.095	9.087	0.002	1.431
Datolite	0.048	0.001	0.174	0.035	0.966	0.008	0.109	0.088	21.46	0.001	0.152
Biotite	11.67	0.000	0.314	0.112	9.842	0.117	4.018	7.874	0.005	0.014	3.900
Talc	21.85	15.015	0.459	1.255	0.410	0.212	0.017	0.014	0.055	0.027	0.074
Serpentine	0.214	60.134	0.008	0.004	0.001	0.000	-	0.000	0.010	0.000	-
Illite-smectite	3.020	-	0.118	0.180	31.22	1.076	33.49	52.32	0.043	0.480	20.51
Smectite	3.524	0.014	1.576	4.689	2.027	2.666	0.583	0.911	0.810	1.476	1.480
Zeolite	0.009	-	0.001	0.016	0.153	0.156	0.357	0.336	0.092	0.590	0.580
Titanite	1.532	0.031	0.882	8.574	1.403	7.164	1.180	1.222	3.044	6.673	5.299
Pyrite	0.175	-	0.001	0.000	0.291	0.002	0.120	0.108	-	0.065	1.647
Pyrrhotite	0.031	-	-	-	0.008	-	1.476	1.499	-	1.402	0.149
Apatite	0.030	-	0.003	0.003	0.097	0.001	0.112	0.124	0.014	0.002	0.039
Fe-oxide	0.001	-	0.000	0.023	0.010	0.002	0.029	0.154	0.002	0.015	0.041
OPX	0.105	0.083	0.000	0.001	0.001	0.000	0.002	0.003	0.065	0.004	0.000
Muscovite	0.007	-	0.002	0.001	0.015	0.006	0.211	0.327	0.003	0.055	0.065
Vermiculite	0.002	0.000	0.017	0.013	0.042	0.000	0.001	0.004	0.002	0.002	0.015
Kaolinite	0.002	-	0.064	0.000	0.000	-	0.000	0.002	0.000	-	0.000
Other	0.070	0.126	0.778	2.927	1.697	0.355	0.152	0.134	0.622	1.552	1.097

6.5.1 Sample 1

TS1 is a heavily fractured, fragmented fault gouge material with heterogeneous distribution of minerals (Figure 6-6). The matrix is made up of mostly clay size material with larger sized clusters (0.5-2 mm) The clusters are mostly made up of concentrated areas of quartz grains in a darker matrix, quartz is also present in other areas of the thin section. The matrix most likely consists of chlorite minerals, however, the fine-grained nature of the samples makes it hard to distinguish minerals. There appears to be a presence of zeolite, talc and mica (muscovite/biotite) in the samples. A variation of fractures in a webbed pattern throughout the sample is seen from the FL-image in Appendix G (Figure 4). There is also evidence of either pyrite or pyrrhotite in the sample (RL-image).

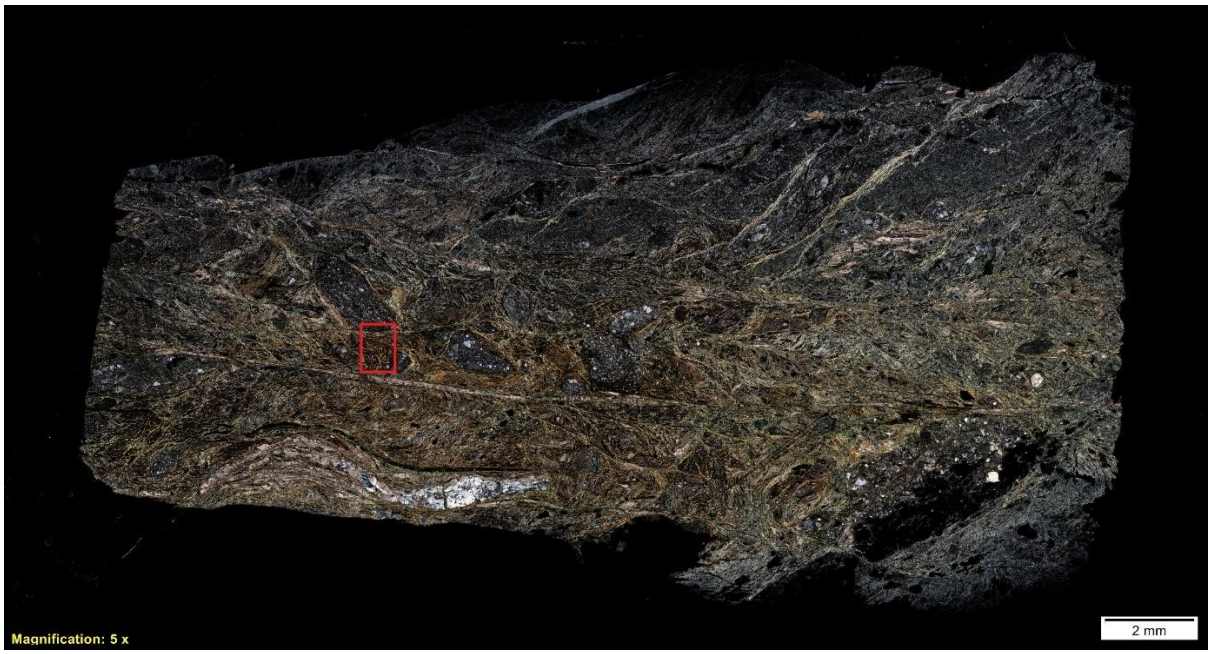

Figure 6-6: Sample TS1 in XPL image with AMS area (red).

The AMS mineral map of TS1 in Figure 6-7 indicates a mixture of mostly talc, chlorite and illite-smectite where the talc minerals are mostly found located around the fracture zones and the others are in the main matrix part, this feature is hard to distinguish from the XPL image. Clasts of plagioclase/albite (ca. 2-10µm) are spread throughout the sample. Titanite minerals are observed in several places in the area with cpx along the edges. A cut out of the quartz rich areas is also a part of the AMS scan, the matrix of the cluster is made up of chlorite and talc. Several large calcite minerals (up to 100µm) are distributed along the edge of the quartz cluster, which is partly observed in the XPL image. Smectite (neon green) is distributed evenly throughout the area and makes up 3.52%.

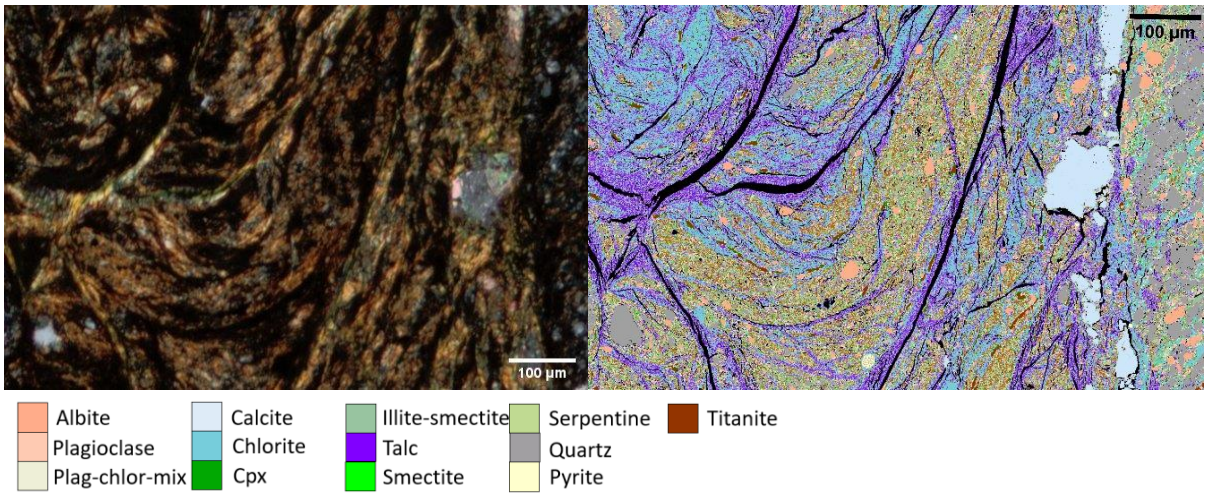

Figure 6-7: XPL area and false-colored mineral map of TS1.

6.5.2 Sample 2

TS2 is a mostly homogenous, fine-grained rock dominated by serpentine minerals with spots of larger mm-sized grains of diopside up to 3 mm (Figure 6-8). A dominant fracture orientation can be observed from top left to bottom right (Appendix G, Figure 8). The fracture filling consists of a variation of minerals, including serpentine and talc. A mesh structure can be observed in the sample mainly created by talc minerals. Other minerals include titanite and large blocks of serpentinized orthopyroxene.

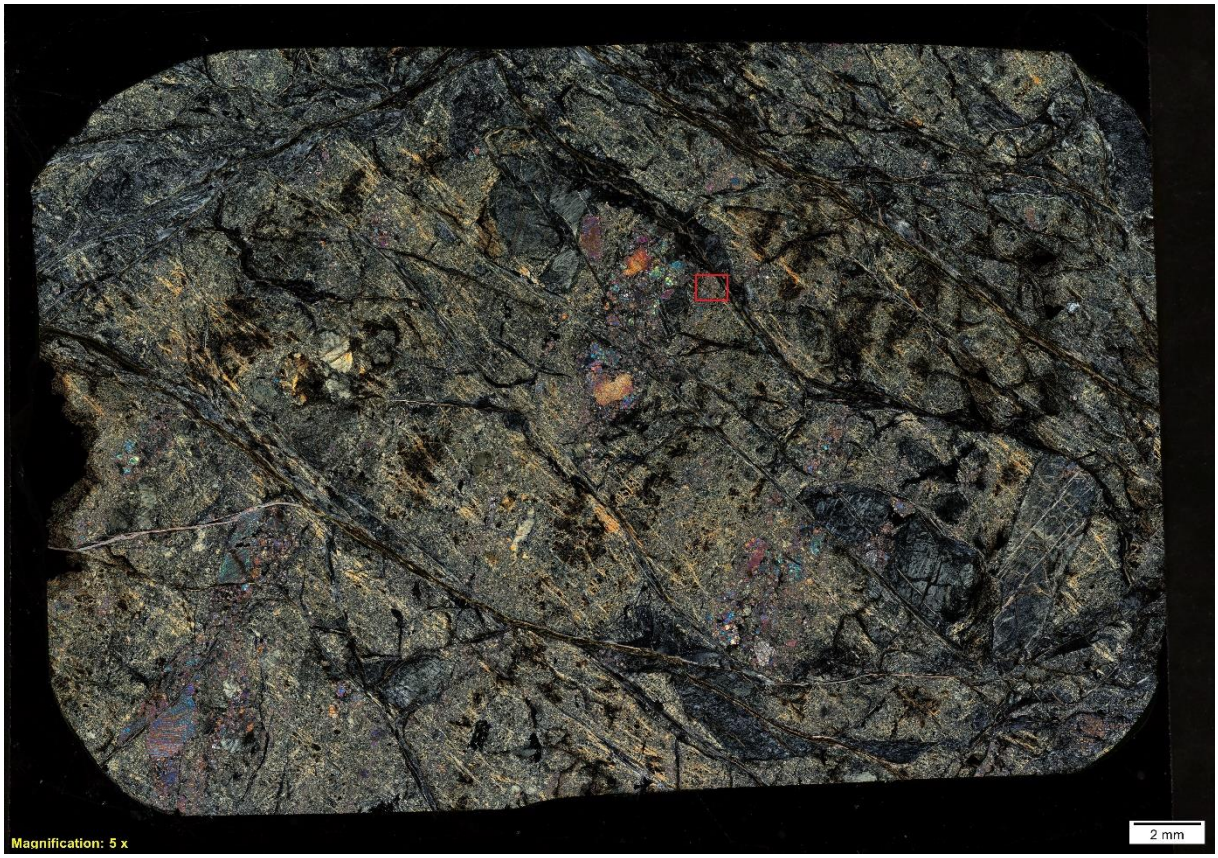

Figure 6-8: Thin section image of sample TS2 in XPL with AMS area (red).

Figure 6-9 displays a close-up XPL image of the scanned AMS area with the corresponding false-colored mineral map. Serpentine makes up the main mineral of the area (ca. 60%) along with clinopyroxene (cpx) (ca. 20%) and talc (ca. 15%). Both serpentine and talc are clay sized minerals and can be observed in the XPL image. The distribution of talc is not corresponding between the XPL image and the mineral map as the talc is observed in a thicker mesh structure (orange) in the XPL image and as small spots in the mineral map (purple). The clinopyroxene, mainly diopside, is varying in size from a few µm to approximately 80µm and is observed in both images. Approximately 0.01% smectite is detected in the sample area. The smectite (neon green) is located in larger clasts spread through the area, however, they are not observed in the XPL image. Chlorite, titanite and quartz minerals are also observed.

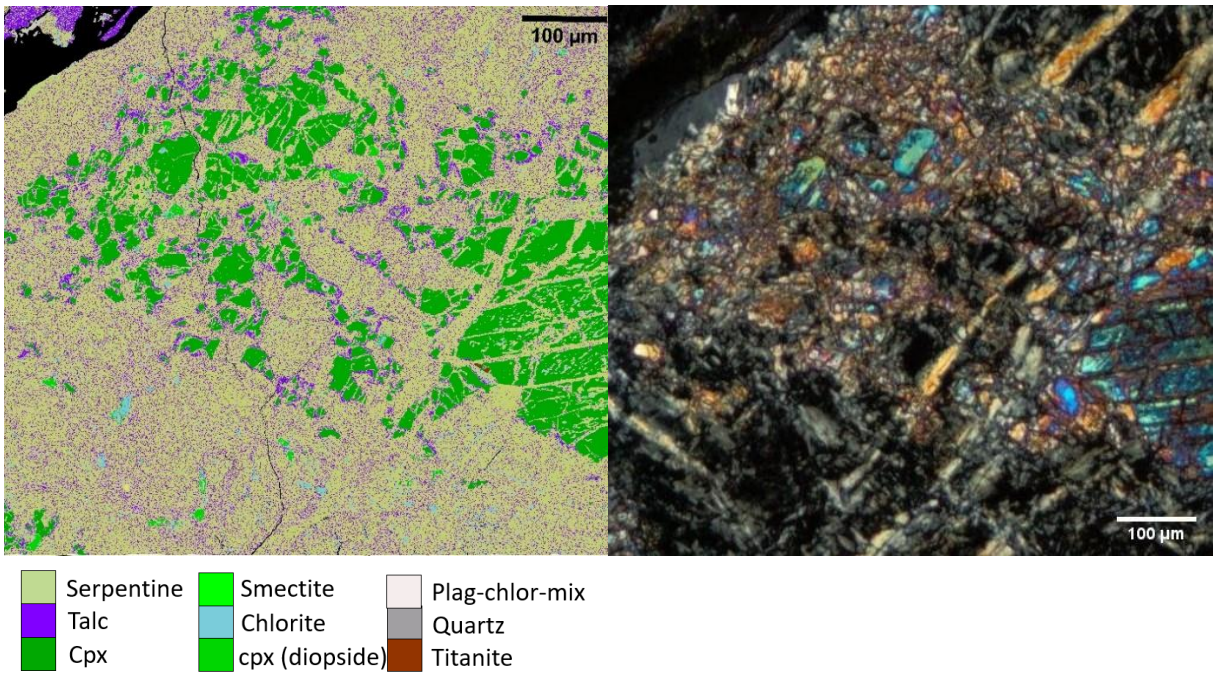

Figure 6-9: False-colored mineral map with corresponding XPL image of TS2.

6.5.3 Sample 3

The rock sample is split into two dominant lithologies, chlorite rich rock and carbonate rock, separated by a transition zone (Figure 6-10). There are some fractures and mineral filled veins in the rock mass. The main focus of sample 3 is in the leftmost area of the thin section (chlorite rich rock). This area is dominated by clay sized chlorite minerals. A large section of carbonate (calcite) is incorporated into the chlorite rich zone. Other observed minerals are serpentine, quartz, and probably some pyrite or pyrrhotite. The thin section sample is very fine-grained, thus making it hard to identify minerals. The rightmost part of the sample is a homogenous carbonate rock dominated by calcite minerals with a few other incorporated minerals.

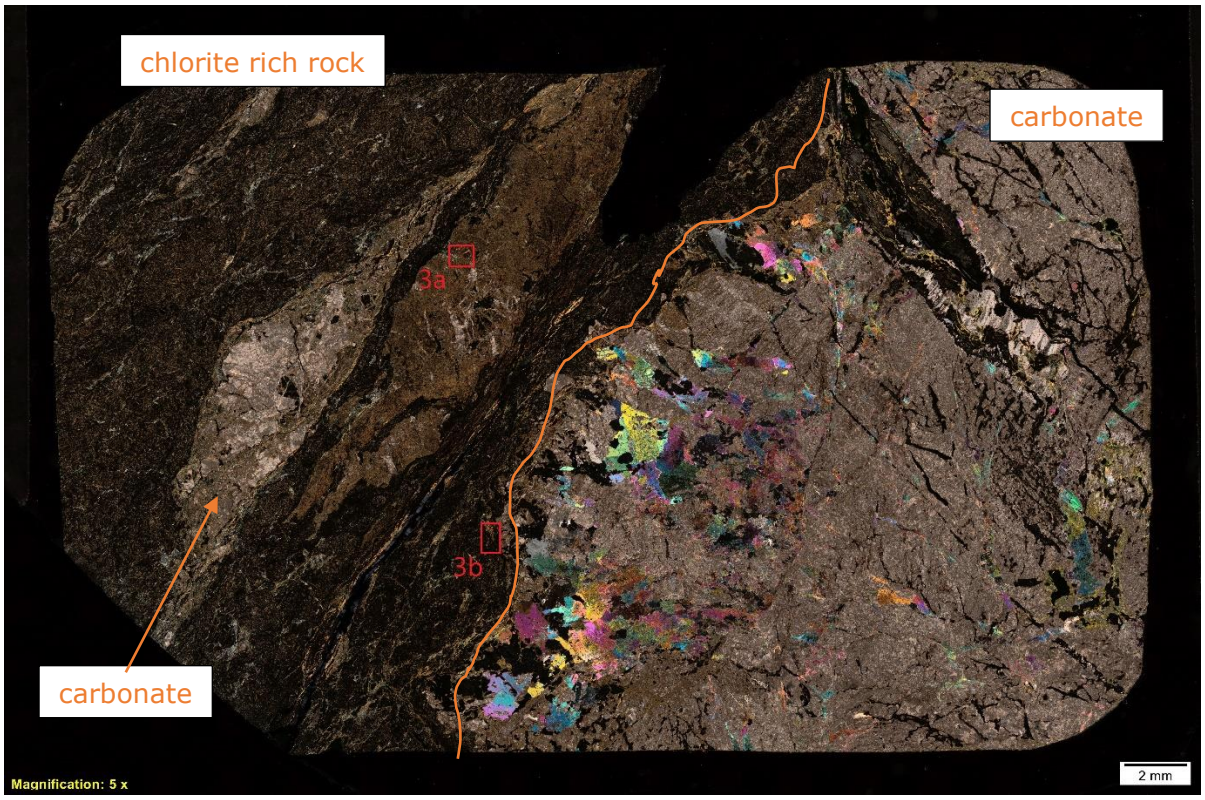

Figure 6-10: Thin section image of sample TS3 in XPL with AMS area of TS3_a and TS3_b (red).

The AMS analysis conducted on TS3 was done in two points to get a better representation of the mineral composition and incorporate the transition zone between the two lithologies. TS3_a is composed of ca. 79% chlorite minerals in a clay size fraction (Figure 6-11). Grains of calcite of varying size from a few µm to approximately 200µm (length) is present in the area. Other noticeable minerals are titanite, plagioclase, cpx, talc and smectite. The smectite minerals (1.58%) are located throughout the sample, however, it is concentrated around the plagioclase rich areas. The most prominent minerals in the XPL image are the calcite clasts and the fine-grained chlorite, all other minerals are hard to spot.

TS3_b is quite similar to TS3_a in mineral composition (Figure 6-12). Yet, the amount of chlorite mineral matrix has decreased to 52% while the amount of titanite, plagioclase and plagioclase-chlorite-mix have increased. Other observed minerals are feldspar and talc. Similar to TS3_a the smectite (4.69%) is present throughout the area with a concentration along the plagioclase chlorite transition areas. In the XPL image, the areas of a darker matrix (TS3_b) have a larger incorporation of plagioclase and plagioclase-chlorite-mix compared to the areas of the lighter matrix (TS3_a).

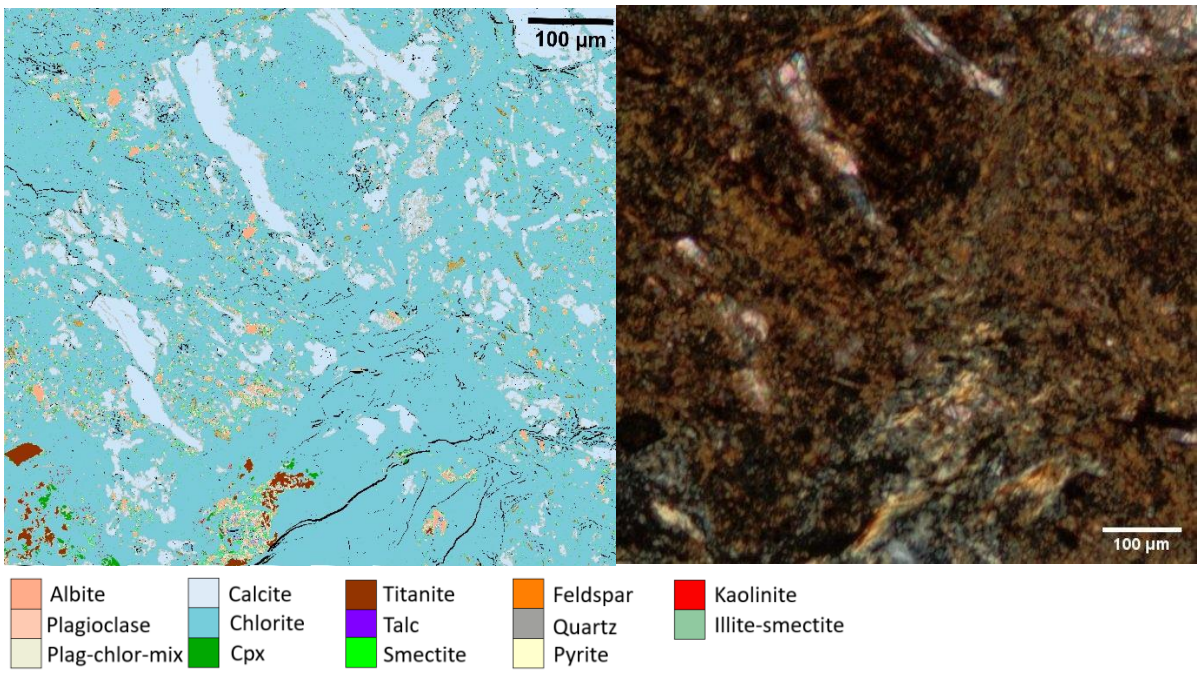

Figure 6-11: TS3_a with false-colored mineral map and corresponding XPL image.

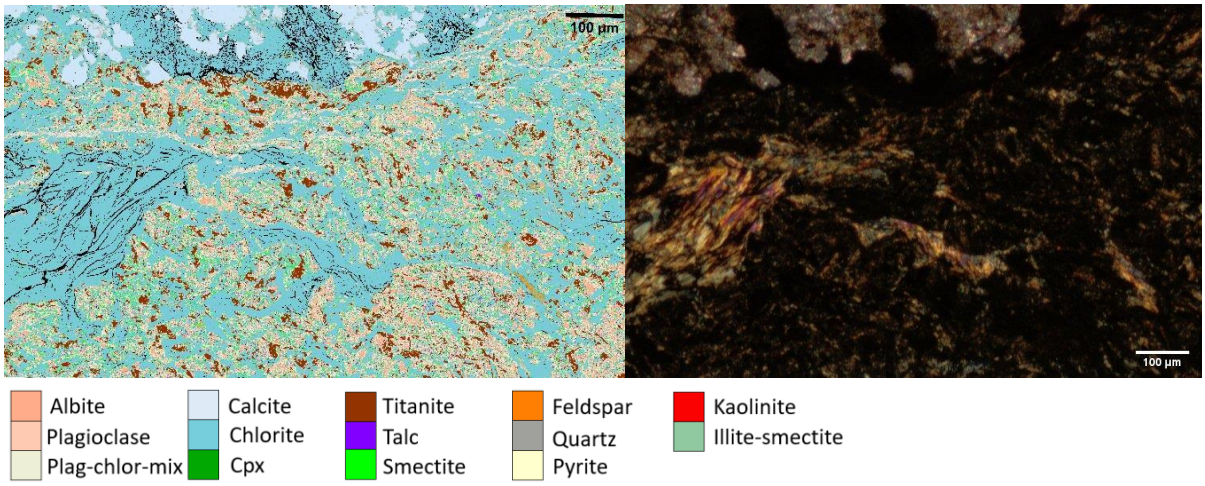

Figure 6-12: TS3_b with false-colored mineral map and corresponding XPL image.

6.5.4 Sample 4

Figure 6-13 is a thin section consisting of two lithologies where each of them have been analyzed as separate samples during this thesis. TS4 is located in the rightmost part of the thin section while TS5 is in the leftmost part.

As seen in Figure 6-13, TS4 is a fine-grained, laminated, sedimentary rock with carbonate porphyroclasts that are tectonically shifted. Most of the carbonate (calcite) clasts appear to be sigma-clasts made up of calcite. The size varies from µm scale to a few mm. The matrix is fine-grained, clay sized with both darker and lighter brown colored minerals. Because the matrix is extremely fine-grained the mineral composition is hard to distinguish only by optical light microscopy. The rock show some fracturing along the lamination.

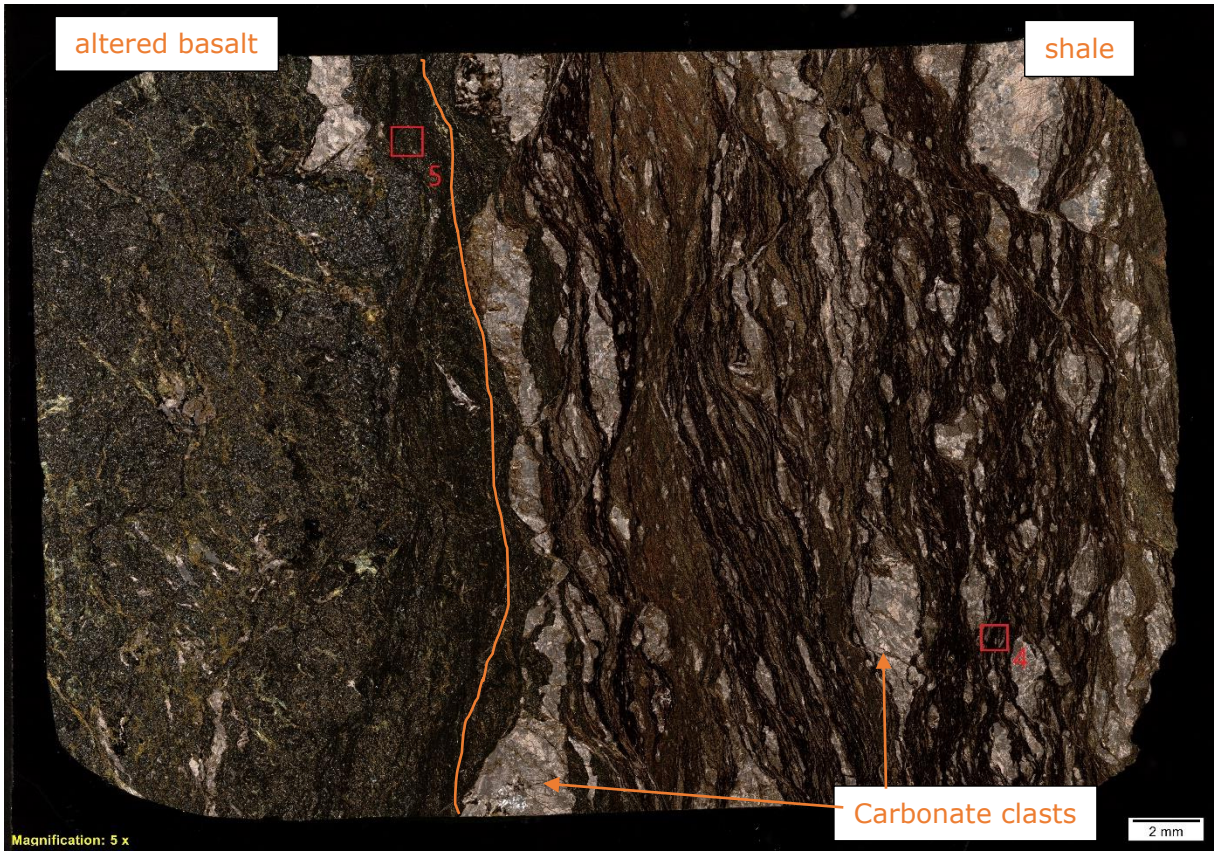

Figure 6-13: Samples TS4 and TS5 in the sample thin section with AMS area (red).

The AMS analysis of sample TS4 indicates the fine-grained matrix as mainly illite-smectite minerals (31,2%), as seen in Figure 6-14. There is also a larger presence of plagioclase, chlorite, plagioclase-chlorite-mix, pyrite and biotite in the matrix speared through the samples. Large calcite sigma-clasts up to 300µm are easily observed in both the XPL image and the mineral map. Because of the very dark, fine-grained matrix in the XPL image the minerals are impossible to interpret without AMS or other mineralogical tests. There is some smectite (neon green), approximately 2%, found in the sample area which is distributed throughout the samples as clay sized spots along with talc and zeolite.

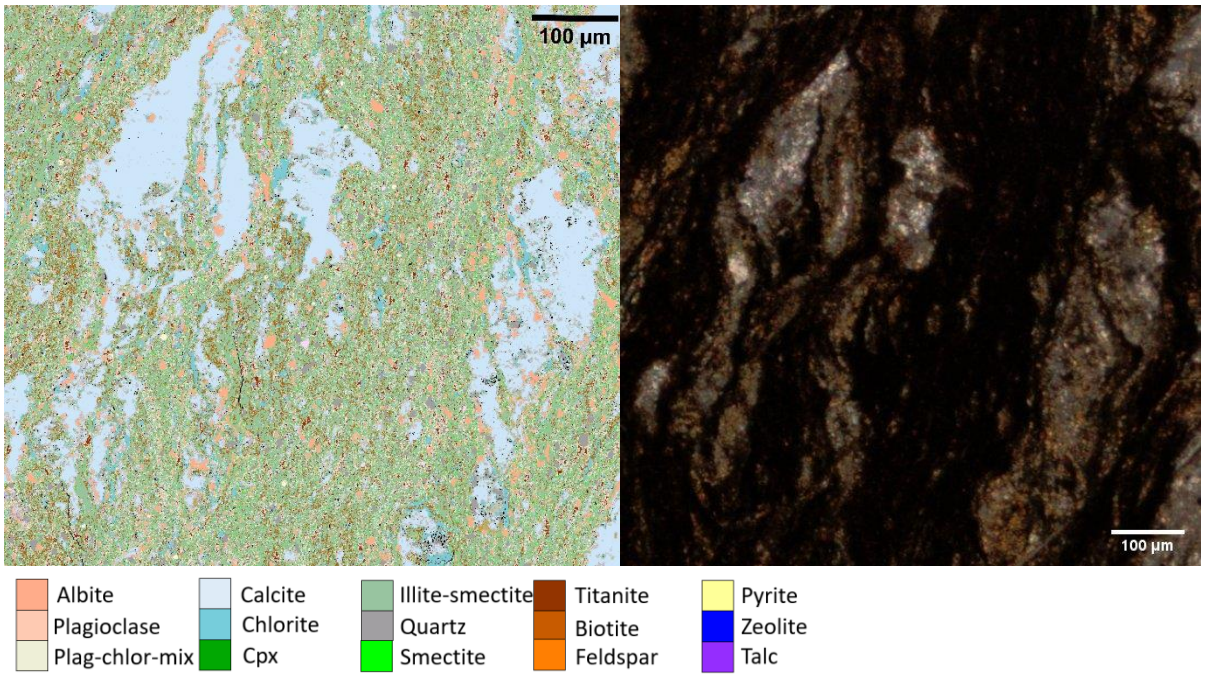

Figure 6-14: TS4 with false-colored mineral map and corresponding XPL image.

6.5.5 Sample 5

Sample TS5 is a fine-grained rock in a dark grey or black matrix (Figure 6-13). The structure is messy and there is no lamination. There are some carbonate (calcite) minerals incorporated in the rock. Observed plagioclase minerals appear to be the main mineral in the matrix, other minerals include chlorite, quartz, clinopyroxene, titanite. The rock sample shows no prominent fracturing.

Based on the AMS analysis, TS5 consists mainly of albite/plagioclase, plagioclase-chlorite-mix and chlorite (Figure 6-15) in a messy structure. Other minerals such as titanite and cpx (ca. 5-10µm) are observed in the sample. A few grains of quartz and calcite minerals are also detected. Ca. 2.67% of smectite is detected throughout the sample.

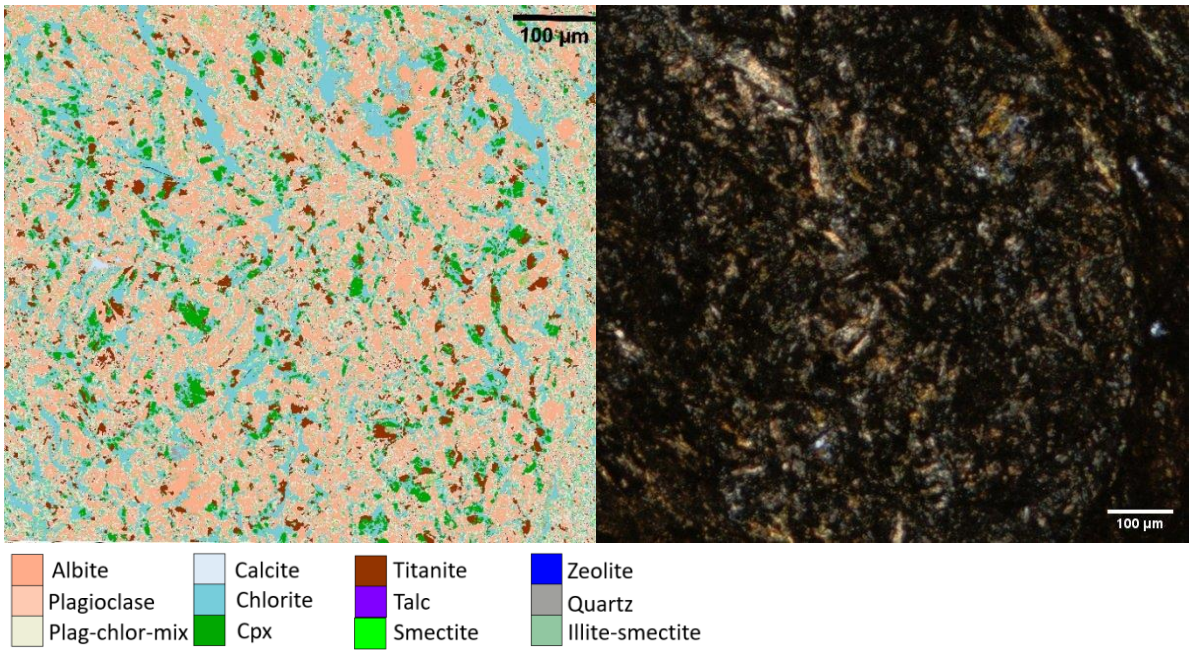

Figure 6-15: TS5 false-colored mineral map with corresponding XPL image.

6.5.6 Sample 6

TS6 is a homogenous, fine-grained rock with randomly oriented fracturing, as seen in Figure 6-16. The matrix is of clay-sized brown mineral. Clusters of small-scale quartz minerals (ca. 10-100 µm) are present all over the rock sample. The veins are mainly filled with a brown/orange mineral. Other observed minerals are calcite, pyrite/pyrrhotite and chlorite. The fine-grained character of the thin section makes it hard to distinguish the complete mineral composition from optical microscopy.

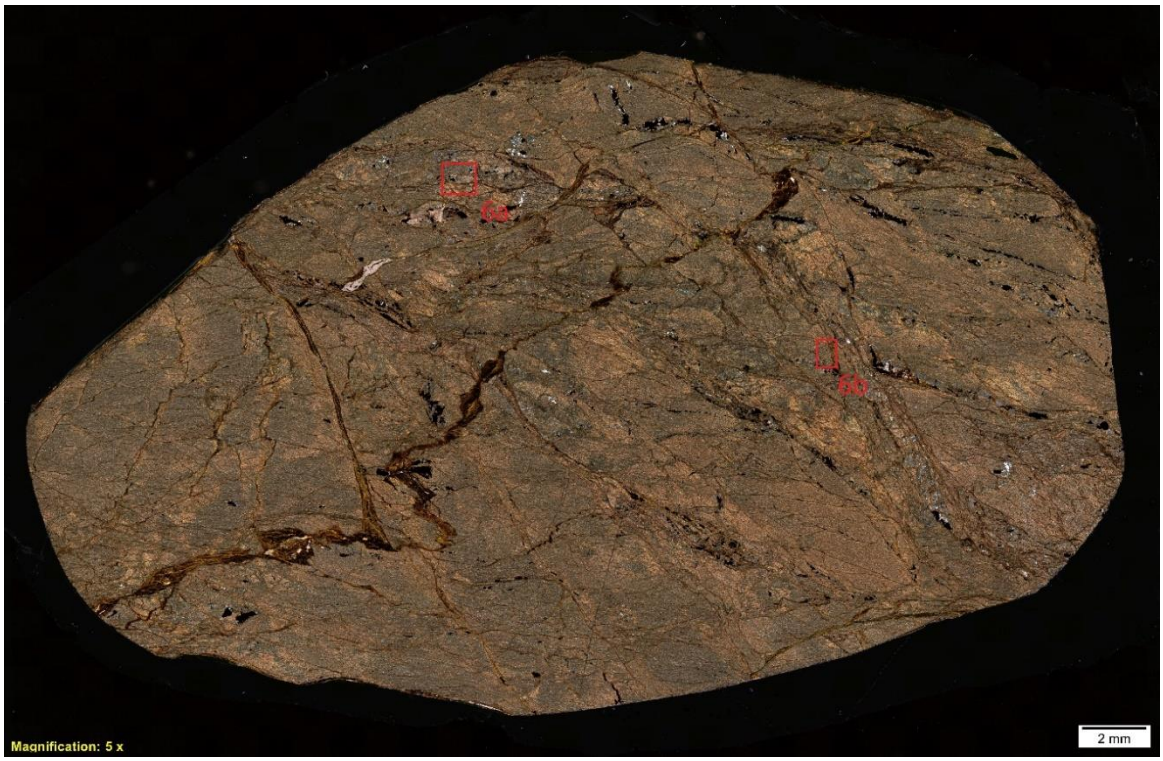

Figure 6-16: Thin section of sample TS6 with AMS area (red) of TS6_a and TS6_b.

The AMS analysis performed on the thin section is done in two separate areas. The two main minerals detected in TS6_a are quartz (ca. 41%) and illite-smectite (ca. 33.5%), as seen in Figure 6-17. There is also a large presence of plagioclase, chlorite and Feldspar. Titanite minerals are located mostly in fractures. 0.58% smectite is detected in TS6_a. Other observed minerals are pyrite, pyrrhotite, calcite, muscovite and biotite.

In Figure 6-18, the main mineral composition of TS6_b is illite-smectite (52%) with quartz (15%) also making up a large part of the area, along with plagioclase, chlorite and biotite. The smectite found in TS6b is 0.91%. In both areas titanite minerals (red) are concentrated in the fractures. Further, the chlorite (blue) is concentrated along the quartz (grey) areas.

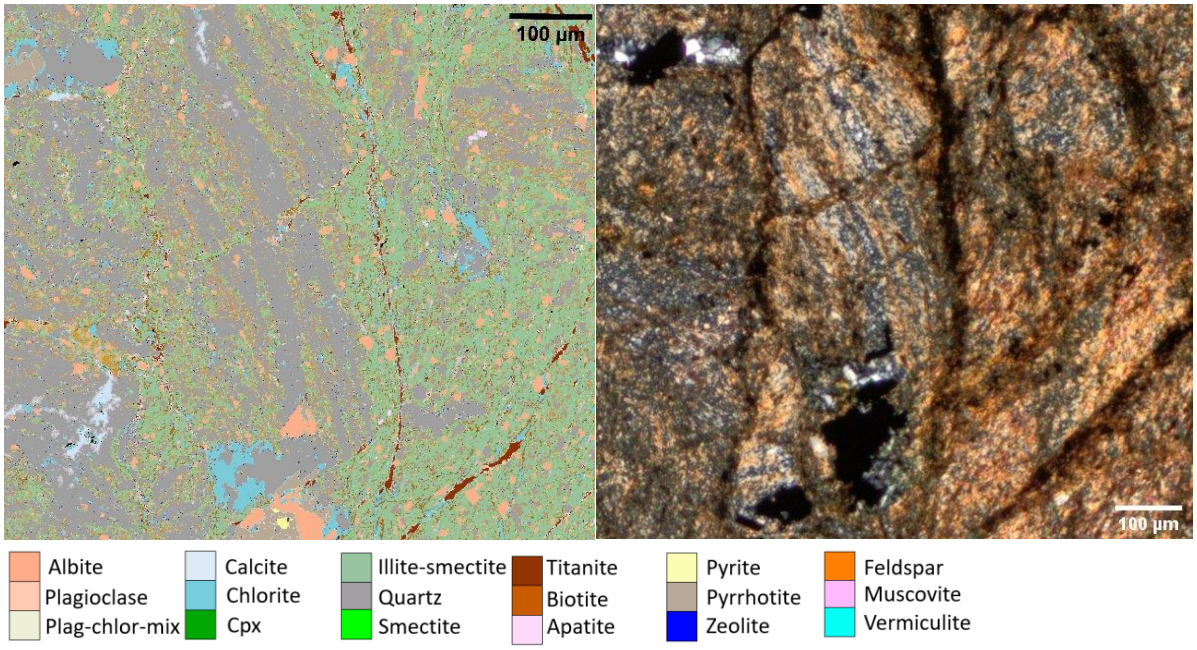

Figure 6-17: Sample TS6_a with false-colored mineral map and corresponding XPL image.

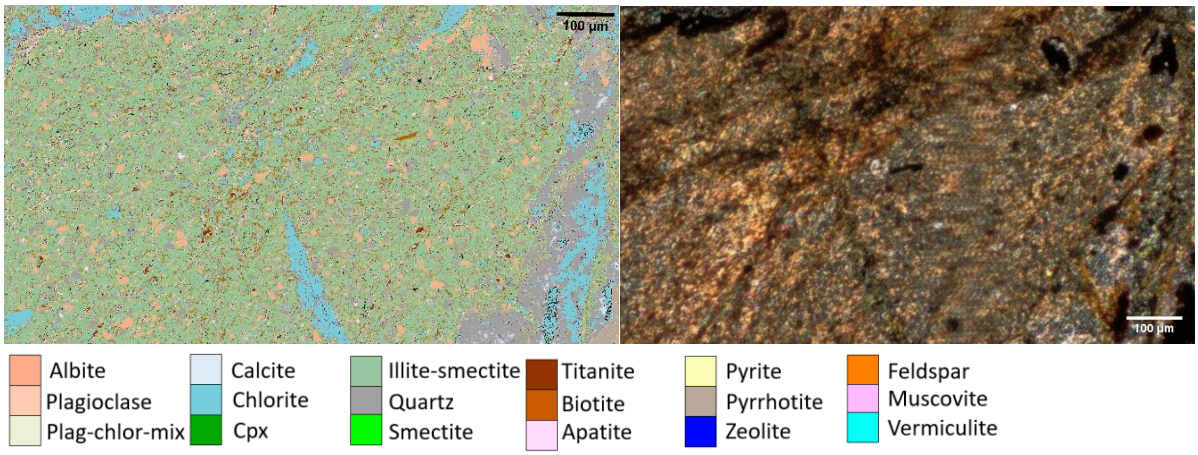

Figure 6-18: Sample TS6_b with false-colored mineral map and corresponding XPL image.

6.5.7 Sample 7

TS7 is an altered basalt rock with incorporated carbonate clasts. As seen in Figure 6-19, the rock is heterogeneous consisting of a carbonate rich part and a magmatic, fine-grained rock. The carbonate rich part is composed of mainly calcite, datolite and quartz. The mineral grains vary in size from µm to a few mm. The magmatic part consists of fine grained (µm scale), dark matrix with some calcite veins and clasts. Observed minerals are plagioclase, chlorite and pyroxene. The remaining minerals are hard to classify. The rock is somewhat fractured.

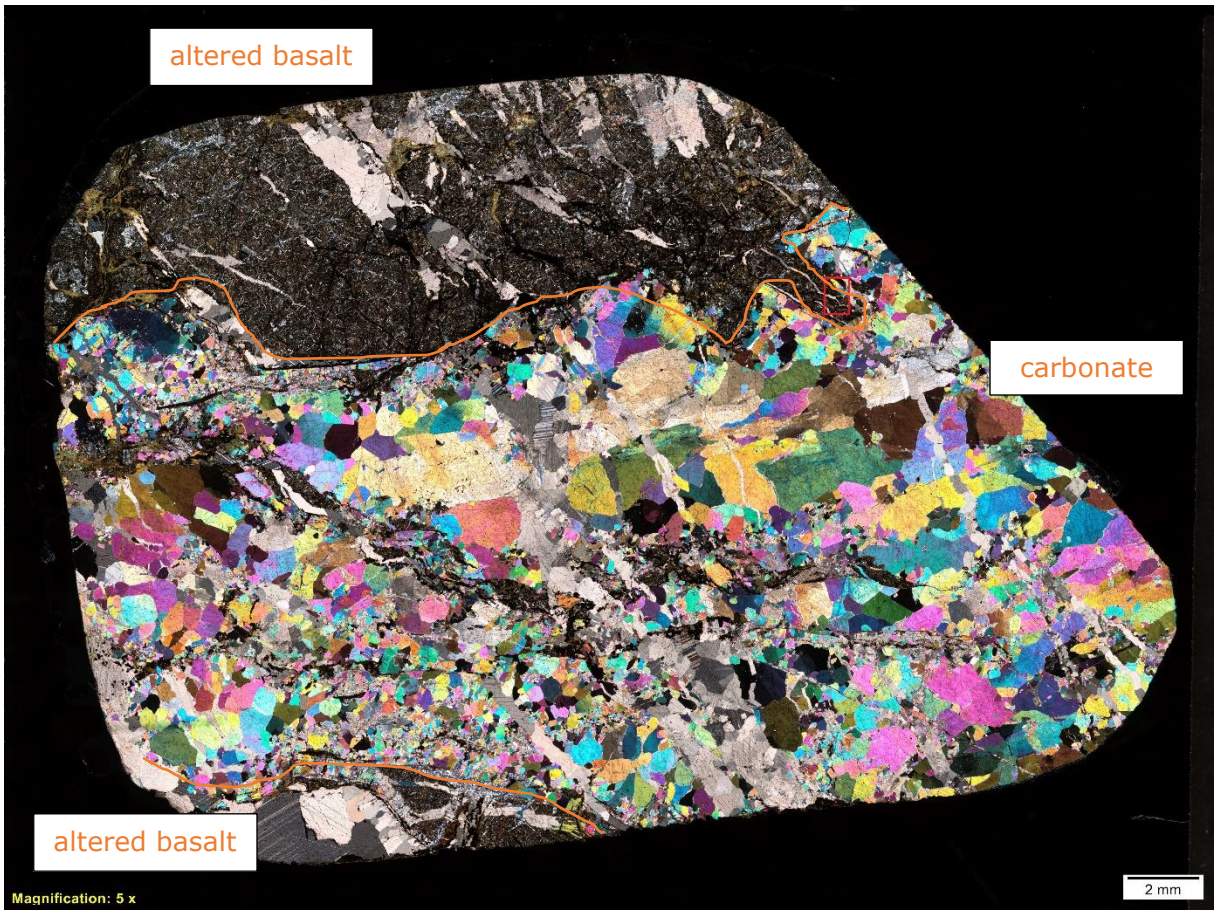

Figure 6-19: Thin section of sample TS7 in XPL with AMS area (red).

The large lithological difference in the sample makes it harder to get a good representation of the entire rock mass through AMS. The close-up area of TS7 has attempted to incorporate both lithologies of the rock mass, with the main focus on the magmatic rock type (Figure 6-20). There are three main minerals in the sample area, chlorite (ca. 22.8%), plagioclase (ca. 22%) and datolite (ca. 21.5%), respectively. The chlorite is fine-grained and scattered throughout the sample matrix. The plagioclase, along with cpx, have larger grains (10-100µm). The datolite is shown as one or more large scale minerals going through the altered basalt matrix along with some veins of calcite and is observed in both the XPL and mineral map. Other minerals observed are titanite and quartz along with clay sized zeolite, talc and smectite (ca. 0.81%).

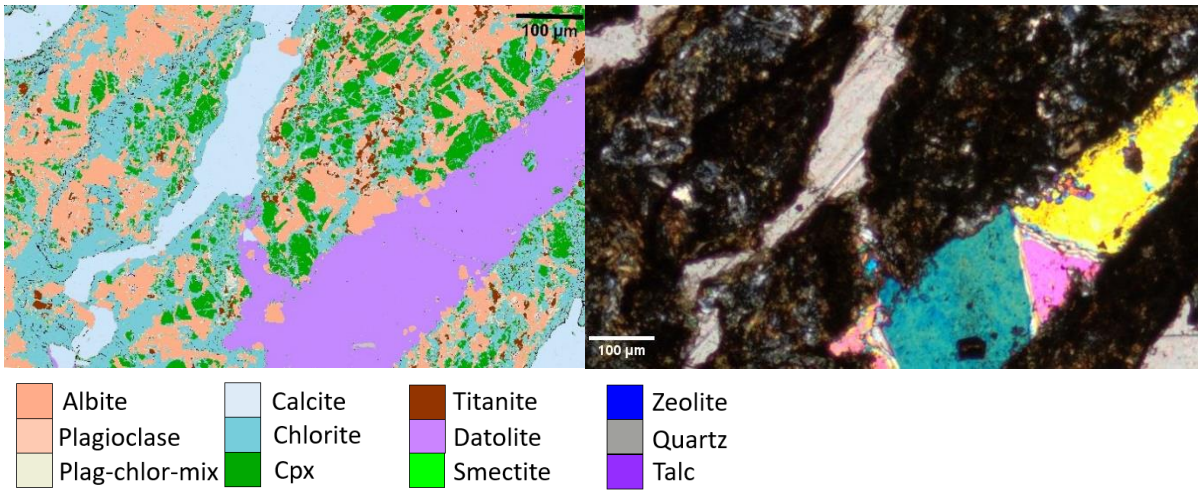

Figure 6-20: False-colored mineral map with corresponding XPL image of TS7.

6.5.8 Sample 8

TS8 is an heterogenous, altered basalt rock type with dark, fine-grained matrix in a messy structure (Figure 6-21). Several yellow/light green elongated minerals are present throughout the sample. The sample consists of plagioclase, pyroxene, chlorite, serpentine, pyrite/pyrrhotite and quartz minerals. A carbonate rich lithology is incorporated into the altered basalt rich in calcite, quartz and possibly mica and chlorite. The rock sample is somewhat fractured with one prominent fracture plane/vein going through the sample (Appendix G, Figure 28). The more fine-grained minerals are not able to be interpreted by optical light microscopy.

Figure 6-21: Thin section image of sample TS8 in XPL with AMS area (red).

The structure of TS8 is very messy with a fine-grained chlorite matrix and several large grain minerals like albite/plagioclase, cpx, quartz, pyrrhotite and titanite scattered throughout (Figure 6-22). The AMS analysis detected chlorite (ca. 34.7%), plagioclase (ca. 25.9%) and cpx (ca. 15.8%) as the main minerals of the rock sample. Clay sized zeolite and smectite (ca. 1.48%) is seen in clusters around the sample. The smectite minerals appear to be concentrated around the plagioclase-chlorite-mix.

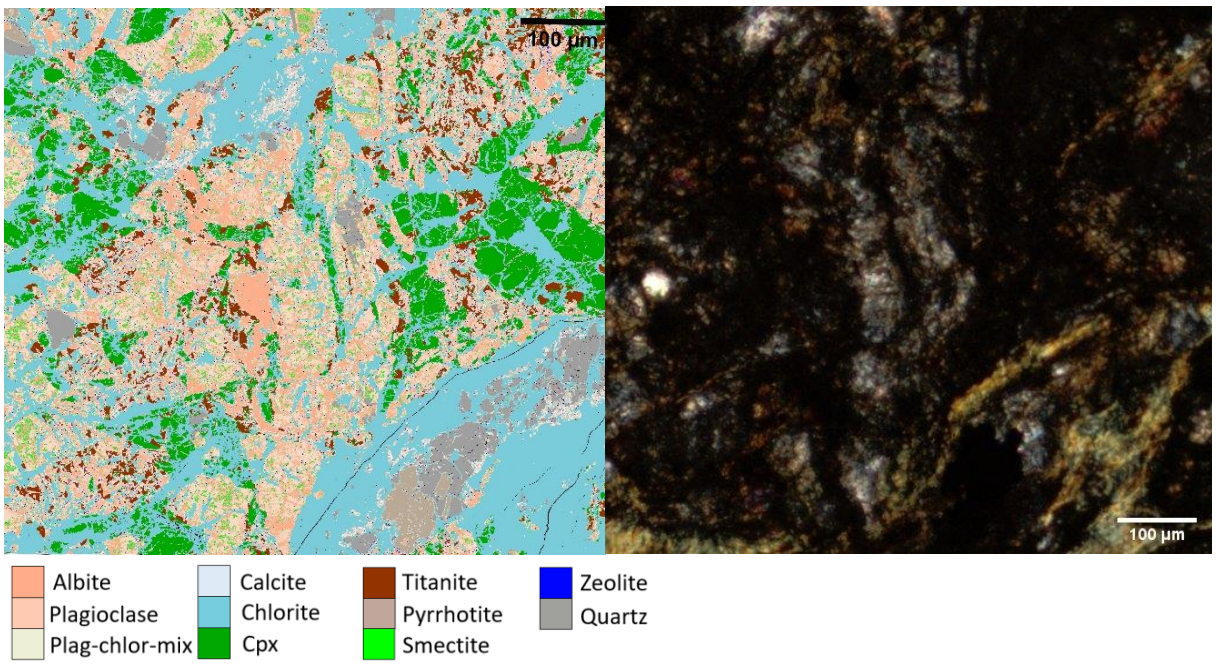

Figure 6-22: False-colored mineral map with corresponding XPL area of TS8.

6.5.9 Sample 9

TS9 is a heterogonous rock mixed from various rock types found in the rock cores, more specifically a shale-marble-mix. As can be seen in Figure 6-23, the thin section consists of carbonate clasts mixed into a fine-grained, dark brown matrix. There appears to be some layering and orientation in the rock. There is a somewhat alteration between the marble-rich and shale-rich lithologies. There is some fracturing in the rock sample. The mineral composition in the rock consists of calcite, quartz, chlorite, pyrite/pyrrhotite. The remaining minerals are not able to detect.

Figure 6-23: Thin section image of sample TS9 in XPL with AMS area (red).

The main minerals detected in TS9 are plagioclase (ca. 21.8%), chlorite (ca. 22.9%) and illite-smectite (ca. 20.5%), as seen in Figure 6-24. There is a concentration of pyrite in the illite-smectite rich area of the sample. Approximately 1.48% smectite is detected and scattered around the sample along with zeolite, both have clay size minerals. Other minerals observed are calcite, titanite, quartz and pyrrhotite.

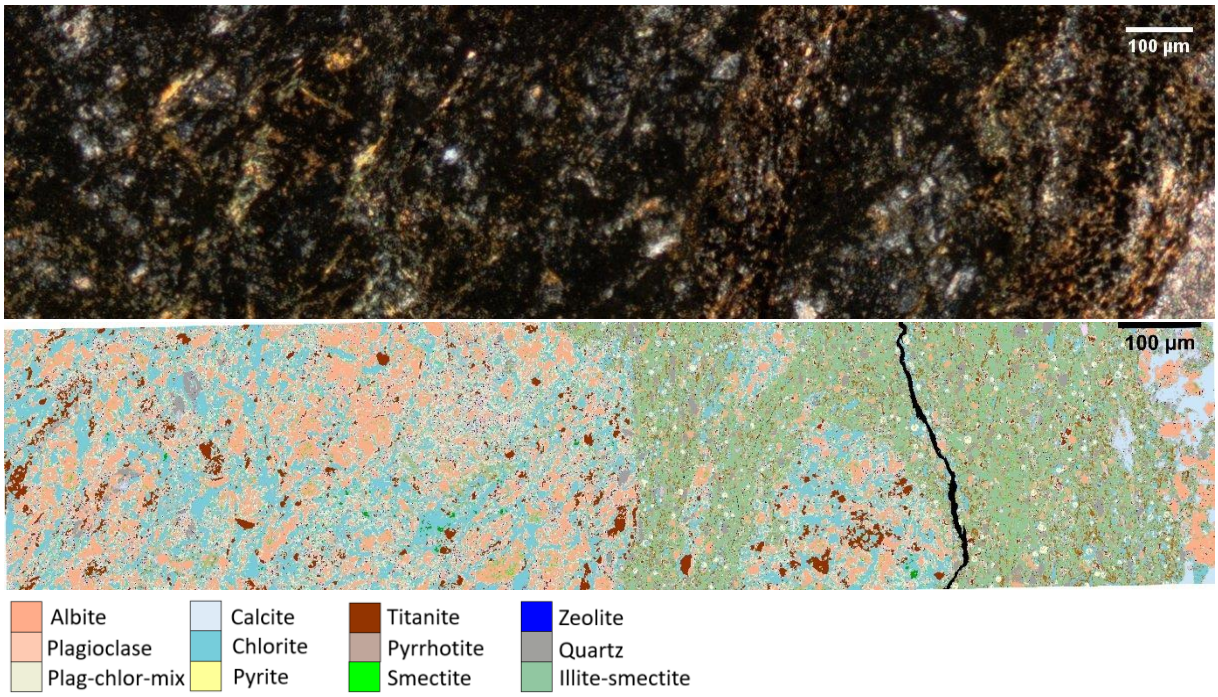

Figure 6-24: False-colored mineral map with corresponding XPL area of TS9.

6.6 Results from SEM-based automated mineralogy and optical microscopy on the powder samples

The AMS results from the powder samples are shown in Table 6-10 and Table 6-11. The original data is displayed in Appendix J. Unfortunately, because of time pressure and a long queue at the AMS apparatus the three samples MOD3, MOD6 and MOD7 were not analyzed.

Both samples 1 and 2 had a high presence of chlorite, serpentine and talc. The main mineral in sample 3 is chlorite, with a high presence of plagioclase and plagioclase-chlorite-mix. Illite-smectite was the main mineral in samples 4 and 6. MOD4 had a higher detection of calcite (18.38%) compared to STD4 (11.45%). Sample 6 had a high detection of quartz as well. Plagioclase and chlorite were the main minerals found in sample 5 in both modified and standard samples. Sample 7 detected plagioclase (27.98%) as the main mineral. Swelling clay (smectite) was detected in all tested samples with a range from 0.76% in STD7 to 4.04% in STD4. In three of the four samples where both standard and modified samples were tested, there was an increase in the smectite amount. Sample 4 shows the opposite. A low amount of zeolite minerals is uncovered in all samples, except sample 2, which could give an impact on the swelling properties of the rock.

Table 6-10: AMS results from standard powder samples in Wt%.

	Standard (STD) [Wt%]						
Mineral	1	2	3	4	5	6	7
Quartz	11.40	0.00	0.37	12.68	2.01	24.53	9.84
Plagioclase	3.77	0.01	13.54	13.01	28.52	9.59	27.98
Plag-chlor-mix	2.83	-	12.17	6.42	8.24	2.54	3.09
Chlorite	19.84	12.21	33.70	9.14	24.88	3.58	4.37
K Feldspar	0.05	-	0.12	0.98	0.26	3.01	0.61
Amph (Actinolite)	0.04	0.07	0.94	0.09	0.53	0.02	0.23
Epidote	0.01	0.01	0.33	0.63	2.62	0.25	3.82
Cpx	0.67	3.08	9.00	0.51	7.41	0.05	2.20
Calc-sil-mix	0.43	0.11	6.05	6.70	6.23	1.43	11.83
Calcite	5.38	0.41	5.55	11.45	1.94	0.78	11.33
Datolite	0.21	0.00	0.52	1.46	4.73	0.30	13.09
Biotite	1.93	0.00	0.17	8.28	0.18	9.82	1.14
Talc	17.60	19.24	5.93	1.64	1.58	0.28	0.26
Serpentine	27.70	58.43	0.13	0.00	0.01	0.00	0.00
Illite-smectite	0.54	0.00	0.57	21.16	1.15	39.28	4.99
Smectite	1.75	0.82	4.04	2.17	2.41	1.31	0.76
Zeolite	0.00	-	0.00	0.03	0.05	0.01	0.07
Prehnite	0.00	0.00	0.08	1.18	0.27	0.12	3.07
Titanite	1.36	0.01	6.61	1.63	6.74	0.93	0.88
Pyrite	0.27	0.00	0.01	0.19	0.03	0.21	0.06
Pyrrhotite	0.06	-	0.00	0.02	0.00	1.25	0.01
Apatite	0.05	-	0.01	0.14	0.02	0.14	0.08
Fe-Oxide (altered)	0.01	0.01	0.01	0.04	0.03	0.06	0.02
Opx	3.57	5.21	0.04	0.02	0.04	0.01	0.00
Muscovite	0.01	-	0.04	0.27	0.07	0.41	0.14
Vermiculite	0.00	0.00	0.02	0.07	0.02	0.01	0.07
Kaolinite	0.01	0.01	0.01	0.04	0.01	0.02	0.02
Other	0.48	0.35	0.03	0.03	0.02	0.04	0.03

Table 6-11: AMS results for modified powder samples in Wt%. Sample MOD3, MOD6 and MOD7 are not analyzed.

	Modified (MOD) [Wt%]						
Mineral	1	2	3*	4	5	6*	7*
Quartz	10.98	0.00	-	10.03	1.93	-	-
Plagioclase	3.42	0.01	-	8.93	22.50	-	-
Plag-chlor-mix	2.95	0.01	-	5.35	6.10	-	-
Chlorite	25.11	12.05	-	12.67	32.19	-	-
K Feldspar	0.05	-	-	0.88	0.29	-	-
Amph (Actinolite)	0.05	0.08	-	0.10	0.53	-	-
Epidote	0.00	0.00	-	0.30	3.39	-	-
Cpx	0.83	2.84	-	0.46	7.78	-	-
Calc-sil-mix	0.45	0.07	-	1.84	4.58	-	-
Calcite	2.90	0.38	-	18.38	4.47	-	-
Datolite	0.29	0.00	-	1.09	6.04	-	-
Biotite	2.28	0.00	-	8.81	0.11	-	-
Talc	20.02	18.27	-	0.74	0.60	-	-
Serpentine	23.61	59.32	-	0.03	0.04	-	-
Illite-smectite	0.59	0.00	-	26.31	0.82	-	-
Smectite	2.05	1.04	-	1.48	1.46	-	-
Zeolite	0.00	-	-	0.01	0.03	-	-
Prehnite	0.00	0.00	-	0.13	0.26	-	-
Titanite	1.10	0.01	-	1.52	6.57	-	-
Pyrite	0.08	-	-	0.21	0.06	-	-
Pyrrhotite	0.01	0.00	-	0.03	0.02	-	-
Apatite	0.05	-	-	0.13	0.02	-	-
Fe-Oxide (altered)	0.00	0.01		0.08	0.04	-	-
Opx	2.95	5.49	-	0.06	0.07	-	-
Muscovite	0.01	-	-	0.29	0.04	-	-
Vermiculite	0.00	0.00	-	0.03	0.01	-	-
Kaolinite	0.01	0.01	-	0.04	0.01	-	-
Other	0.21	0.40	-	0.03	0.02	-	-

*None tested samples

Figure 6-25 and Figure 6-26 display the BSE image (backscattered electron micrograph) and false-colored mineral maps of STD5 and MOD5. The images show a close-up of the samples, the original images are displayed in Appendix I along with the images of all other powder samples.

The figures showcase the textural differences between the samples. The STD5 material in Figure 6-25a shows a variety of grain sizes from agglomerated, fine-grained material (dust cloud) up to 250 µm. The grains are mostly subrounded with some incorporation of angular grains. The MOD5 sample material in Figure 6-25b,c and d are angular with a low amount of crushed matrix material. The two former have a larger grain size from approximately 50µm up to 300 µm, while the latter have a grain size of <100 µm. Several of the grains display a mixed mineral composition. This is better showcased in Figure 6-26 as both STD5 and MOD5 detected chlorite, plagioclase/albite, plagioclase-chlorite-mix, calcite, datolite, titanite and cpx. There is also a presence of quartz and feldspar mainly observed in Figure 6-26c. Smectite clay minerals can be observed in several of the grains.

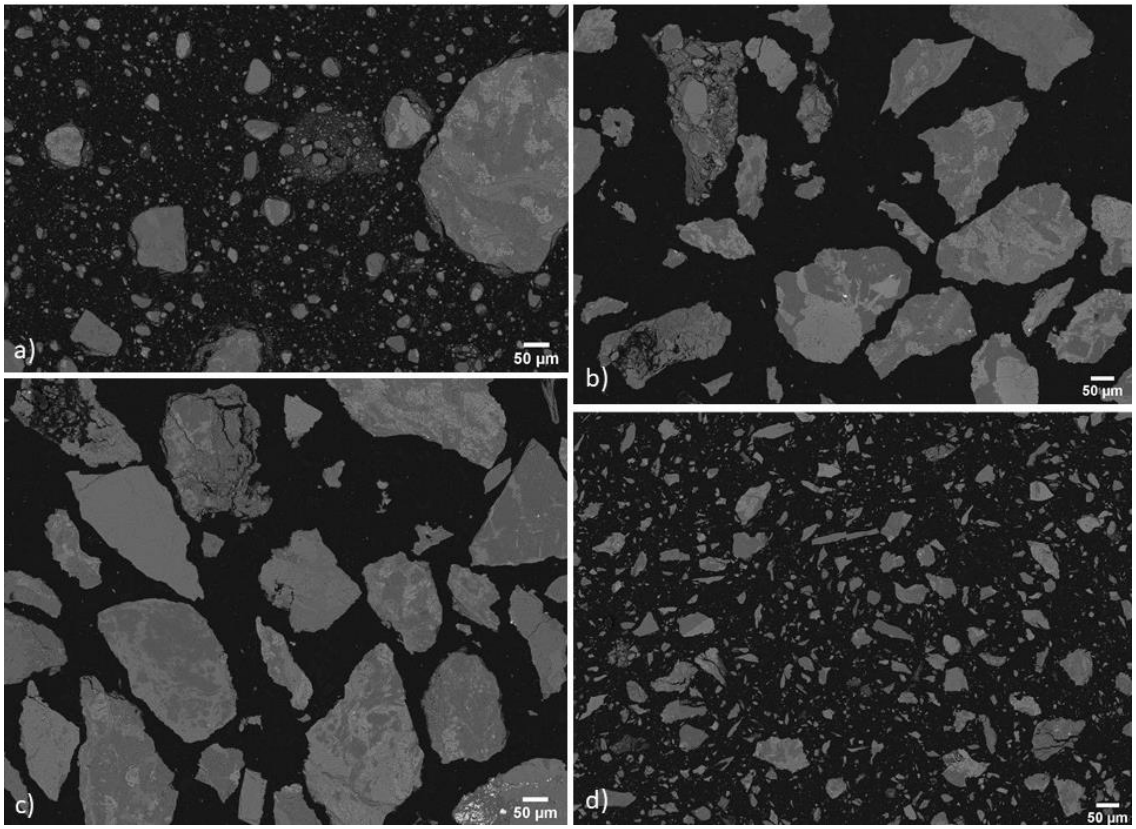

Figure 6-25: BSE image of a) STD5. b) & c) MODA5 (100-300µm) d) MODB5 (<100µm).

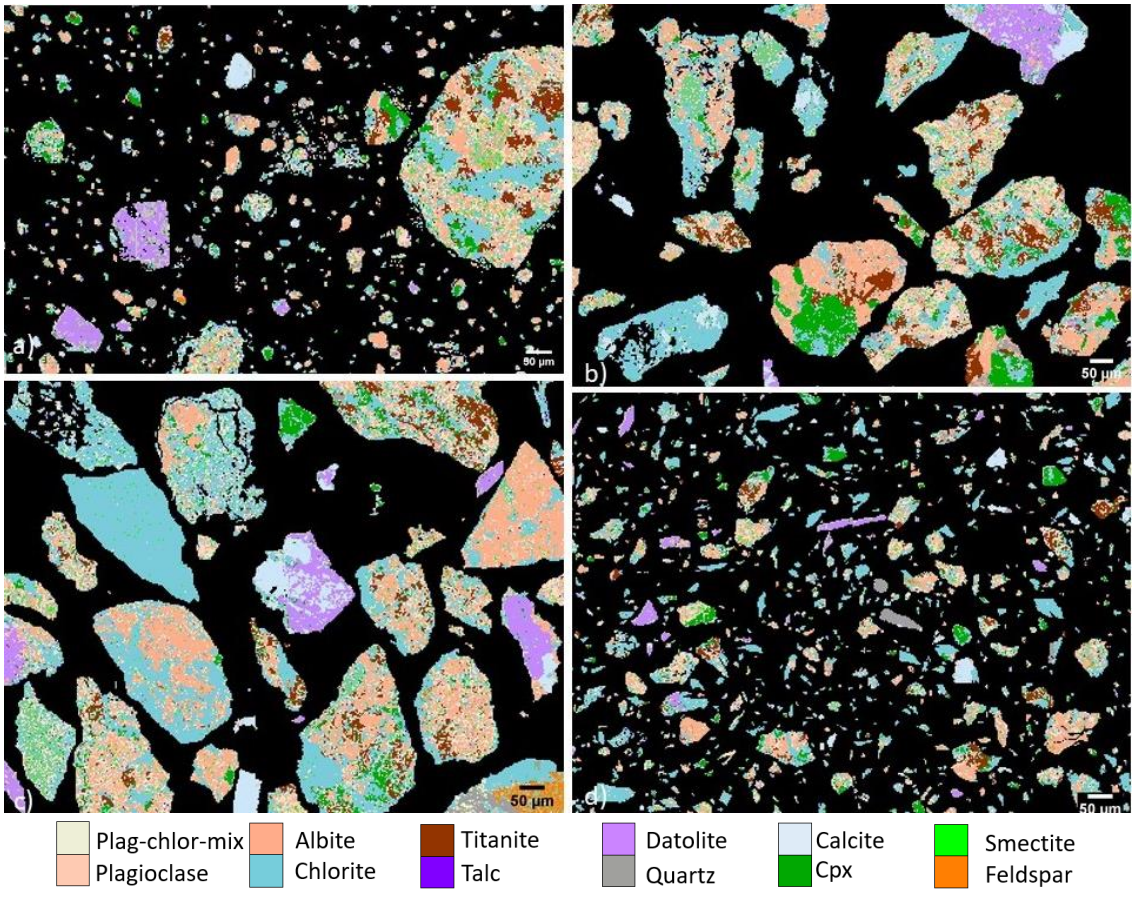

Figure 6-26: Mineral map of sample a) STD5. b) & c) MODA5 (100-300µm) d) MODB5 (<100µm).

In Figure 6-27 the BSE image and mineral map of STD4 and MOD1 are shown. As described above the standard samples often contain a dust cloud of the mixed matrix material. A closer inspection of the figure shows a difference in the mineral cluster between the BSE image and mineral map in STD4. In several areas of the figure (red circles), it appears that the AMS is unable to interpret all minerals. Note that there are more such areas than what is marked by the red circles. A similar occurrence can be observed in MOD1 as well. In this case, a more-or-less intact calcite mineral partly disappears in the false-colored mineral map. Likewise, this can be observed in samples 4 and 7 in Appendix K.

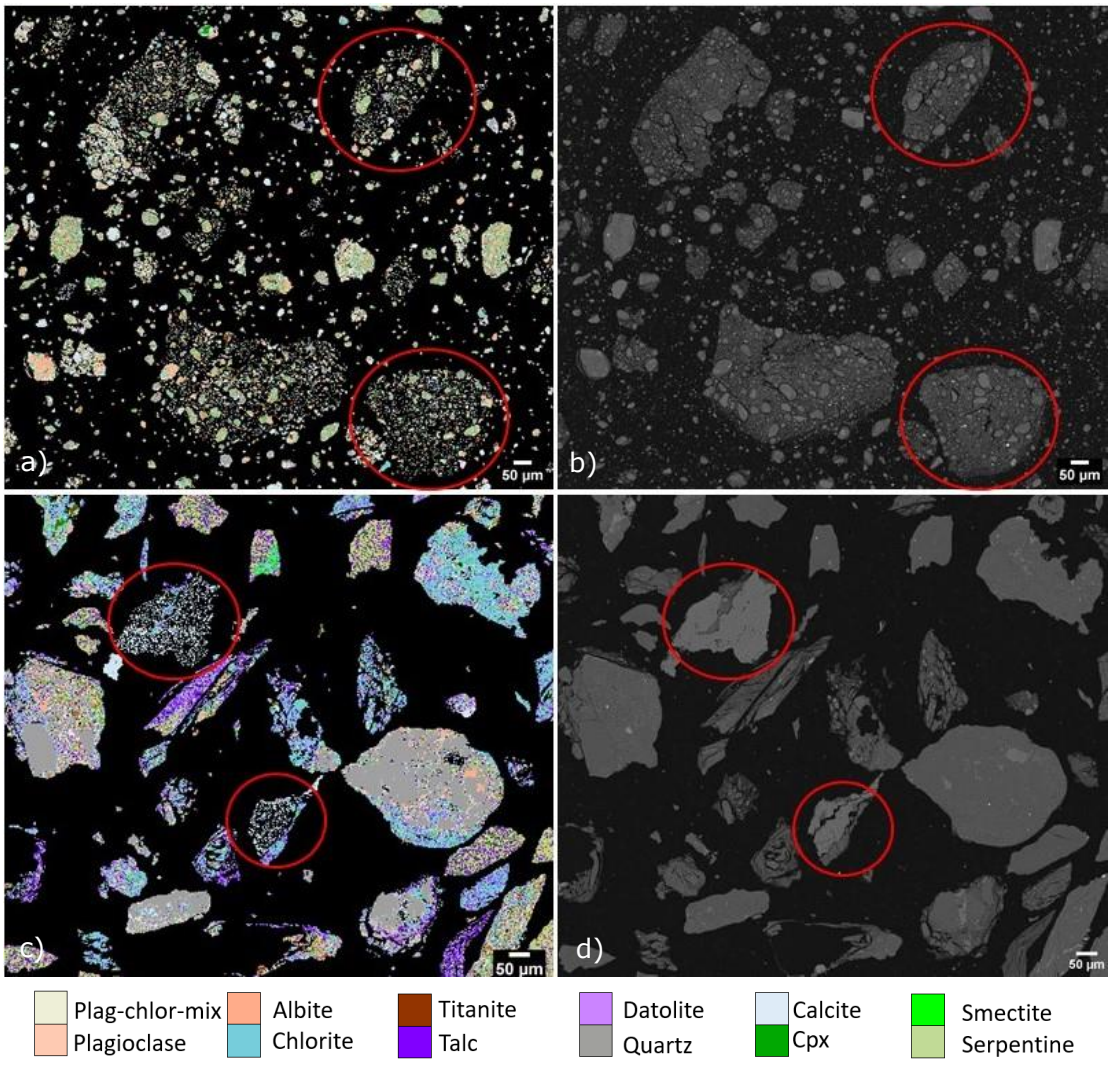

Figure 6-27: a) STD4 mineral map. b) STD4 BSE image. c) MODA1 mineral map. d) MODA1 BSE image. Red circles showcase the differences between the BSE image and the mineral map.

Figure 6-28 to Figure 6-31 display comparison charts between the standard and modified mineralogical results obtained from AMS in samples 1, 2, 4 and 5. Both samples 1 and 2 have a fairly good correlation. Soft minerals such as chlorite, serpentine and talc show a poor correlation in sample 1, in addition to calcite (hard mineral). A few other minerals have some small differences as well, for example, smectite. In sample 2 only talc and cpx have a noticeable difference. One could argue that smectite, opx and chlorite have some differences as well. A poor correlation is revealed in samples 4 and 5 with a variation of both soft and hard minerals. Most of the minerals indicate a higher mineral detection in the standard samples, however, the opposite is also observed in some minerals.

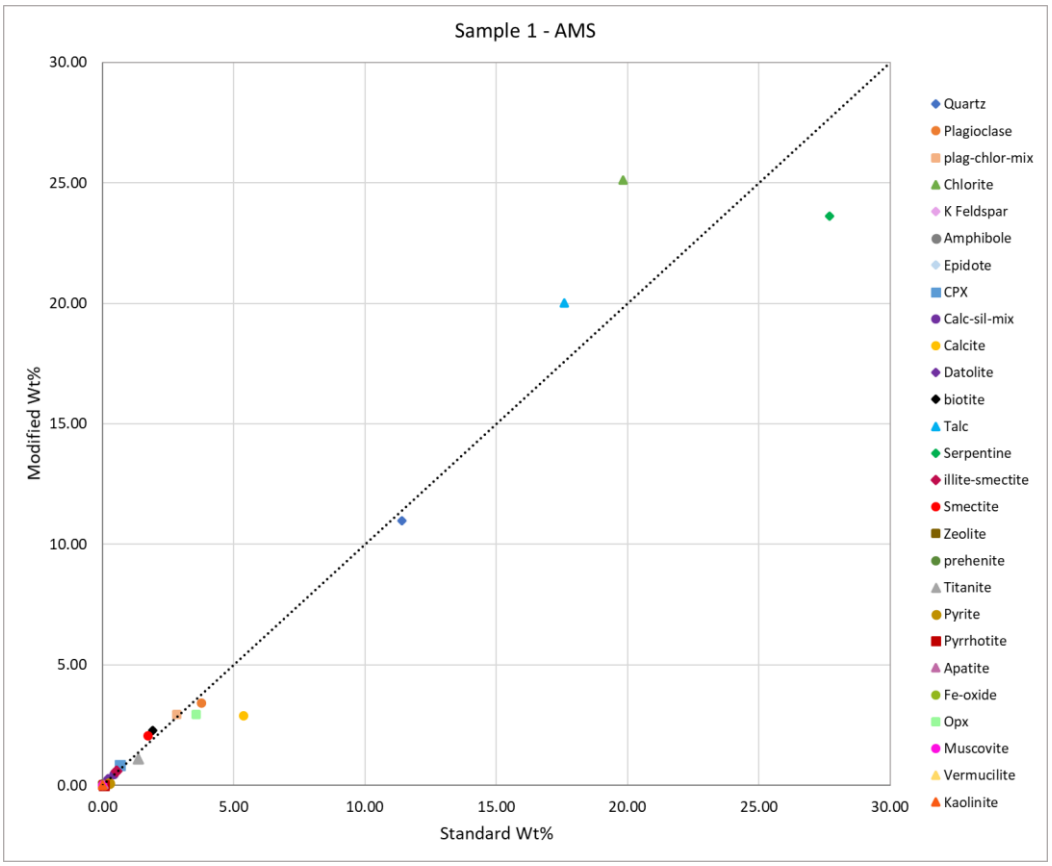

Figure 6-28: Comparison chart of modified (y-axis) and standard (x-axis) AMS results in sample 1.

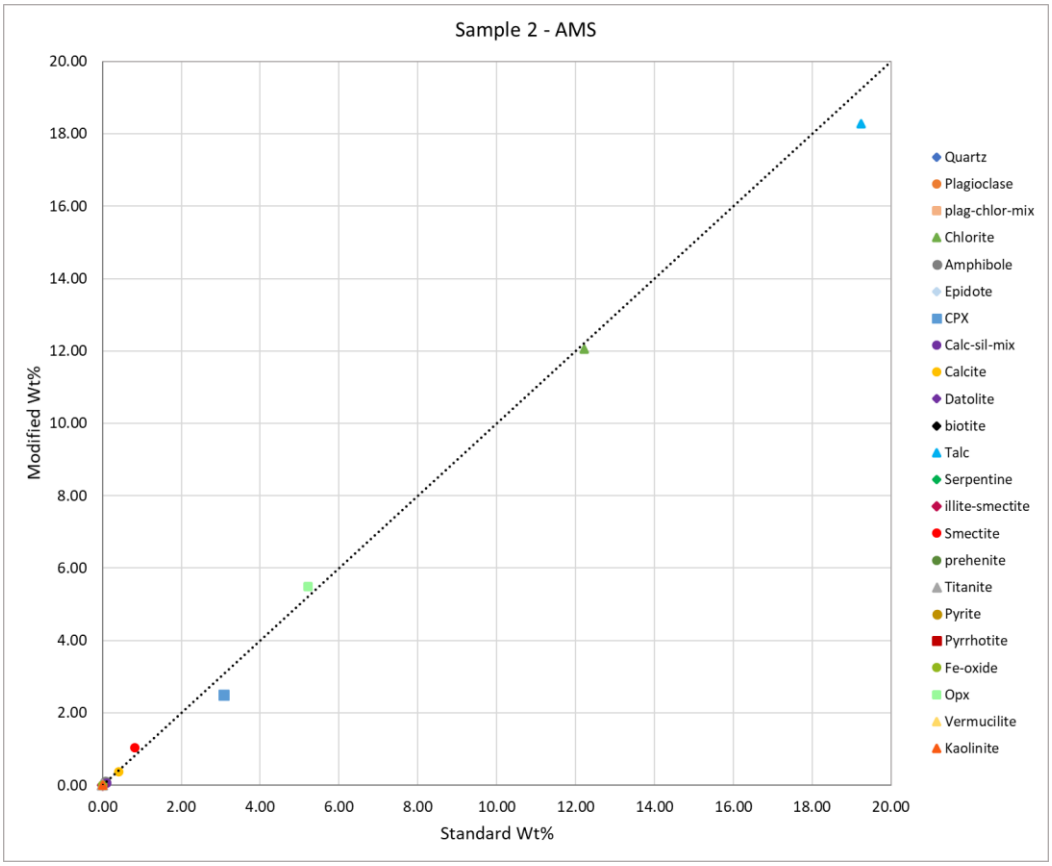

Figure 6-29: Comparison chart of modified (y-axis) and standard (x-axis) AMS results in sample 2.

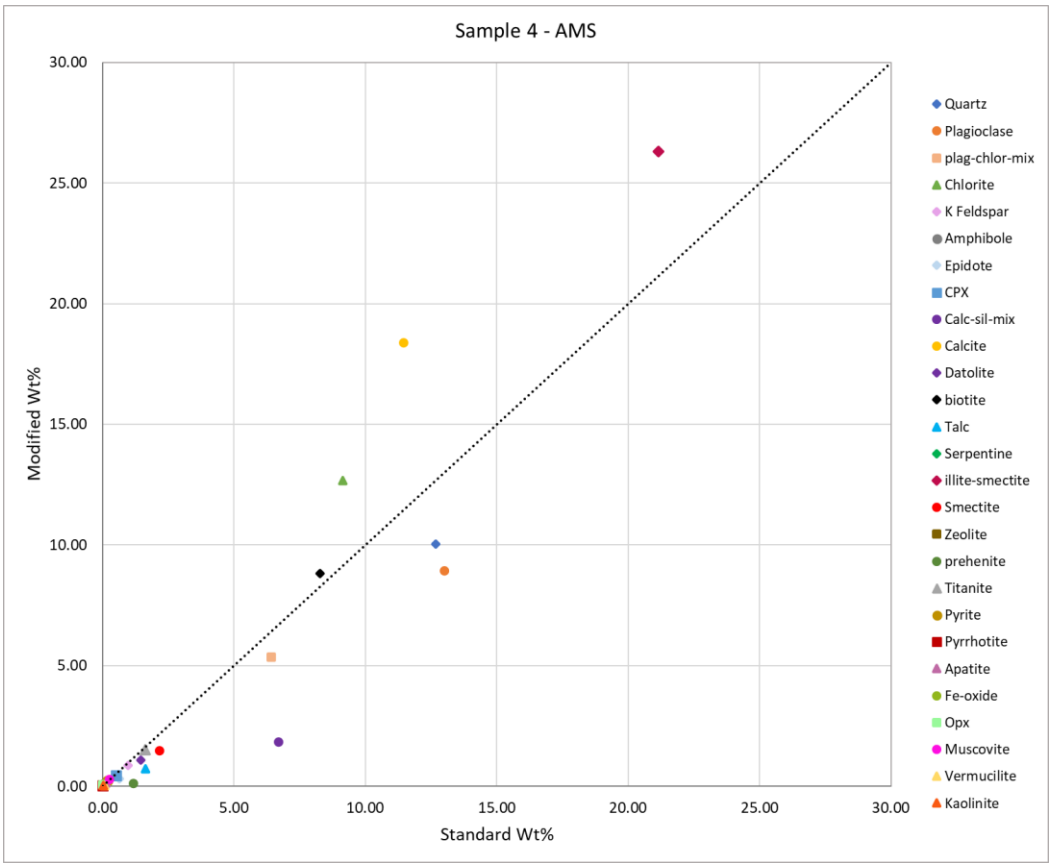

Figure 6-30: Comparison chart of modified (y-axis) and standard (x-axis) AMS results in sample 4.

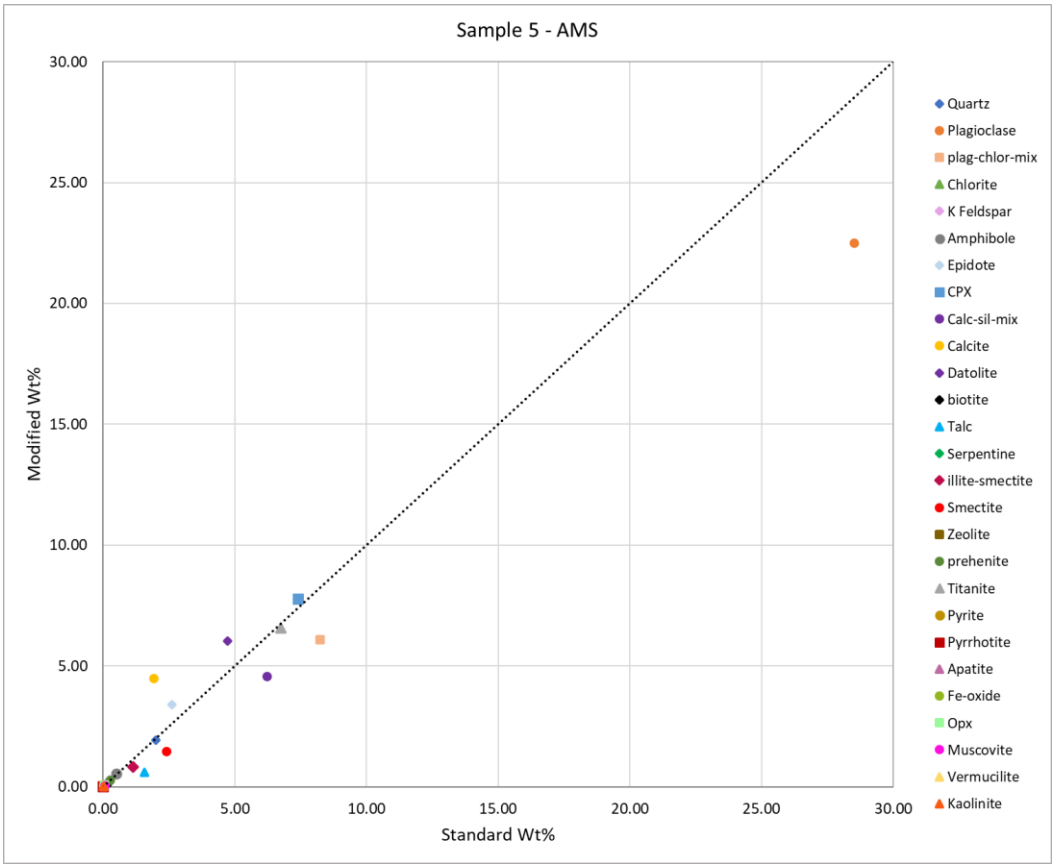

Figure 6-31: Comparison chart of modified (y-axis) and standard (x-axis) AMS results in sample 5.

The amount of detected smectite from the AMS analyses is plotted in Figure 6-32. Note that samples 3, 6 and 7 do not have the modified results and can be somewhat overlooked because of this. The graph is meant to illustrate the smectite differences between the standard and modified samples, a positive deviation (%) describes an increase in modified detection, as seen in samples 1 and 2, while a negative deviation (%) implies a decrease in smectite detected in the modified sample material as seen in samples 4 and 5. The deviation is calculated from Equation 6.1.

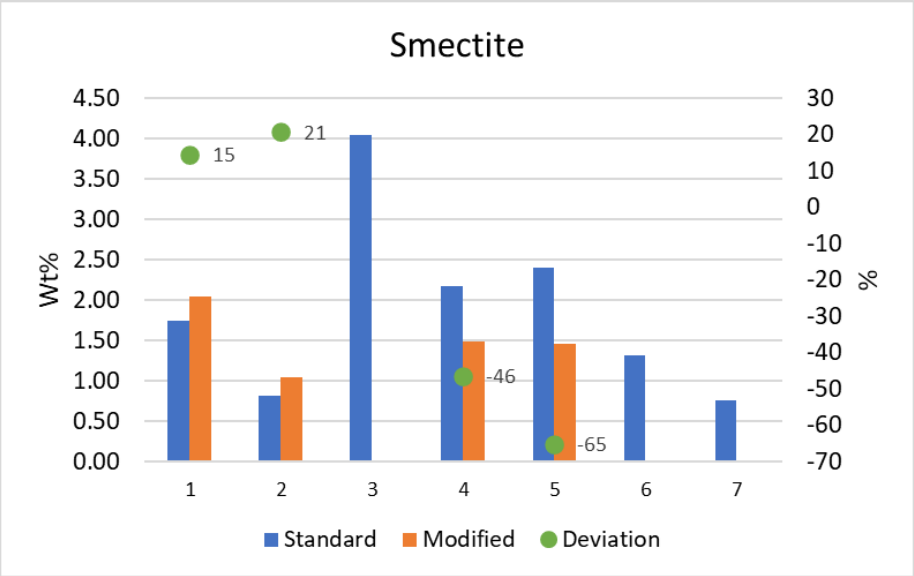

Figure 6-32: Comparison of standard and modified smectite detection from AMS with deviation (%).

6.7 Hyperspectral Imaging

The hyperspectral imaging results obtained from the core boxes and rock samples are presented in this section. The data processing was performed by Jessica Ka Yi Chiu. Core logging data, sample observation and the results obtained from XRD and AMS were used to help determine the mineralogical composition of the samples. The data from SWIR spectra was solely used for the mineral classification of the sample specimens and rock cores. A selection of minerals was investigated through hyperspectral data. These were chosen because of their possible negative effect on the tunnel stability, including smectite, illite, talc, serpentine, kaolinite, vermiculite, chlorite and zeolite. Carbonate minerals were also included. Minerals such as quartz, plagioclase, feldspar, pyroxene and biotite are spectrally inactive and will not be evaluated by the hyperspectral data. A description of the post-processing procedure and results is given in the report by Chiu (2022) in Appendix L.

The mineralogical classification maps (top) produced from hyperspectral data of samples 2-4, 8 and 9 are shown in Figure 6-33 along with the RGB representation (bottom). The results are provided from the SWIR camera with a 30 cm lens. The dominant mineral of the scan area is montmorillonite, montmorillonite-illite and smectite-talc (neon green color). A large portion of the samples is classified as unknown. The mineral classification is displayed in Table 6-12. Of these, the smectite-talc was the main mineral in all five samples. In addition, sample 3 and sample 9 had a high amount of smectite-vermiculite-chlorite. Other detected minerals include zeolite, talc, serpentine-carbonate and carbonate.

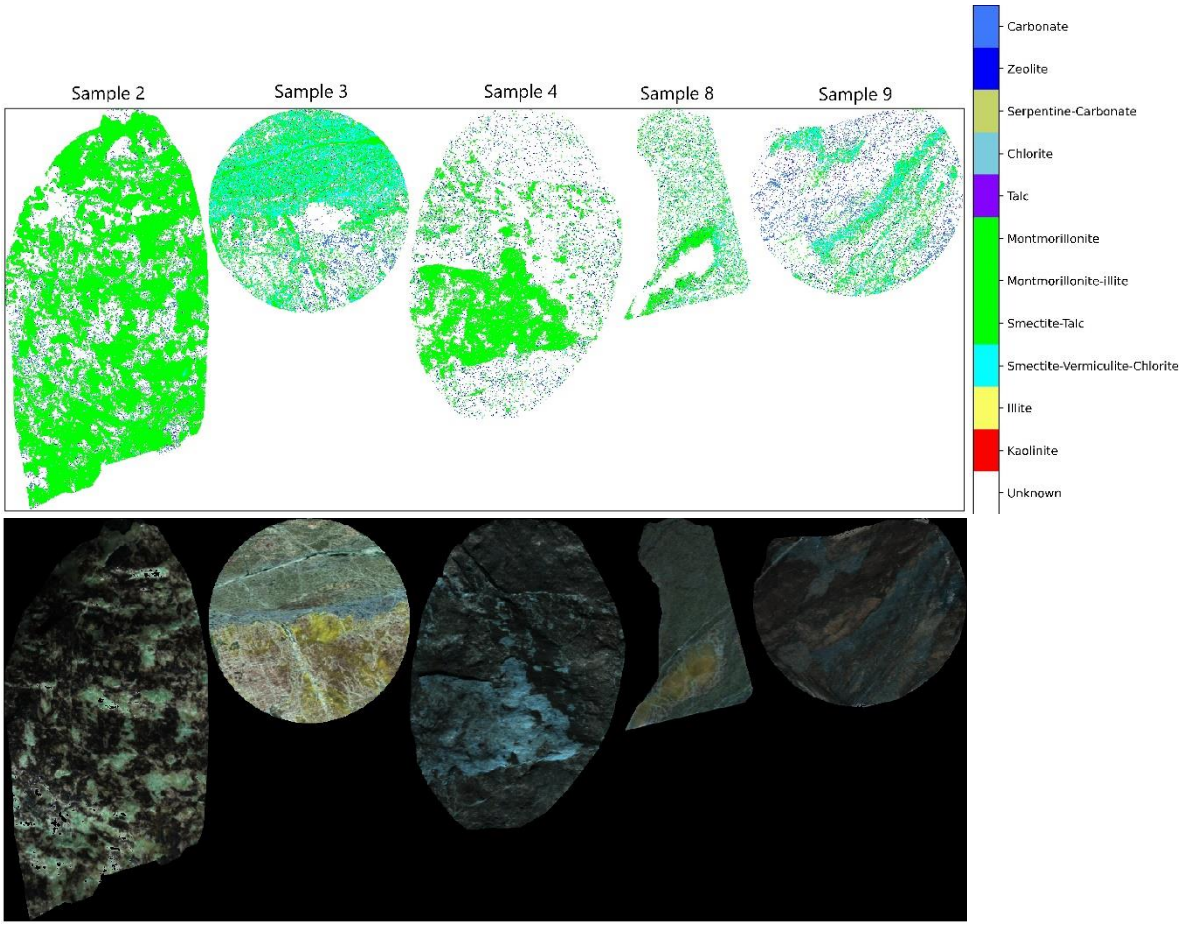

Figure 6-33: mineral classification results (top) and RGB representation (bottom) from SWIR of samples 2-4, 8 and 9 with 30cm lens.

Table 6-12: Classification results of possible minerals detected in the samples with a 30cm lens.

	Sample 2	Sample 3	Sample 4	Sample 8	Sample 9
Possible mineral(s)	% of analyzed pixels				
Unknown	31.3	40.04	68.93	69.98	71.39
Kaolinite	0.0	0.0	0.0	0.0	0.0
Illite	0.0	0.0	0.0	0.0	0.0
Smectite-Vermiculite-Chlorite	0.79	23.88	0.77	5.32	7.19
Smectite-Talc	63.82	29.98	26.13	20.91	11.98
Montmorillonite-illite	0.05	0.65	0.07	0.1	0.0
Montmorillonite	0.19	0.98	0.44	0.68	0.1
Talc	0.46	0.02	0.02	0.03	0.6
Chlorite	0.04	0.01	0.01	0.0	0.07
Serpentine-Carbonate	0.4	0.12	0.03	0.03	0.44
Zeolite	0.85	1.72	2.79	2.74	2.49
Carbonate	2.1	2.61	0.82	0.22	5.74

Figure 6-34 displays the mineralogical classification (top) of the rock cores (68-80 m depth) along with the RGB representation. The results are derived from a SWIR camera with a 1m lens. The total mineral classification from the rock cores is shown in Table 6-13. Smectite-talc is the main mineral composition detected in the rock cores whereas zeolite is following

with a much lower percentage. Approximately 44% of the rock core is unclassified (unknown). Other detected minerals are smectite-vermiculite-chlorite, montmorillonite, talc, serpentine-carbonate and carbonate.

The mineralogical composition for the nine sample areas (Figure 6-35) was also investigated in more detail. The values are shown in Table 6-13, showing that smectite-talc is the main mineral in all samples except S4 where zeolite is detected as the main mineral (3.67%). There is a large percentage variation in the smectite-talc detection ranging from S8 with 88.9% to S4 with 2.67%. A similar distribution is shown with the unknown minerals which range from 3.63% (S5) to 93.45% (S4). There are some variations between the mineral compositions in the samples, however, none of the samples detected kaolinite, illite, montmorillonite-illite or chlorite.

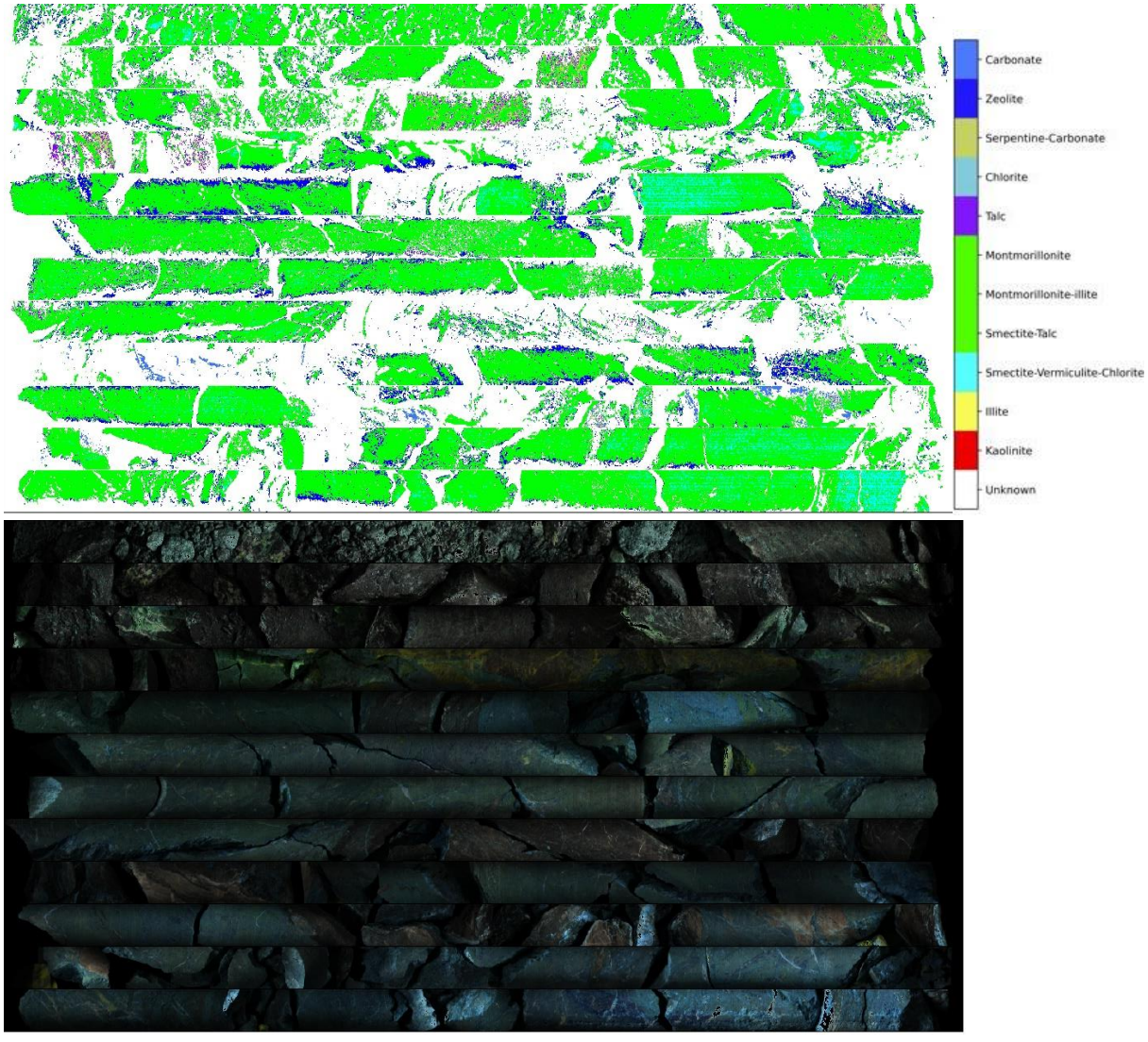

Figure 6-34: Mineral classification (top) and RGB representation (bottom) from SWIR of the rock cores with 1m lens. The rock cores have a depth from 68.00m (top-left) to 80.00m (bottom-right). Each core is approximately 1 m in length.

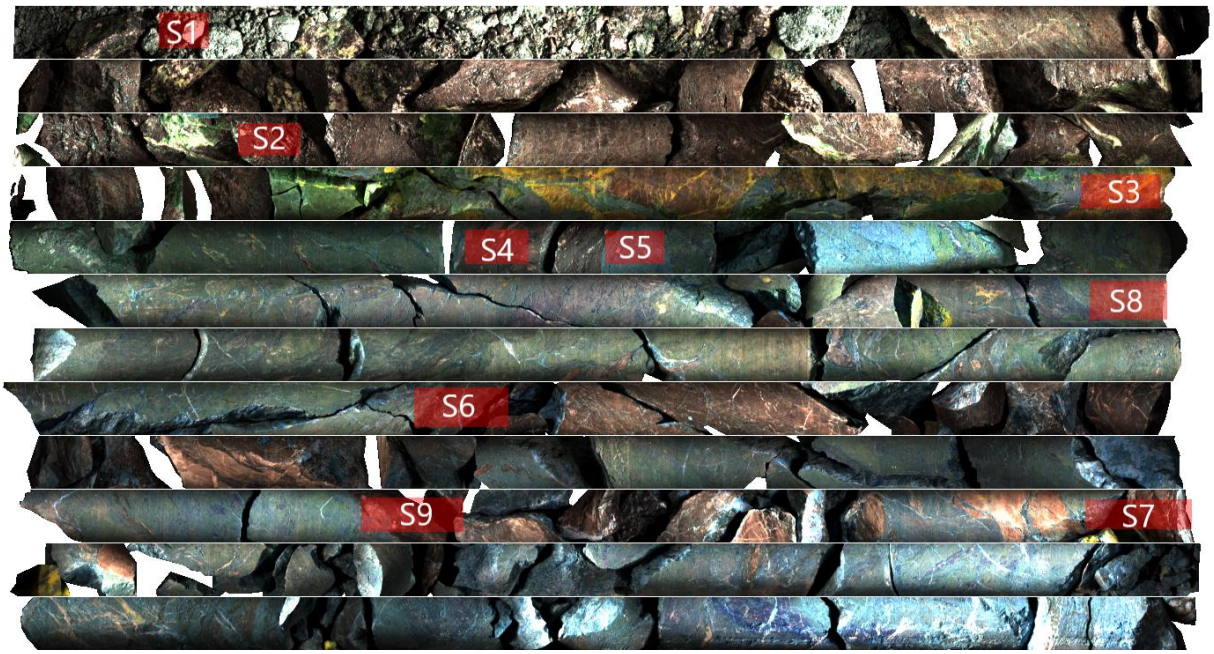

Figure 6-35: Overview of nine sample locations (S1-S9) for extracting the classified pixels. The rock cores have a depth from 68.00m (top-left) to 80.00m (bottom-right). Each core is approximately 1 m in length.

Table 6-13: Summary of possible minerals detected in the rock cores and nine sample areas (S1-S9).

	Rock cores	S1	S2	S3	S4	S5	S6	S7	S8	S9
Possible mineral(s)	*% of analyzed pixels*									
Unknown	43.94	45.58	43.8	77.09	93.45	3.63	85.05	69.22	5.96	80.33
Kaolinite	0	0	0	0	0	0	0	0	0	0
Illite	0	0	0	0	0	0	0	0	0	0
Smectite-Vermiculite-Chlorite	2.21	7	0.04	0.91	0	20.65	0	0.54	3.14	1.47
Smectite-Talc	46.48	40.96	43.91	21.17	2.67	75.43	12.34	28.34	88.9	15.9
Montmorillonite-illite	0	0	0	0	0	0	0	0	0	0
Montmorillonite	0.04	0	0	0.06	0.04	0	0	0.13	0	0
Talc	0.71	0	7.36	0	0	0	0	0.05	0	0.16
Chlorite	0	0	0	0	0	0	0	0	0	0
Serpentine-Carbonate	0.61	0	3.05	0	0	0	0	0	0	0.09
Zeolite	5.66	6.47	1.56	0.68	3.67	0.28	2.62	1.23	2.01	1.02
Carbonate	0.35	0	0.27	0.09	0.18	0	0	0.49	0	1.04

6.8 Oedometer swelling tests

Results from the powder oedometer swelling test are given in Table 6-14. The results show the maximum swelling pressure obtained during the time of the test, which is the first 24 hours. All seven standard samples were tested with the oedometer apparatus to quantify the maximum swelling pressure. A majority of the samples were classified as low. STD1 detected the highest swelling pressure at 0.15 MPa with a medium classification. Two of the modified samples were tested by oedometer swelling test, MOD1 and MOD6 respectively. Both samples corresponded with the standard classification and were classified as low. However, there were some changes in maximum swelling pressure as shown in Table 6-14. The swelling pressure charts are presented in Appendix M.

Table 6-14: Results from the oedometer swelling test for both powder and intact rock samples. Classification after NTNU standard (Mao et al., 2011). Swelling classification is displayed in Appendix B. L = low, M = medium, H = high, V-H = very high.

Sample	Standard [MPa]	Class.	Modified [MPa]	Class.
1	0.15	M	0.05	L
2	0.06	L	-	-
3	0.08	L	-	-
4	0.07	L	-	-
5	0.04	L	-	-
6	0.001	L	0.02	L
7	0.02	L	-	-

7 Rock mechanical tests

The uniaxial compressive strength (UCS) test and Brazil test (BTS) were the two rock mechanical tests performed during this thesis. E-modulus, Poisson ratio, velocity and density measurements were done in addition to this.

7.1 Material Description

Five sample specimens were chosen for the UCS test, as presented in Table 7-1. According to the ISRM (1979a) standard for uniaxial compressive strength, the height to diameter ratio for the specimen should be between 2.5–3.0. At the rock mechanical laboratory at NTNU, a suggested absolute minimum height to diameter (h/D) ratio is 2. As previously stated, the samples arrived in extremely broken condition and the testable material became scarce. Three samples fulfilled the minimum requirement and were used for UCS, E-modulus, Poisson ratio, sonic velocity and density tests.

Table 7-1: UCS samples with the collected area, rock type and length to diameter ratio. Collected areas are displayed in Appendix C.

Sample	Area	Rock type	Ratio
UCS1	71.45-71.70	Chlorite rich shale with carbonates	2.1
UCS2	72.14-72.36	Altered basalt	-
UCS3	74.27-74.49	Altered basalt	2.6
UCS4	79.00-79.20	Altered basalt	-
UCS5	77.72-77.95	Altered basalt, large carbonates	2.1

- Unsuccessful preparation

Eleven samples were chosen for Brazil tensile strength test, as presented in Table 7-2. The requirement is to have a minimum of 10 samples for testing. All remaining samples were altered basalt rock types. Fifteen samples were originally chosen for BTS testing, but all samples were not prepared.

Table 7-2: Chosen samples for Brazil test with area and rock type classification. The collected areas are showed in Appendix C.

Samples	Area	Rock type
BTS3	73.80-73.88	altered basalt
BTS4	74.00-74.14	altered basalt
BTS5	74.50-74.63	altered basalt
BTS6	74.50.74.63	altered basalt
BTS8	78.70-78.90	altered basalt
BTS9	78.70-78.90	altered basalt
BTS11	78.60.78.70	altered basalt
BTS12	79.00-79.23	altered basalt
BTS13	79.00-79.23	altered basalt
BTS14	79.00-79.23	altered basalt
BTS15	79.00-79.23	altered basalt

7.1.1 Specimen Preparation

The five successfully and unsuccessfully prepared samples are shown in Figure 7-1. The samples were prepared at the Rock Mechanics Laboratory at NTNU. Preparation was done under wet conditions. During preparation, it was discovered that two of the rock samples, UCS2 and UCS4, were not fit for testing. Because of large irregularities and fracturing during preparation, it was decided not to use them. The three prepared rock samples UCS1, UCS3 and UCS5 have a height-to-diameter ratio between 2.1 to 2.6 (Table 7-1).

Figure 7-1: Successfully and unsuccessfully prepared UCS rock specimens. UCS1 to UCS5 from left to right.

Sample preparation for the Brazil test was done at the Rock Mechanics Laboratory at NTNU. The specimen is cut to a disc with dimensions where the thickness is 0.5xD. The surface should be free of tool marks and irregularities. The diameter of the specimen should not go under 54 mm, in this case, the diameter is approximately 70 mm (ISRM, 1978c). The specimens are wrapped with tape around the periphery to keep the samples intact after the testing procedure. All prepared samples are displayed in Figure 7-2 with varying conditions.

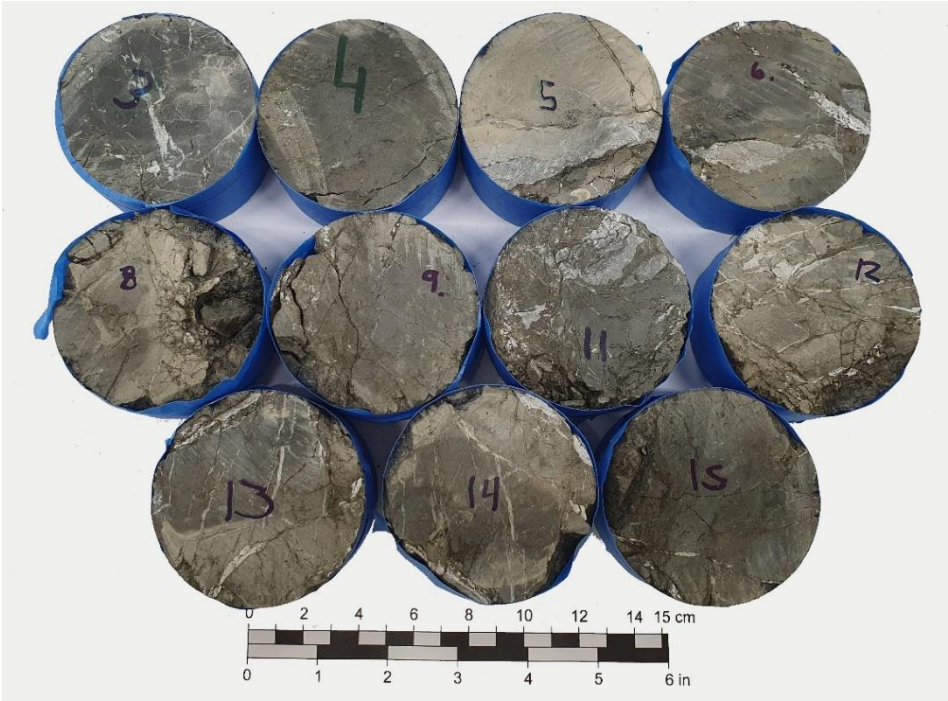

Figure 7-2: Prepared samples for Brazil test.

7.2 Uniaxial Compressive Strength test and Deformability

The uniaxial compressive strength test (UCS) is a method for strength classification and characterization of the intact rock mass. A cylinder specimen is tested and should ideally have a diameter of approximately 54 mm and a height to diameter ratio of 2.5-3.0. The ends of the sample should be flattened and perpendicular to the axis of the specimen. The sides should ideally be smooth and free of irregularities (ISRM, 1979a). During the testing procedure the cylinder specimen is placed in the apparatus (Figure 7-3). A constant axial load is applied to the specimen between two steel plates while simultaneously measuring the load. The point of failure represents the maximum load the specimen can carry. The uniaxial compressive strength is calculated by dividing the maximum load on the cross-sectional area of the specimen (ISRM, 1979a).

The E-modulus, E, and Poisson's ratio, v, can be calculated from the measurement during UCS testing. A stress-strain curve is created during testing by recording the axial stress, σ, and axial/radial strain, ε. The E-modulus is the ratio of the axial stress change to the axial strain change in the linear part of the curve. Poisson's ratio is the ratio of the radial and axial strains. This is calculated from the point $\sigma_{50\%}$ where the curve is more or less linear (ISRM, 1979a).

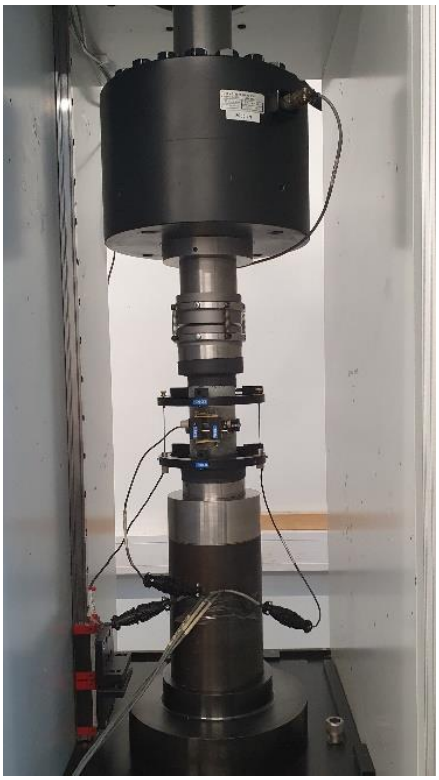

Figure 7-3: The GCTS RTR-4000 Rapid Triaxial Rock Testing System.

The GCTS RTR-4000 Rapid Triaxial Rock Testing System (Figure 7-3) was used during UCS testing. The three samples UCS1, UCS3 and UCS5 were tested under laboratory conditions. The samples had a diameter of approximately 71.5 mm and lengths varying from 147 to 187 mm. Two of the tested cores, UCS1 and UCS5, did not meet the (ISRM, 1979a) criteria and had a ratio of 2.1. On the other hand, the rock mechanical laboratory at NTNU suggests an absolute minimum ratio as h/D = 2 which was followed during the test where all tested samples lie within this range. This is a method used for avoiding an artificially high UCS value (Hawkes and Mellor, 1970 in Frengen, 2020). It was necessary to use a lower ratio than the standard as it was hard to get undamaged samples with the correct height.

The results obtained from the UCS test along with the E-modulus and Poisson's ratio are presented in Table 7-3. The corresponding stress-strain curve is shown in Figure 7-4. The UCS values vary from 18 MPa to 67 MPa. According to the rock strength classification by ISRM (1978), UCS1 is characterized as a strong rock, UCS3 is a medium strong rock and UCS5 is a weak rock (Appendix B). The failure modes on the samples during the uniaxial compressive strength test are shown in Figure 7-5. The Poisson ratio obtained from the samples is to an excessive degree affected by fractures and cracks in the rock specimen, because of this it was decided not to use the data. As for the Poisson ratio in UCS1 it was presumed reasonable to place the tangential point below $\sigma_{50\%}$ as the stress-strain curve is linear at that point and the tangential line at $\sigma_{50\%}$ is influenced by the fractures. The table and stress-strain curve with the tangential points are shown in Appendix N.

Table 7-3: Values of uniaxial compressive strength, E-modulus and Poisson ratio of samples UCS1, UCS3 and UCS5.

Sample	Uniaxial compressive strength [MPa]	Class.	E-modulus [GPa]	Poisson's ratio
UCS1	67 ± 7.1	Strong	66.7	0.3*
UCS3	26.2 ± 2.8	Medium strong	32.0	-
UCS5	18.4 ± 2.1	Weak	15.6	-

*Poisson ratio is calculated below $\sigma_{50\%}$

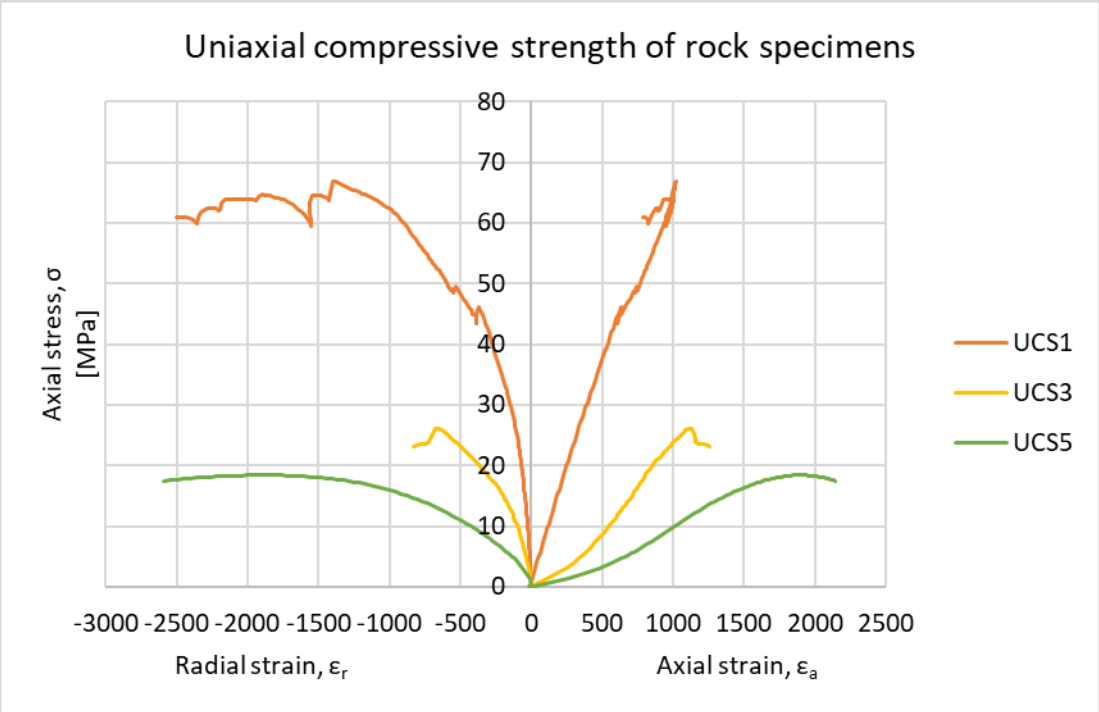

Figure 7-4: Stress-strain curve from UCS1, UCS3 and UCS5.

Figure 7-5: Failure planes created during uniaxial compressive strength test on UCS1, UCS5 and UCS3.

7.3 Brazil test

Brazil test is a method used to test the tensile strength (σ_t) of the rock specimen that is further used for classification and characterization of the intact rock mass. The test is performed by placing the prepared rock specimen in a machine where the tensile load is applied and measured, as illustrated in Figure 7-6. The load should be applied at a constant stress rate until failure (ISRM, 1978c; Li, 2018). The alignment of the specimen should be such that weakness or fractures are not parallel to the loading points. The test is approved if the failure goes directly through the two loading points of the specimen, as seen in Figure 7-6. Tensile strength is calculated from Equation 7.1 where P is the load at failure (N), D is the diameter (mm) and t is the thickness (mm) (ISRM, 1978c).

$$\sigma_t\,[MPa] = \frac{2}{\pi} * \frac{P}{D * t} \tag{7.1}$$

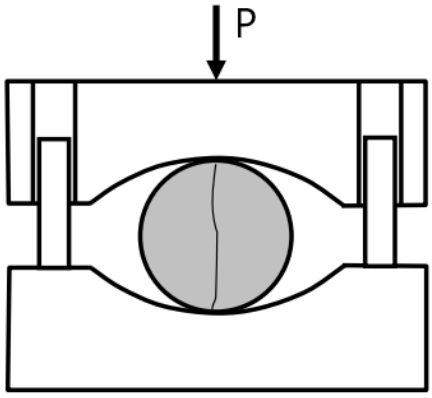

Figure 7-6: Brazilian test setup and illustration of load. Modified from Li (2018).

The Brazil tensile strength test was performed by Jon Runar Drotninghaug due to time constraints. Out of eleven samples, only five were approved during testing, BTS8 and BTS9 were not usable for testing as they had largely broken up pieces. BTS3, BTS6. BTS13 and BTS14 were not approved during testing. The remaining samples (BTS4, BTS5, BTS11, BTS12, BTS15) were approved and had a tensile strength range from 1.25 MPa to 5.27 MPa with a mean value of 2.35 MPa (Table 7-4). The full overview of Brazil test results is found in Appendix N.

Table 7-4: Brazil tensile strength results.

	Tensile strength, σ_t [MPa]
Min value	1.25
Max value	5.27
Mean value	2.35

7.4 Density and Velocity

Velocity measurements are done by sending pulses of P-waves through the rock specimen and by measuring the travel time through the core. A transmitter and receiver are placed on each side of the rock core. The velocity (v_p) is calculated based on the travel time (t_p) and the distance (d) between the transmitter and receiver (Equation 7.2) (ISRM, 1978a). The procedure was used on the prepared UCS sample cores under dry conditions. The velocity is used to explain potential differences in the rock cores when conducting other tests, as it gives information about the characteristics of each rock specimen. Hence, it is important to maintain the calculated values for each sample rather than finding a mean value. The velocity that was calculated is presented in Table 7-5.

$$v_p = \frac{d}{t_p} \tag{7.2}$$

The density (ρ) is calculated using Equation 7.3, where *m* is the mass and *V* is the volume of the specimen. The calculated density is shown in Table 7-5.

$$\rho = \frac{m}{V} \tag{7.3}$$

Table 7-5: Calculated velocity and density of the specimens.

Sample	Velocity [m/s]	Density [g/cm^3]
UCS1	6352.1	2.7
UCS3	4461.9	2.8
UCS5	2909.7	2.7

8 Analysis and discussion

8.1 Analysis of the results

A considerable amount of laboratory testing has been performed during this thesis to evaluate the rock characteristics concerning swelling and/or difficult minerals. The laboratory methods are to be assessed based on their achieved results. In addition, the standard and modified crushing methods are to be compared and evaluated based on the results.

8.1.1 Analysis of the crushing

The first step to evaluate the modified crushing method up against the established standard crushing method is to look into the crushing procedure. Both the standard and modified methods experienced advantages and drawbacks during the crushing procedures. The occurring problems may impact the laboratory test results following this.

The standard crushing method provides an effective way of grinding the samples down to approximately <10µm grain size with the Retch Vibratory Disc Mill RS 200. It is a relatively simple method where only a few steps need to be considered. Yet, one problem was discovered. Large grains (ca. 2 mm) were found in STD3, STD4, STD5 and STD6 specifying that the material was not sufficiently milled down. A possible explanation could be an exceeding of the disc mill jar which can only hold a maximum of 20-30 g each round. Even though the samples were divided into smaller parts during the milling procedure, the material was not weighed to establish acceptable limits. The additional milling of the samples added to the loss of material and an added risk of damaging the material. The loss of material for three of the four samples, namely STD3-STD5, has a much higher material loss compared to the samples with only one run of crushing, ranging from 6.8% to 9.9% (Table 6-2). Sample STD6 has a 2.1% material loss. Then again, STD1 has a material loss of 4.4%, higher than STD2, STD7 and STD6. A source of material loss is related to the equipment as some materials will stick to contact surfaces, particularly soft and fine-grained material are prone to this. This might explain the large material loss of STD1 which derives from a fault gouge rock type.

The modified crushing method did also experience some difficulties. Firstly, the method proved to be very time-consuming with each sample taking half a workday (approximately 4-5 hours) to fully grind down and get through the sieves. The main problem occurs in the hard minerals, such as quartz, which are harder to fully grind down. The amount of sample material is also an influential factor. For this thesis, a larger amount of sample material was needed as several laboratory methods were to be tested. In other projects, the extent of material might be reduced. Secondly, the Fly Press Rock Crusher apparatus can get damaged when such small grains are being crushed, causing the two steel discs to press against one another continuously. The mortar and pestle were added to reduce some of this damage. Thirdly, there was a significant loss of material since the crushing did not take place in an isolated area and the material easily got flung out. Some measurements were taken, such as placing sheets of paper around the equipment to catch some of the grains. However, a significant amount of material was still lost, between 5.6% to 10.3% (Table 6-2). Hard minerals like quartz are more difficult to mill down and thus can easily

be flung out of the apparatus during crushing, adding to the loss of material. Loss of material through the equipment is also occurring in the modified crushing. It was attempted to reduce the loss as much as possible, however, when cleaning the apparatus there were found traces of sample material.

Washing of the equipment was done between all samples during both methods. However, it cannot be guaranteed that some contamination did not occur. Another point to consider is that the modified procedure is done by manual labor. The handling of each sample will vary based on the person performing it and also through the development of technique. This will give a larger impact on this method compared to the standard automated method. It is thus recommended to make the modified crushing procedure automated, both to save time and to remove some of this bias.

Lastly, considering that there was found a large loss of material in both the standard and the modified samples none of them can be used as a true mean value. As explained previously, the standard values were used as the mean value during calculations of relative deviation. These results need to be interpreted with caution.

8.1.2 Analysis of X-Ray Fluorescence (XRF)

The XRF results were used to determine potential differences between the two crushing methods. According to Table 6-8, the greatest deviation is found in SiO_2 and CaO. There appears to be a loss and/or gain of the elements where SiO_2 shows a loss in all samples but two. A gain of material is not attainable in this situation and is in connection with the loss of other elements, as the total chemical composition is adjusted when others disappear. As mentioned, hard minerals rich in SiO_2 (silicate minerals) have a likelihood of being lost as they are harder to mill down, especially in the modified crushing method which is not performed in a closed space. This would explain the large deviation of SiO_2 found in the samples.

Sample 7 stands out from the other samples when viewing the standard deviation (SD). While all others are quite similar with a maximum of 1.86 in sample 5, sample seven has a standard deviation of 5.76. This deviation mostly comes from SiO_2 and CaO components. This is consistent with the other samples and is most likely explained by the loss of hard silicate minerals, such as quartz or plagioclase.

It is important to remember that even if the loss of material can be interpreted from these results, the exact minerals cannot be determined. This is because of the complex chemical composition of the minerals, particularly soft and/or clay minerals such as montmorillonite ($(Na,Ca)_{0.33}(Al,Mg)_2(Si_4O_{10})(OH)_2*nH_2O$). It is believed that a portion of soft minerals disappears in both crushing methods due to the apparatuses and equipment. Soft minerals will easier stick to contact surfaces and be washed away later. However, the complex chemical composition makes it hard to spot this effect in the XRF results and classify which mineral got lost.

8.1.3 Analysis of the mineralogy

The mineralogical composition of a rock is important knowledge when evaluating critical conditions, such as the swelling potential. The mineralogy in this thesis is determined from the XRD (MOD, STD), AMS (MOD, STD and TS) and optical microscopy results (TS).

8.1.3.1 X-Ray Diffraction (XRD)

The minerals composition in the samples of the two crushing methods runs very similar with some differences in quantification (Table 6-3 and Table 6-4). However, STD6 and STD7 did not identify smectite minerals in contrast to all other samples. Other noticeable differences are found in plagioclase and titanite which is increased in the standard samples, as supposed to smectite and serpentine which is higher in the modified samples. The remaining minerals have no distinct connection to either standard or modified samples. The lithological differences between the rock samples may have led to the large differences observed in the correlation charts, thus making them more difficult to compare.

The swelling clay (smectite) detection is higher in the modified samples compared to the standard samples. It is questioned why the relationship between the modified and standard smectite show such large variation, especially concerning sample 6 and 7. These relationships may be explained by differences in sample lithology and thus their effect from preparation (crushing, splitting, material loss). The loss of material was not cohesive between samples, adding to the sample differences. A suggested trendline (blue) based on the smectite results is shown in Figure 8-1 and does not portray a particularly good correlation. One could argue that samples 1 and 3 are anomalies. If the values from samples 1 and 3 are discarded there seems to give an improved correlation (red) using the remaining values, as seen in the figure. Another detected mineral with swelling possibility is zeolite (mordenite). This mineral was only detected in STD1 (5%) and MOD1 (8%). The influence of zeolite minerals will be further analyzed in Chapter 8.2.1.

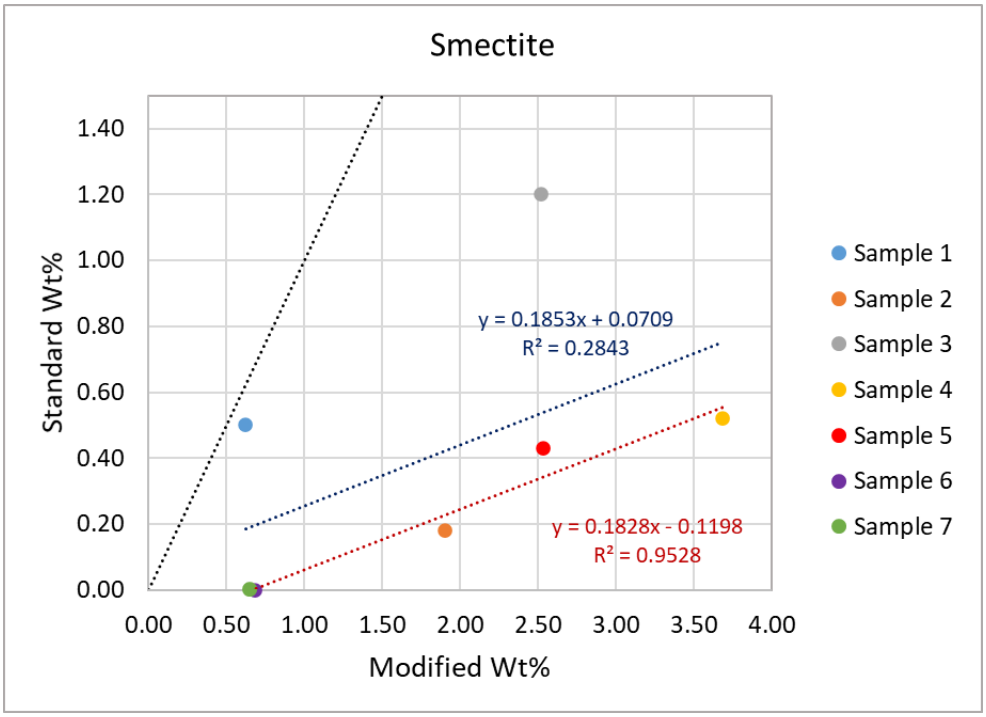

Figure 8-1: Comparison chart of the smectite clay content in standard (y-axis) and modified (x-axis) samples with two alternative trendlines. Blue: trendline to fit all samples (1-7). Red: trendline to fit samples 2, 4, 5, 6 and 7. Black: 1:1 line.

The smectite/zeolite observations may support the hypothesis that the modified crushing method preserves weak minerals. When plotting all hard and soft minerals (Figure 6-4) the amount of detected soft minerals does increase in the modified samples simultaneously as hard minerals decrease, with the exception of sample 2. There is no solid explanation

for why sample 2 differs from the other samples. The mineral quantification is influenced by the total weight in the sample, meaning that if the amount of e.g., smectite or zeolite were to increase, other minerals would have to decrease. It is hard to determine which minerals are influenced by this, as it could be both weak/soft or hard minerals. Further, some minerals would also be influenced by the crushing (preparation) methods. Nevertheless, one could argue that the modified crushing does have a positive effect on swelling minerals such as smectite. The most obvious reason being the emergence of smectite in MOD6 and MOD7. Still, this could also be caused by errors from preparation, splitting or material loss. All things considered, the number of samples used in this thesis is far too low to give a reasonable correlation or final result based on this.

8.1.3.2 Automated Mineralogy System (AMS)

The use of AMS offers possibilities to visualize and quantify chemical, mineralogical and textural information of the rock samples (Keulen et al., 2020). The obtained backscatter electron micrograph (BSE) and false-colored mineral maps are beneficial for giving detailed, in-situ information on the distribution and placement of minerals. This includes texture, grain size, fracture filling and mineral association, particularly from polished thin section samples. The ability to compare the mineral maps with optical microscopy separated the AMS from other mineralogical methods. Powdered thin section samples do not hold the same optical benefits as intact samples. The in-situ placement of minerals is only obtainable in larger grains. However, the BSE images of the former help visualize detailed mineral texture which is beneficial when evaluating the rock mass quality. This has been helpful when comparing the modified and standard crushing procedures, which will be explained in the section to come.

The chemical composition obtained from the AMS (EDS-spectrum) is helpful when the mineral identification is questioned and has to be reinterpreted (Cook, 2000; Graham & Keulen, 2019). However, it can be challenging when the chemical composition is similar or when there is a mixed signal due challenging to fine-grained material. Also, the use of other methods such as optical light microscopy will be helpful through data processing.

A comparison of the minerals map and thin section image (XPL) was done for all samples. The comparison can be used to locate possible differences and errors in the AMS. TS2 (Figure 8-2) revealed that the talc is not as strongly pronounced as displayed in the XPL image. A somewhat diagnostic concentration of talc can still be seen in the mineral map. It is believed that the issue lies in the distinction between talc and serpentine. The close chemical resemblance of the two minerals (Appendix O) could cause them to get mixed, resulting in quantificational errors. Then again, a closer inspection of the AMS data revealed it as a mixture of antigorite (serpentine) and talc rather than pure talc mineral. This is interpreted based on the chemical composition of the minerals, also the backscatter image shows no clear borders of this mineral. No distinct solution was found for this problem and this will not be further addressed.

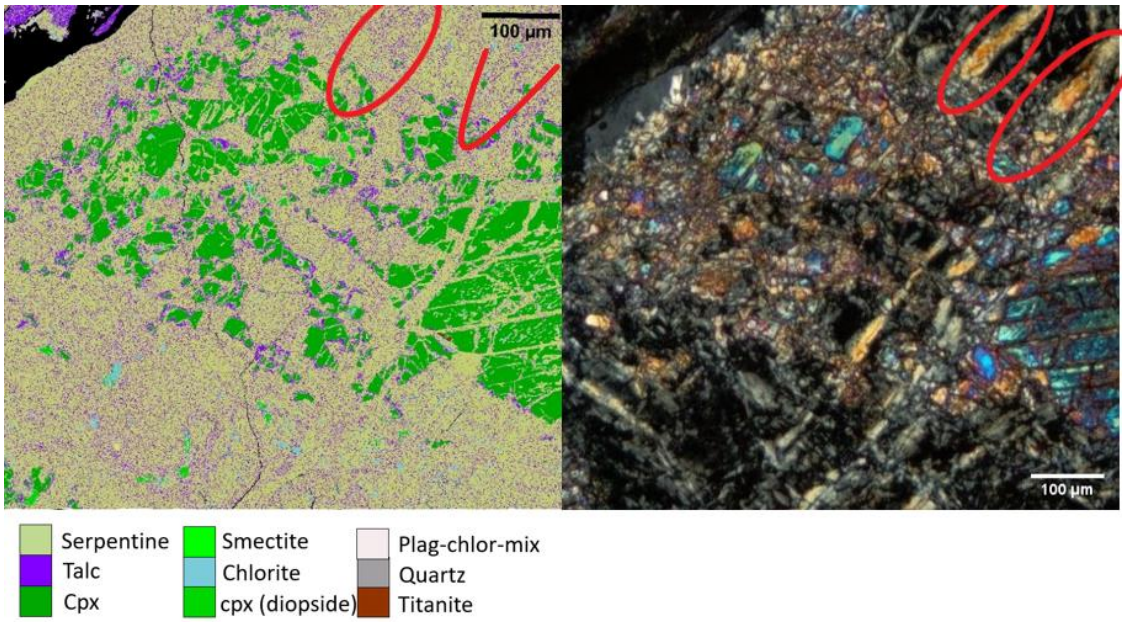

Figure 8-2: False-colored mineral map with corresponding XPL image of sample 2. Red markings highlight the problematic areas of talc and serpentine mineral detection.

One of the study aims was to determine the differences between standard and modified crushed samples. This has been done, among other things, by analyzing the powder thin section with the AMS. The comparison has been somewhat limited due to the three lacking samples (MOD3, MOD6 and MOD7). Another source of uncertainty is the grain representation. The mineral composition can be affected by the chosen area of the sample. The size of the scanned area is aimed to be corresponding from sample to sample to reduce uncertainty related to that.

Smectite was quantified in all samples of the polished thin sections, as well as the powdered thin section samples. The maximum smectite amount was found in TS3_b (4.7%). The smectite clay minerals are distributed evenly throughout the samples, as can be visualized in the mineral maps. It appears that smectite minerals are often concentrated around plagioclase-chlorite-mix/plagioclase minerals which are observed in TS3_b, TS5, TS8 and TS9, as well as some larger grains in the powdered thin section (Appendix I). This observation is reasonable as smectite is altered from silicate minerals such as plagioclase (Fulignati, 2020). The differences between standard and modified smectite results are somewhat unexpected (Figure 6-32). There was an increase in smectite quantification in MOD1 and MOD2 in contrast to a decrease in smectite quantification in MOD4 and MOD5, and there was no correlation between the four samples. The results show no clear evidence that the modified crushing method is superior to the standard crushing method concerning swelling clay minerals. Unfortunately, more samples were not able to be analyzed.

A textural difference between the standard and modified samples were observed from the BSE image and mineral maps. The standard sample material was more rounded and filled with agglomerated mixed-matrix material in contrast to the modified samples which had mainly angular shaped grains (Figure 6-25). This could be an indication that the gentle crushing preserves the original texture of the rock better, thus also perceiving the mineral composition. It was discovered that these "dust clouds" partly disappear in the false-colored mineral maps, as displayed STD5 in Figure 8-3. The mixture of the clustered material and epoxy does not generate enough EDS-counting for the material to be identified, thus causing this problem (S. Lode, personal communication, 2022).

It was discovered dissimilarities between the mineral maps and BSE image related to calcite minerals. In samples MOD1 and MOD2 (Figure 6-27 and Appendix K) calcite minerals partly disappeared in the mineral maps, similar to the "dust clouds" described above. It was questioned whether this is a systematic bug or if there is an issue with quantification. When compared to the XRD results AMS has a lower quantified amount of calcite, this could indicate quantification errors in AMS. However, MOD4 and MOD5 also have low calcite detection without calcite disappearing from the mineral maps.

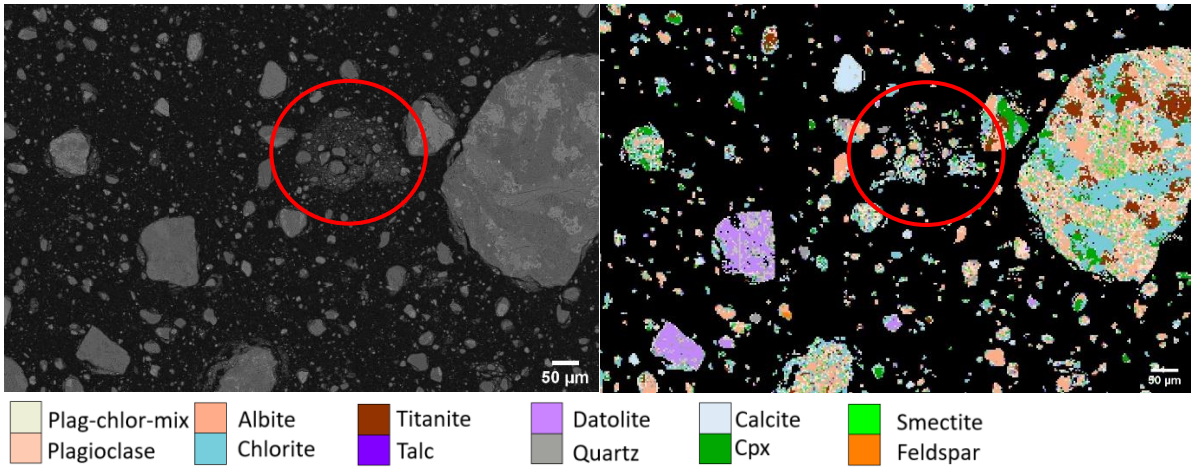

Figure 8-3: BSE image (left) and mineral map (right) of STD5 with focus on agglomerated mixed-matrix material (red circle) in the sample, also referred to as "dust clouds".

Whilst this method can be promising for future projects, there are also some limitations. The preparation of thin sections is a time-consuming process, as well as the AMS analysis and post-processing itself. Sometimes decisions have to be made fast in hydropower tunneling projects, thus this might not be a suitable method. In other cases, for example during project investigations, the time aspect would not be as problematic. Depending on the required information, the AMS analysis can be adjusted to save time by selecting the scan area, step size, and have a detailed mineral list which will make the analyzes less time-consuming (Keulen et al., 2020). An approach described in the article by Keulen et al. (2020) would be to run the initial area with a larger step size and use smaller step sizes for detailed information in selected areas. In addition, the use of powdered thin sections for AMS could provide a better solution as the duplicate crushed material used in, for example, XRD or swelling test can be used. This method could possibly be easier to compare considering the same crushed material is used.

The AMS analyzed areas in each thin section are extremely small, especially compared to the entire rock mass. Ideally, the scan area would have been increased, however, the fine-grained composition of the rock samples would have made this time-consuming and thus the scan area and step size were reduced (S. Lode, personal communication, 2022). The chosen area of the analysis will be a significant influence on the final mineral composition. This is best demonstrated by TS3_a/b and TS6_a/b (Table 6-9). For example, the quartz in TS6_b is reduced to 15.28% from 41.07% in TS6_a, while both illite-smectite (33.49 to 52.32%) and chlorite (4.25 to 8.40%) have increased. Then again, some materials have almost identical mineral compositions such as plagioclase, plagioclase-chlorite-mix, zeolite and titanite. In samples TS3_a and TS3_b the quartz, plagioclase, plagioclase-chlorite-mix and titanite have increased significantly, while the chlorite has decreased (79.16 to 52.01%).

The use of AMS was particularly helpful to clarify the rock type in the core logging and makes it easier to locate similarities or differences between rock types. The AMS results do give a good indication of the mineral compositions, however, they can be limited in terms of quantification. An approach to reduce uncertainties and errors in the AMS data is a longer and more thoroughly data processing.

8.1.3.3 Optical microscopy

The thin section study is used to evaluate the mineral composition of the thin section samples and find representable areas to perform AMS analysis. Optically, there is a large difference between the rock samples in relation to fracturing, mineral composition and alteration. Even though the chosen rock samples are collected from the same rock core, the lithologies are very different. Some minerals like quartz, serpentines, calcite and muscovites are easy to locate in the samples, others are much harder to detect as the fine-grained nature of the samples makes it hard to separate and distinguish one mineral from another, particularly clay minerals such as smectites. The attempt to find swelling minerals optically did thus not succeed. The use of thin sections is still important as it may help to find other valuable information about the rock sample and contribute to the use of AMS analysis, as explained in the preceding section.

8.1.4 Analysis of the swelling results

The oedometer swelling pressure test was performed to assess the swelling potential of the various rock samples. The results from the oedometer swelling test conducted on the bulk powder samples were classified as low swelling in all samples apart from sample 1 which was classified as medium swelling. The results indicate maximum swelling pressure [MPa] with zero volume change.

The reliability of the swelling pressure test is rather questioned. The characterization of swelling pressure used at NTNU is based on swelling gouge material as opposed to intact rock (Selen, 2017). Furthermore, there is no control of temperature, grain size, sample density or other parameters leading to unknown differences between the rock samples (Selen, 2020).

An issue when using the zero-volume change condition for the modified bulk material samples is the particle size of the material. High porosity in the sample material will reduce the detection of swelling as the material is expanding into the pores. A direct comparison of the milled bulk material (<10µm) in the standard crushing with the two fractions (100-300µm and <100µm) of the modified will not be possible as the porosity will differ. The results were inconsistent as the maximum swelling pressure from sample 1 was reduced from 0.15 MPa to 0.05 MPa in MOD1. In contrast, the maximum swelling pressure increased in sample 6 from 0.001 MPa to 0.02 MPa in MOD6. The tests were performed to give an illustration of possible swelling differences between the two bulk samples, however, the values have questionable reliability.

8.1.5 Analysis of the hyperspectral imaging results

The hyperspectral imaging (HSI) aimed to determine the mineralogic composition of the rock mass with regards to swelling and difficult minerals. The given classification of the Moglicë samples is simplified, hence caution should be taken when interpreting the results. The fine-grained nature of the rock cores and rock specimens makes it harder to determine the mineral composition of the samples. Hyperspectral imaging is a pixelated method that

cannot give a classification of individual minerals given the spatial resolution (Chiu, 2022). This causes distinguishing problems in some of the minerals. Based on the knowledge of the rock cores the amount of smectite is overestimated in the mineral maps. The hyperspectral data does provide valuable knowledge of smectite clay presence in the rock cores, with limitations of true mineral distribution.

The five sample specimens all displayed a large amount of smectite-talc (neon green), which was found strange as the same samples classified with low swelling and a low amount of smectite from other mineralogic analyses. This could be from exaggeration, as explained above. However, the close resemblance of smectite and serpentine features may cause problems in the distinction. If smectite and serpentine are present in the same pixel the absorption feature of smectite will likely overprint the serpentine minerals (Chiu, 2022). This is believed to have happened in Sample 2 which is a known serpentinite rock (Figure 6-33).

The distribution of zeolite minerals is questioned as they are concentrated at the edges of the rock cores, as seen in Figure 6-34. This is more likely a topographic effect creating noise in the spectral data. Additionally, zeolites will not be detected if other clay minerals are located within the same area (pixel), such as smectite or illite, as explained in the report by Chiu (2022) in Appendix L. The zeolite should be interpreted as something artificial. An improvement of the hyperspectral data would be to remove this edge effect, as has already been done in some of the rock cores.

As smectite-talc/smectite/smectite-illite minerals are the dominating mineral classification, fully representable mineral composition and distribution are hard to achieve using hyperspectral data. Other minerals such as serpentine, chlorite, talc and calcite cannot be excluded from the rock cores as they have likely been overprinted by either smectite or zeolite. This issue may be resolved by thorough post-processing of the data. Additionally, there is a large portion of unknown minerals which are spectrally inactive.

The hyperspectral result from the laboratory samples was provided 1-2 weeks before the submission deadline. Because of this, a detailed evaluation of the results has not been performed. The hyperspectral data collected from the field trip to Albania have not been processed in time for the submission deadline as the fieldwork was performed quite late. Hyperspectral imaging is found useful when qualitatively detecting minerals, however, the quantitative results must be further evaluated and adjusted. Based on the laboratory results it is recommended to improve the machine learning approaches and adjust the data processing to distinguish between some of the problematic minerals, particularly smectite and serpentine. The data processing for the laboratory minerals is explained in Appendix L, however, a different approach might be necessary to reduce the uncertainty of the results. Moreover, try to reduce the artificial effects caused by topographic differences, as this issue may be even more problematic in the field data.

8.1.6 Analysis of the rock mechanics results

Rock mechanical tests are used to achieve the quality of the rock mass by testing the mechanical behavior of the rock. The rock mass quality is interpreted through classification systems. The tests are often performed on homogenous, intact rock specimens with few discontinuities. The tested rock specimen is thus stronger than the actual rock mass (Panthi, 2006). In this case, the rock mass is of extremely broken, inhomogeneous and highly altered material which is expected to have a weak rock mechanical classification. The rock mechanical test was performed on the most intact, homogenous material which

is expected to be far stronger than the rock mass. The tests were still performed to give an indication of the "strongest" rock material in the samples, however, they are not representative of the rock mass strength. In addition, there were a limited number of appropriate sample specimens adding to the uncertainty of the achieved results.

The three rock specimens tested by the UCS test had very different rock strength classifications, ranging from weak rock to strong rock. This is somewhat expected considering the three samples were of different lithologies, also the velocity measurements indicated differences in the rock mass. The chlorite rich shale with carbonate clasts (UCS1) was classified as a strong rock. Weak chlorite minerals and fractures controlled the mechanical properties of the rock. Both UCS3 and UCS5 were altered basalt rock types, whereas UCS5 had larger incorporation of carbonate clasts. UCS5 was classified as a weak rock while UCS3 was classified as a medium strong rock. Both failures were heavily influenced by cracks and fractures in the rock sample which makes the results unreliable. Additionally, the ISRM recommended number of samples was not reached, which for UCS is five duplicate samples (ISRM, 1979a). As for the Brazil test (tensile strength test) it was recommended at least ten sample specimens (ISRM, 1978c), however many of the chosen samples were either not usable or not approved during testing (Appendix N). Thus, only five samples were approved during testing. The average tensile strength gained from the Brazil test is 2.35 MPa. The tensile strength of a rock is important to avoid fracturing and must be sufficient to do such (Li, 2018).

During testing, the strain of the rock was heavily influenced by external factors making the Poisson ratio unusable. The Poisson ratio is normally calculated from 50% of UCS because this point is normally the more-or-less linear (ISRM, 1979a), as explained in Chapter 7.2. It can in special cases be suggested to place the tangent point above or below 50% when such situations occur. As the top part of the stress-strain curve is somewhat strange it was argued that the stress-strain curve below the 50% tangent point was more fitted for the sample UCS1 (Figure 1 in Appendix N), making the Poisson ratio 0.3. The top part has most likely been affected by the fractures and weakness zones in the rock specimen as described above.

Overall, rock mechanical testing on the Moglicë rock samples was found hard to perform and the values need to be interpreted with caution as they are heavily affected by weakness zones, weak minerals and fractures in the rock. Also, the transportation, storage and preparation of the rock cores will have an impact on the rock characteristics. The number of test results was below the recommendation from the International Society of Rock Mechanics (ISRM) and not conducted in a homogenous rock mass, creating large uncertainties. This type of rock mechanical test is not appropriate for weak rocks. Even if the tested samples were approved, they would still not be entirely representable.

8.2 Comparision of results

8.2.1 Comparison of the mineralogy and swelling results

To evaluate whether the mineralogical analysis from XRD and AMS are corresponding to the measured swelling pressure [MPa] the results were compared with the amount of detected smectite. Furthermore, as presented in Chapter 2, zeolite minerals may affect the swelling ability of rocks and will be evaluated alongside smectite. In Figure 8-4 the swelling mineral results from XRD and AMS are compared with the obtained swelling pressure to evaluate the relationship. The results are presented as trend lines with R-squared values. The closer the R-squared (R^2) values are to 1, the better the correlation.

The high swelling pressure of sample 1 did not correspond to the low amount of detected smectite from the XRD results. A significant improvement was noticed when both smectite and zeolite minerals were compared to the swelling pressure (Figure 8-4). The R-squared value increased from 0.2921 to 0.8001 (standard) and 0.0049 to 0.8817 (modified), indicating a considerably better fit when adding the zeolite. This observation supports the hypothesis that zeolite does contribute to the swelling of rocks. Having said that, the AMS results seem to suggest otherwise. When comparing both zeolite and smectite the R-squared values indicate a slightly worse correlation. It should be noted that the amount of detected zeolite is very different in the two methods. Zeolite was solely discovered in sample 1 of XRD with a much higher amount (ca. 5-8%) than any of the zeolite detected from AMS (mean value ca. 0.03%). It was questioned whether the zeolite minerals were misidentified as anorthite because of the chemical resemblance (Appendix O), although there is not found as much anorthite as 5-8% in the AMS (B. E. Sørensen & S. Lode, personal communication, May 2022).

From the following figure, it is obvious that the XRD results provide a better correlation with the measured swelling pressure [MPa]. Interestingly, a combination of smectite and zeolite shows the best correlation thus indicating that zeolite holds a swelling potential. This finding supports the results from Selen (2017) where zeolite (laumontite) had a clear connection with the swelling potential. Mordenite is the zeolite mineral detected from the XRD results in this study (Appendix E). Previous studies referring to swelling in specifically mordenite zeolites were not found, however, the possibilities should not be dismissed as other zeolites such as laumontite have shown to swell (e.g., from Selen, 2017). The paper by Bish (2013) acknowledges zeolite minerals as influential in swelling environments. In contrast to smectite, zeolites have an upper swelling limit and cannot swell to the extent of smectites. However, zeolites have the ability to be hydrated in even low water environments thus being more likely to swell than clay minerals. Further, hydration and dehydration structural changes are observed far more in zeolites (Bish, 2013).

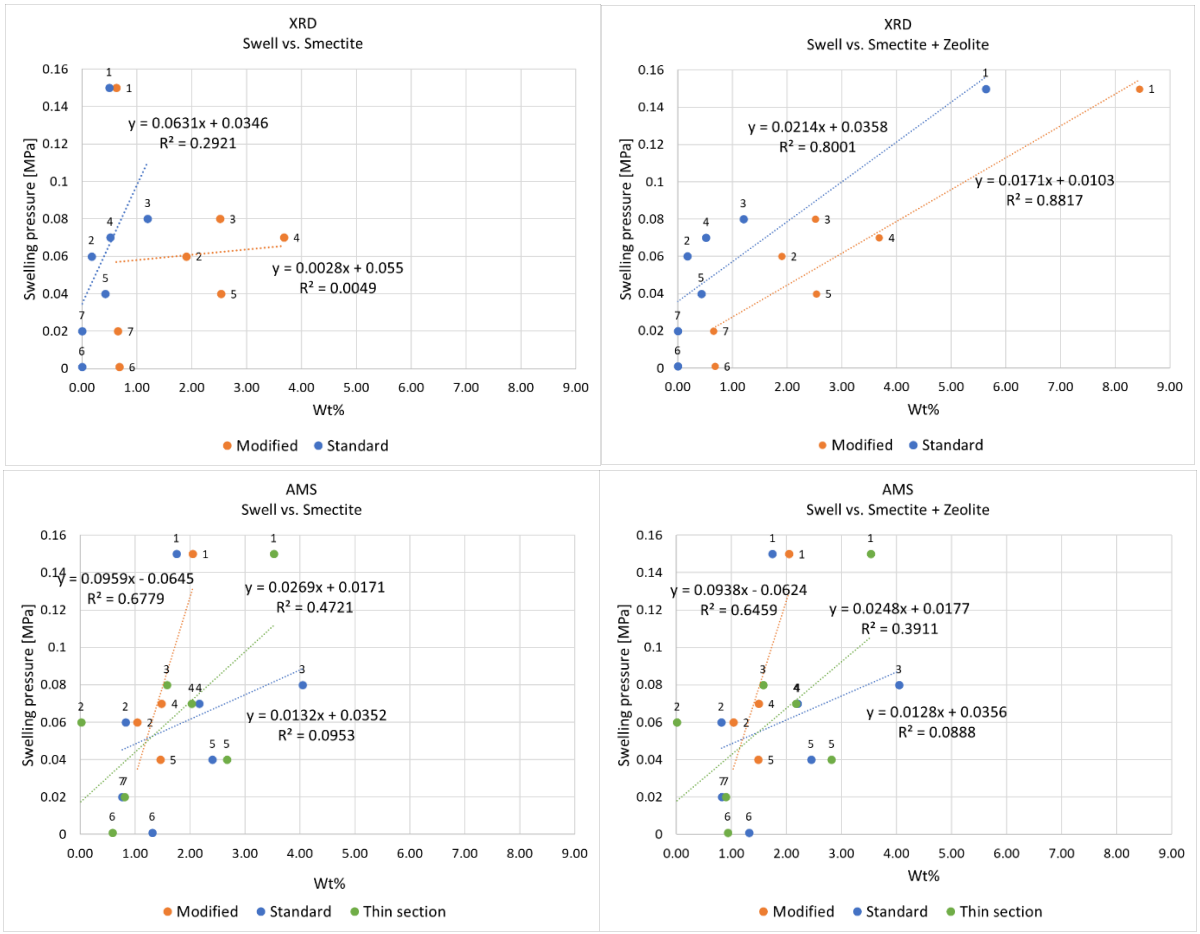

Figure 8-4: Swelling pressure [MPa] compared to XRD and AMS mineralogical results of smectite and smectite + zeolite.

The XRD graph in Figure 8-5a validates the zeolite (mordenite) detection in sample 1 (MOD1). The blue line (mordenite) matches the peak heights of the diffraction pattern with the peaks of the mineral phase. However, the width of the peaks creates uncertainties with the quantification. It is proposed that amorphous or mixed-clay material is the explanation for this, thus overestimating the detected amount of zeolite in the sample (B. E. Sørensen, personal communication, May 2022). It is believed that some mineral phases are not modeled by the XRD which may be swellable material, possibly mixed-clay material. It was suggested to add laumontite (zeolite) to the classification with success (Figure 8-5b). However, the amount of zeolite was still overestimated. It is interpreted that zeolite is present in sample 1 with high certainty.

It is surprising that the correlation with the AMS results is as poor as displayed in the charts (Figure 8-4). It is believed that the low detection of zeolite in AMS (sample 1) is the main reason for this. It would thus be of interest to reinterpret the zeolite minerals using the AMS, particularly in sample 1.

The comparison of the findings should be interpreted with caution as the oedometer swelling pressure test has its limitations and the obtained swelling pressure results can be deceiving. The use of modified sample material for the oedometer swelling test should also be investigated in future projects.

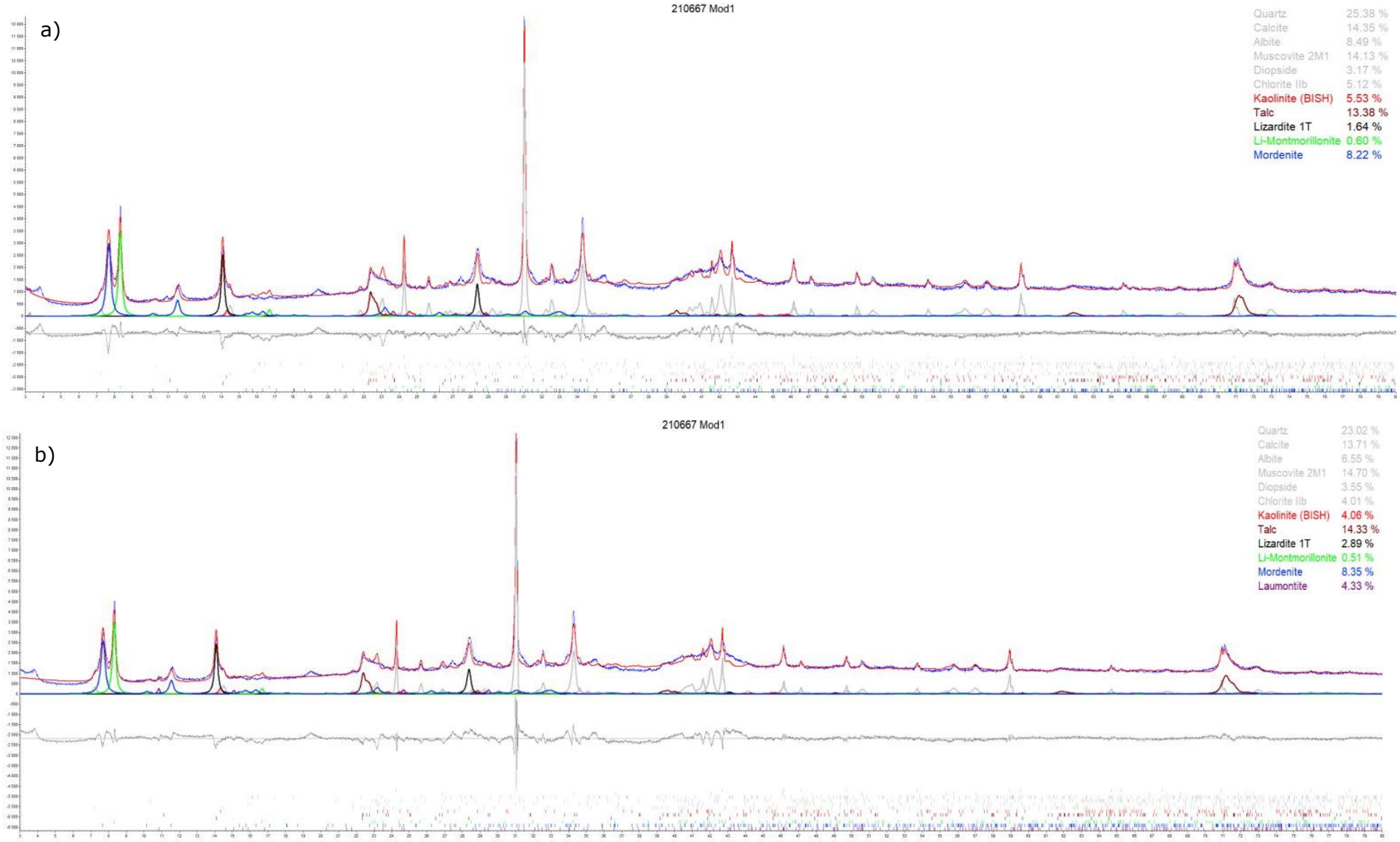

Figure 8-5: XRD peaks of MOD1 with focus on a) mordenite (zeolite), b) mordenite and laumontite (zeolite), as well as other clay minerals.

8.2.2 Comparision of standard and modified preparation methods

A new, modified preparation method has been tested as the standard preparation method has given ambiguous results in previous studies. A comparison between the standard and modified crushing material has been performed in four laboratory investigation methods, namely XRD, XRF, AMS and oedometer swelling test.

There is a clear increase in the quantified amount of smectite in the modified XRD samples, as shown in Figure 8-6. STD6 and STD7 had no identification of smectite in contrast to MOD6 and MOD7. This finding is significant as it showcases the poor reliability of the standard preparation method. Additionally, when combining all soft and hard minerals there is a favored increase of soft minerals in the modified samples and a decrease of hard minerals, except for sample 2. As the modified crushing method is meant to preserve soft minerals these results are promising.

The relationship between standard and modified methods in the AMS results is unclear (Figure 8-6). The smectite minerals increased in MOD1 and MOD2 similarly to the XRD results. Surprisingly, there was a decrease in smectite in MOD4 and MOD5. It is unfortunate that the three remaining samples were not analyzed, as the four obtained results do not indicate that any of the preparation methods are more favorable than the other, at least concerning smectite minerals. That said, the texture of the samples showcased in the BSE images indicated that the modified crushing does preserve the rock material better. As seen in Figure 6-25, the modified samples had more angular, relatively undamaged grains while the standard samples were subrounded with "dust clouds" of mixed-matrix material. The question remains why there was no clear difference displayed in the quantified results. It could be argued that MOD4 and MOD5 were anomalies, thus giving negative results. Especially considering the correlation of samples 4 and 5 were poor compared to samples 1 and 2. The poor correlation could be a consequence of the material loss or splitting errors. Another possibility is problems related to the AMS software and post-processing. The AMS results are limited by the low number of samples.

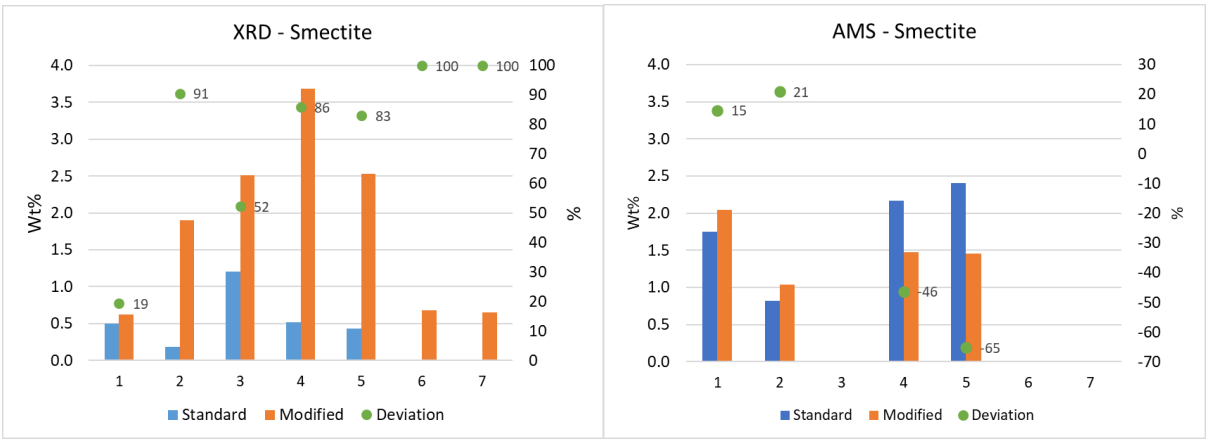

Figure 8-6: Comparison of quantified smectite [Wt%] in the standard and modified samples with deviation [%] in XRD (left) and AMS (right) laboratory results.

A comparison of standard and modified swelling potential was attempted in the oedometer swelling pressure test. Even though there were some differences in the maximum swelling pressure [MPa] measured. The comparison of standard and modified is not reliable as the two materials were different in grain size. The former has grain sizes <10µm and the latter has grain sizes up to 300µm. Further, only two samples (MOD1 and MOD6) were tested and are not a good enough representation of modified swelling pressure for all samples. This comparison method is thus overlooked.

The modified crushing method has shown potential, especially from the XRD results. The textural difference in the AMS results also shows that the modified crushing reduces the structural breakdown of the rock specimen. More tests would have to be run with duplicate samples to reduce the uncertainty and to get a better distribution of the results. The modified method also needs to be improved according to the material loss as this may have caused some of the deviations in the results.

8.2.3 Comparision of XRD and AMS results

One of the objectives of this study was to review the potential of the Automatic Mineralogy System (AMS) for mineralogical assessment. This laboratory method is compared with X-ray diffraction (XRD) which is the traditional mineralogic method. There were some clear differences in the mineral detection between XRD and AMS. Not only was the number of detected minerals larger in the AMS, but there were also quantificational variations of almost all minerals, with a few exceptions. An overview of mineral composition is presented in the graphs in Appendix P. The large differences between mineral detection in XRD and AMS are very unfortunate as the choice of method will influence the interpretation of the rock mass in tunneling or other projects. It appears hard minerals such as quartz and plagioclase are more favorable in XRD. A comparison of hard and soft minerals in the two methods is given in Figure 8-7 and Figure 8-8. The AMS detected a lower amount of hard minerals compared to the XRD in all samples except sample 7 where they were close to similar.

The identified amount of smectite is very different between the XRD and AMS, as seen in Figure 8-6. The differences are large both in the compared amount and in the deviations calculated from modified and standard samples. Thus, making it hard to draw a connection between the methods. Sample 1 has the closest relationship between the two methods, however, there is detected far more smectite in AMS compared to XRD. The finding in sample 1 is not associated to the other samples.

One of the most noticeable differences between XRD and AMS is in the muscovite (mica) and illite-smectite quantification (Appendix P). The muscovite detection from XRD was high compared to the AMS, and illite-smectite is only identified in the AMS results. As previously stated, there is an issue of distinguishing muscovite and illite using XRD (Sari, 2018). The highest presence of illite-smectite is found in samples 4 and 6a/b (31.22, 33.49 and 52.32%). When comparing with the muscovite detection in the XRD there seems to be a possibility that the illite-smectite has been wrongly detected as muscovite in the XRD samples.

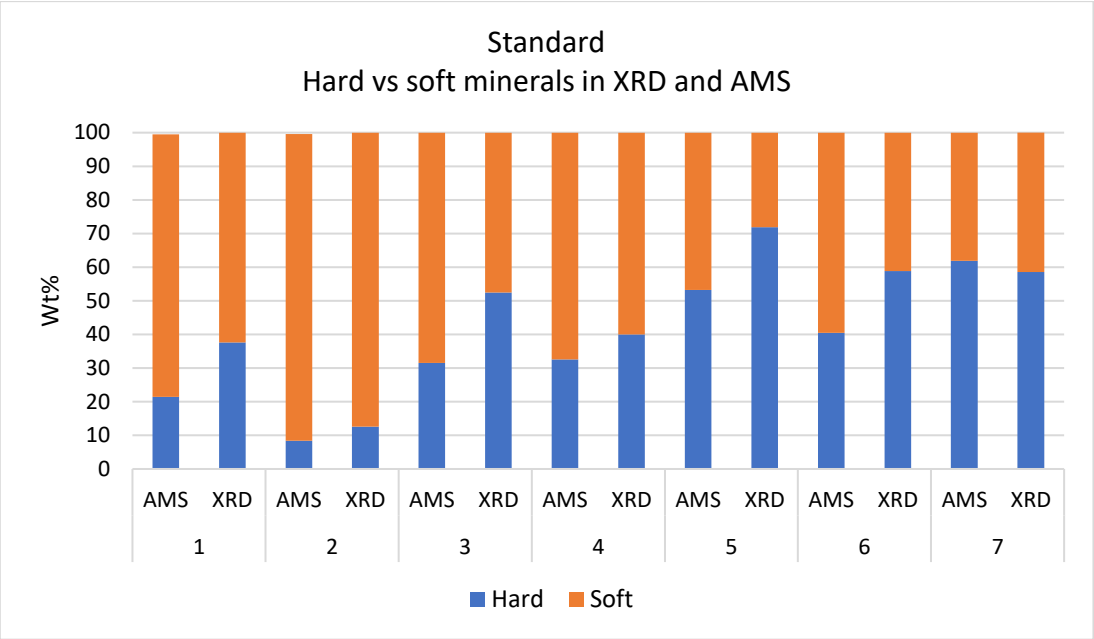

Figure 8-7: Hard vs soft minerals in standard XRD and AMS samples.

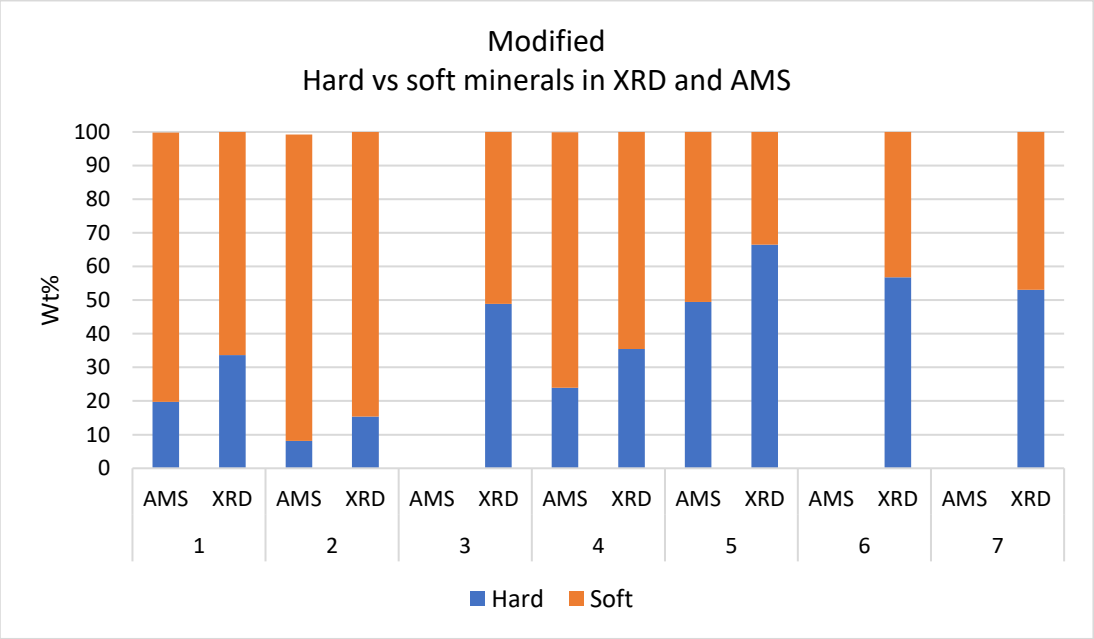

Figure 8-8: Hard vs soft minerals in modified XRD and AMS samples.

As presented earlier, the relationship between the mineralogy and swelling pressure are possibly more favorable towards the XRD results. The detection of zeolite + smectite from XRD had a better fit with the measured swelling pressure. It was also discussed whether reclassification of the AMS, particularly related to the zeolite minerals, would give an improvement in the results. Then again, there exist some uncertainties related to the oedometer swelling test results. It is also worth mentioning that the standard XRD results did not detect swelling clay in STD6 and STD7. If only this method would have been used to quantify the mineral composition of the rock, which is normally done in projects, the smectite content of samples 6 and 7 would have gone unnoticed. The AMS analysis did detect swelling minerals in all samples and is thus beneficial even if the correlation was not as promising.

In situations where there is some deviation between the XRD and AMS results, other methods may be valuable to decide the right classification. Geological knowledge of what minerals to expect is also an important tool in such situations. For example, both sample 4 and sample 6 which detected a high amount of illite-smectite have been classified as shale rock types. Illitization of smectites is common in diagenesis of shales (Lanson et al., 2009) and thus a high amount of illite-smectite could be expected in shales. In contrast to muscovite which is more common in metamorphic and igneous rocks (Deer et al., 2013). Even though there can occur some muscovite in shales, the XRD detection problems have to be taken into consideration.

There are several uncertainties related to the study which may cause the differences in the mineralogical classification. Firstly, some errors could have occurred during the preparation and splitting. Ideally, the material used in XRD and AMS should be identical, however, there is no guarantee for this. Secondly, the XRD material had additional crushing with the McCrone micronize mill which is in contrast to AMS. This may have inflicted the rock mass characteristics of the XRD material. Thirdly, there are limitations within both methods which causes a bias, for example, in the illite and muscovite situation. Lastly, only a small portion gets analyzed in each method and the mineral composition will be heavily influenced by this.

Overall, both XRD and AMS results have some advantages and drawbacks. The comparison of AMS and XRD does showcase large differences in mineral composition and quantification, making it hard to determine which method is the most reliable. The use of XRD for mineralogical quantification in hydropower projects is the standard practice. This study has raised some questions whether this method is good enough, particularly in soft rocks. It is clear, however, that the modified preparation method combined with XRD gives the best results concerning swelling minerals. One suggestion would be to improve the modified XRD method and only use this method for mineralogical classification. Another possibility is to use both XRD and AMS analysis as it can be beneficial to compare results. Approvements must be made in data processing approaches to distinguish similar minerals in both XRD and AMS methods. The knowledge of regional geology, mineral chemistry and the use of optical light microscopy is beneficial to this.

8.2.4 Comparison of HSI and AMS

As previously stated, five of the thin section specimens were chosen to represent a corresponding hyperspectral scan area with the idea to have a direct comparison (Table 5-2). Although it is possible to compare the data, the results should be interpreted with caution. As illustrated in Figure 8-9 the thin section (orange) takes up a small part of the sample area, also samples TS2 and TS4 do not represent the exact hyperspectral scan area. Furthermore, the AMS scan area is limited to a very small portion of the thin section because of the fine-grained state of the rock specimens.

The minerals in the hyperspectral scans are somewhat consistent with the AMS results as both have detected several of the swelling and difficult minerals. The presence of smectite, talc, zeolite, serpentine, carbonate and chlorite is found using both methods. The spectrally inactive minerals including quartz, plagioclase, feldspar, pyroxene, biotite and the other remaining minerals are excluded from this. As the hyperspectral classification groups, as well as the scan areas, are fairly different it was not possible to evaluate the two methods quantitatively. That being said, some of the hyperspectral results are questionable. Sample 2 which has been classified as a serpentinite rock type has only detected 0.4% serpentine minerals from the hyperspectral data, with approximately 64% smectite-talc instead (Table

6-12). Even though the thin section and hyperspectral scan area are not perfectly matched, it is reasonable to assume this is an error from the hyperspectral data. A possible explanation could be that serpentinite rock has some issues in hyperspectral scanning. A similar explanation could be given from the rock cores. Figure 8-10 shows the AMS scan mineral maps. Compared to the hyperspectral mineral maps the AMS maps are far more detailed with the mineral distribution. It is noticeable that the five samples have a varying mineral composition from AMS, whereas the hyperspectral maps look more or less similar. Further, the smectite minerals only make up a small portion in Figure 8-10 compared to Figure 8-9.

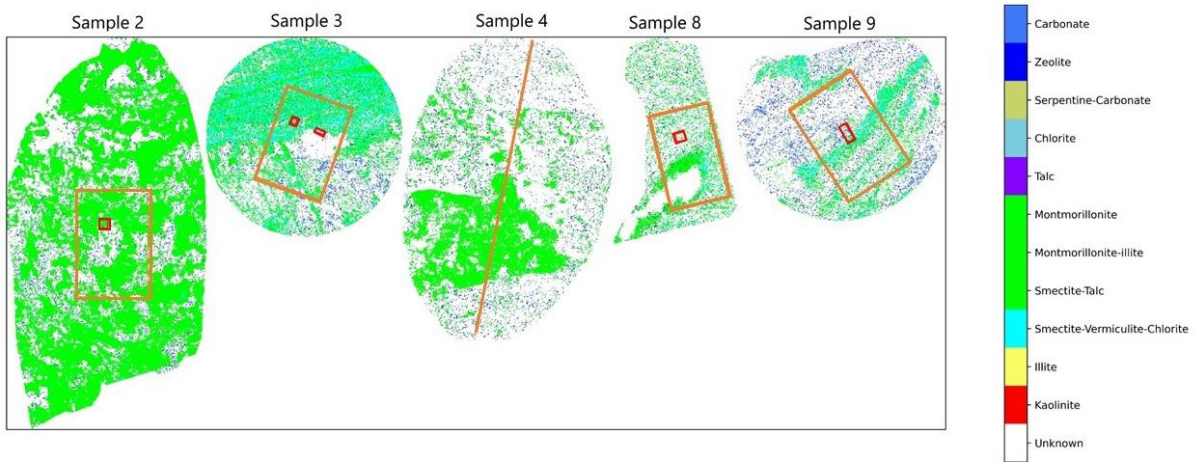

Figure 8-9: Overview of thin section area (orange) with corresponding AMS scan area (red) displayed on the hyperspectral mineral maps of samples 2, 3, 4, 8 and 9.

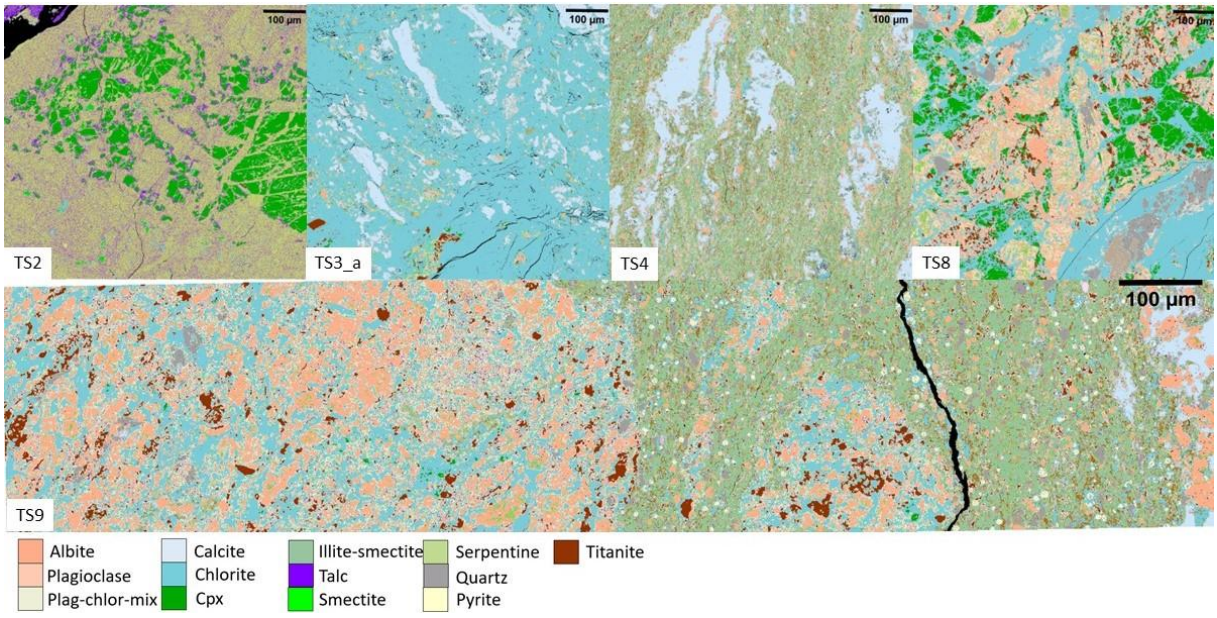

Figure 8-10: False-colored mineral maps obtained from AMS of TS2, TS3_a, TS4, TS8 and TS9. The images in this figure are meant to illustrate mineralogical differences, full scale images can be viewed in Appendix I.

A thorough comparison of hyperspectral imaging results with the other laboratory work has not been performed as the former results were delayed. This comparison indicated that hyperspectral imaging lacks when displaying mineral distribution and overestimates the smectite content. There are also issues with distinguishing the fine-grained minerals

as they get classified into the same groups. Still, hyperspectral imaging is consistent with regard to revealing the presence of swelling and difficult minerals. More detailed post-processing needs to be performed.

9 Uncertainties and Error Sources

Table 9-1 displays an overview of some of the uncertainties and errors discussed throughout this master thesis. A short description of uncertainties and recommendations to reduce the uncertainties in future work are also given in the table.

Table 9-1: Uncertainties with description, impact and recommendation.

Uncertainty related to:	Description:	Impact of uncertainties:	Recommendations to reduce uncertainties:
Transportation and storage	The rock cores were heavily shifted and broken during transportation. After arrival, the rock core boxes were stored at one of the laboratories at the department with no control of temperature or humidity, with deviation from the in-situ environment.	The repositioning of the rock cores might be incorrect and affect the results. Possible climatic influence as the in-situ environment of the rock cores is not kept.	The problem was mainly caused by low-quality core boxes. In future projects a sturdier packaging should be used. Should have better control of climatic changes in temperature and humidity. Also, in which way this will influence the rock mass.
Crushing and loss of material (standard samples)	The disc mill jar limit was exceeded during sample preparation. Additional crushing of some samples needed to be performed. Soft, fine-grained material will stick to contact surfaces.	An increased loss of material impacted the laboratory results. Loss of material can cause differences between duplicate samples, thus not being reliable when comparing methods or classifying mineral composition.	Make sure not to exceed the jar limit during milling. Make sure to get as much material as possible from contact surfaces.
Crushing and loss of material (modified samples)	The modified crushing was very time-consuming with a large loss of material because of an open crushing system. Soft, fine-grained rock will stick to contact surfaces.	It is not a practical method to use on large sample portions. Loss of material changes the character of the rock sample. Particularly hard minerals get flung out.	Development of the modified crushing method to make it less time-consuming, more automated and reduce material loss. Preferably in a closed space.
General preparation in the laboratory	Errors from measurement, storage, contamination, use of water, and temperature.	May give uncertain outcomes of laboratory results which are hard to evaluate as uncertainty or actual result.	Be aware of the possible error sources and try to reduce them as best as possible. Has to be considered during the interpretation of results.

Bulk material and sample representation (XRD, XRF, thin section, AMS, swelling)	Bulk material needs to be stirred before being taken out of the container to get the best representation of grain sizes. The samples make up a small portion of the entire rock mass (e.g. in AMS, thin section) and it is impossible to get a full representation of the rock mass.	The mineral composition and quantification will heavily rely on the chosen sample material. There will be a bias in the results based on the chosen area or sample material for each test. Hard to fully compare different laboratory tests because of this bias.	There will always be uncertainties related to this, however, one needs to try to get the most representable material/area when testing. Be aware of limitations when interpreting or comparing the results.
XRD VS AMS	Limitations to distinguish illite from muscovite in XRD. Limitations to distinguish zeolite in AMS. Possible other minerals where this occurs as well.	Will give the wrong classification and quantification of minerals. Very hard to compare mineralogic methods as the results are ambiguous.	Need to be aware of this. Maybe some possible solutions in the future. Need to do further research on the problems. Use geological knowledge to help determine the minerals.
Rock mechanical tests (UCS, E-modulus, Poisson ratio, Brazil test)	A low number of samples tested, influenced by fractures, weakness zones and broken rock specimens. Sample disturbance during preparation (cutting).	Most of the rock mechanical results were affected by the poor state of the rock mass. Additionally, a low number of samples were tested, often below the ISRM recommendation of samples which adds to the uncertainty of the results.	Follow the minimum recommendation of rock samples by ISRM. Make sure the tested specimens are not heavily influenced by fractures and weakness zones. Note that the testing of the "best" and intact rock pieces will not be representable in a weak rock mass and only to showcase the "strongest rocks".
Oedometer swelling test	Swelling classification is based on gouge material rather than intact rock. The modified sample material is too coarse (<100µm, 100-300µm), and swelling got lost in the pore volume.	Swelling classification is possibly not fit for the tested rock samples. Did not get a representable swelling measurement as some of the swelling got lost in the pore volume.	Investigate and make a classification based on the swelling of intact rock to fit this type of sample specimen. Find a way to make the modified sample material fit for the oedometer swelling test without damaging the material.

	No control of e.g., grain size, temperature, humidity.	Could be differences within the tested samples that will affect the comparability.	Should establish better control of material, temperature and humidity.
Hyperspectral imaging	About 20 cm of each rock core was not scanned due to setup limitations. Overestimation of smectite/talc/illite minerals. Underestimation of other minerals such as smectite, and calcite.	Will lose information from the rock cores. Quantification of minerals is wrong. The amount of swelling clay was strongly overestimated visually in the mineral maps.	Make sure to scan the entire rock core in future projects by adjusting the scan setup. Adjustment of machine learning approaches is necessary.

10 Conclusions and Recommendations

10.1 Summary and conclusion

To evaluate the long-term stability of hydropower water tunnels the mineralogical composition, swelling capability and rock mechanics are some of the factors which must be estimated. Samples from the Moglicë hydropower plant (HPP) in Albania have been tested during this thesis work. This thesis has contributed to a deeper understanding of the preparation methods and their influence on the quantification of mineralogy rock material. Further, an evaluation of different laboratory methods and their capability to assess swelling minerals was performed. A summary and conclusion based on the discussion is as follows:

- All tested samples contained swelling clay minerals (smectite) and measured varying degrees of swelling. Most samples were classified as low swelling with one sample (fault gouge material) showing moderate swelling.

- The findings suggest that zeolite minerals have a significant influence on swelling in the rock mass, along with smectite. The fault gouge material had a high detection of zeolite which correlated well with the measured swelling pressure.

- The laboratory results have shown the importance of performing several tests and not relying on one single result. X-Ray Diffraction (XRD), Automated Mineralogy system (AMS) and Hyperspectral Imaging (HSI) results detected a very different mineral composition. Identification errors were found in all three methods. The mineral classification of a tested rock sample would depend strongly on which method was chosen. The use of several methods can either confirm the outcome or suggest a quality check of the results. This is a more time-consuming process, but the final results would most likely be better.

- The XRD results have the best correlation to the measured swelling pressure. It is interpreted that XRD has the most correct mineral identification related to swelling clay (smectite) and zeolite. It is believed that some of the minerals are overestimated and also that there are some missing mineral phases in the data. The XRD method also showed problems with distinguishing mica and illite minerals.

- HSI and AMS are valuable for comparing with XRD results but show limitations as sole mineralogical classification methods. Visualization through the obtained mineral maps is valuable and can be compared to optical thin sections or core logging data. Both methods are beneficial when showcasing the mineral composition of swelling and/or difficult minerals.

- AMS did not correlate well with the measured swelling pressure. It is believed that the low detection of zeolite is the reason for this. The chemical composition of minerals detected through AMS can make it easier to distinguish between minerals that have ambiguous results in other methods.

- HSI overestimated the amount of smectite (talc, illite) in both the rock cores and the five individual samples. The method had problems with distinguishing smectite from other fine-grained/clay minerals, particularly serpentine. Topographic effects also caused an overestimation of zeolite.

- The use of optical microscopy was not successful in distinguishing swelling clay minerals in the thin section samples because of the fine-grained state of the samples. Thin section images are useful to find representable areas for AMS and to compare with mineral maps obtained from the laboratory methods.

- An improvement of post-processing and machine learning approaches for the laboratory data will be crucial for reducing uncertainty in the mineralogy classification.

- It is assumed that the standard crushing and preparation method is not suitable for soft rocks as the rock structure gets damaged and weak minerals such as smectite disintegrate.

- The modified crushing method has shown potential to preserve weak minerals in soft rock. This thesis supports the use of a modified crushing method for soft rocks in future projects and recommends this to be an established method at the Department of Geoscience and Petroleum. Development has to be made so to make the method less time-consuming, reduce the loss of material, and make it more automated while still maintaining the same amount of gentle crushing and milling.

- The rock mass quality along the Moglicë headrace tunnel is generally low as the rock mass is disintegrated with several fractures and weakness zones, as well as containing a fault gouge material.

- The rock mechanical results of this study were difficult to perform with few representable rock specimens. A limited amount of rock samples were tested which were below the ISRM suggested sample amount. The results were strongly influenced by weak minerals and fractures, thus creating a high level of uncertainty.

10.2 Recommendation

The following recommendations are given for future work based on this master thesis.

- The modified preparation methods need to be implemented as a standard for soft rock. The current standard intended for hard rocks should not be used on soft or weak rocks.
- A development of the modified crushing method is necessary to make it less time-consuming and preferably automated. The loss of material must also be handled in a way to make it reduced.
- Do not rely on only one mineralogical analysis. The use of XRD along with AMS, HSI and optical thin sections is useful to distinguish mineral composition in a rock mass and get a visualization of the rock material.
- Automated Mineralogy System (AMS) should be evaluated further as the results from this thesis were ambiguous.

- A thorough post-processing and development of machine learning approaches are required for future projects.
- A larger number of samples is suggested in future work to reduce the uncertainties of the laboratory results.
- Swelling test of the modified powder material must be improved as the current sample material is too coarse to measure the maximum swelling pressure. However, the grinding of the material must be done in a way to preserve the weak minerals.
- Perform intact oedometer swelling test to compare with powder oedometer swelling test.
- Further evaluation of hyperspectral imaging data should be executed, both from the laboratory and field. Detailed post-processing should be a focus for a better distinction of fine-grained minerals.

References

Aasen, O., Ødegaard, H., & Palmström, A. (2013). Planning of pressurized headrace tunnel in albania. In *Norwegian Hydropower Tunneling II* (pp. 21–27). Norwegian Tunneling Industry (NFF).

ALS. (2021). *Loss On Ignition (LOI)*. ALS Global. https://www.alsglobal.com/en/news/articles/2021/07/loss-on-ignition

Barla, G. (2002). Tunnelling under squeezing rock conditions. In *Tunnelling Mechanics—Advances in Geotechnical Engineering and Tunnelling* (pp. 169–268).

Bish, D. L. (2013). Parallels and Distinctions Between Clay Minerals and Zeolites. In *Developments in Clay Science* (Vol. 5, pp. 783–800). Elsevier. https://doi.org/10.1016/B978-0-08-098258-8.00026-2

Brevig, L., Bøhagen, Ø., & Ødemark, E. (2011). *Design Basis Report*. Norconsult & Statkraft; Unpublished.

Broch, E., & Palmström, A. (2017). The design of unlined hydropower tunnels and shafts: 100 years of Norwegian experience. *Int. J. Hydropower Dams*, *24*, 72–79.

Brox, D. (2019). Hydropower tunnel failures: Risks and causes. In *Tunnels and Underground Cities: Engineering and Innovation meet Archaeology, Architecture and Art*. CRC Press.

Carter, T. G., Castro, S. O., Carvalho, J. L., Hattersley, D., Wood, K., Barone, F. S., Yuen, C. M. K., & Giraldo, D. (2010). Tunnelling Issues of Chilean Tertiary Volcaniclastic Rocks. *XIII Ciclo Di Conferenze Di Meccanica Ed Ingegneria Delle Rocce*, 215–236.

Chabrillat, S., Goetz, A. F., Krosley, L., & Olsen, H. W. (2002). Use of hyperspectral images in the identification and mapping of expansive clay soils and the role of spatial resolution. *Remote Sensing of Environment*, *82*(2), 431–445. https://doi.org/10.1016/S0034-4257(02)00060-3

Charrier, R., Wyss, A., Flynn, J., Swisher, C., Norell, M., Zapatta, F., McKenna, M., & Novacek, M. (1996). New evidence for Late Mesozoic-Early Cenozoic evolution of the Chilean Andes in the Upper Tinguiririca Valley (35°s), central Chile. *Journal of South American Earth Sciences*, *9*, 393–422. https://doi.org/10.1016/S0895-9811(96)00035-1

Chiu, J. K. Y. (2022). *Report—Hyperspectral image analysis*. Unpublished.

Clark, R. N. (1999). Spectroscopy of rocks and minerals and principles of spectroscopy. *Manual Remote Sensing*, 3–58.

Cook, N. J. (2000). Mineral characterisation of industrial mineral deposits at the Geological Survey of Norway: A short introduction. *NGU-BULL*, *436*, 189–192.

Deer, W. A., Howie, R. A., & Zussman, J. (2013). *An introduction to the rock-forming minerals* (3rd ed.). Mineralogical Society of Great Britain and Ireland.

Devoll HPP. (2011a). *Harnessing of Hydropower Potential of Devoll River Geological Report HPP Moglicë* (EST-000-600). Unpublished.

Devoll HPP. (2011b). *Moglicë waterway—Geological logitudinal section waterway* (Appendix EST-000-600 Map 2). Unpublished.

Dutrow, B., L., & Clark, C., M. (2021). *X-ray Powder Diffraction (XRD)*. https://serc.carleton.edu/research_education/geochemsheets/techniques/XRD.html

Einstein, H. H. (1996). Tunnelling in difficult ground—Swelling behaviour and identification of swelling rocks. *Rock Mechanics and Rock Engineering*, *29*(3), 113–124. https://doi.org/10.1007/BF01032649

FELMI-ZFE. (2022). *Zeiss Sigma 300 VP*. FELMI ZFE. https://www.felmi-zfe.at/instrumentation/sem/zeiss-sigma-300-vp/

Frengen, R. B. (2020). *Assessment of swelling pressure on sprayed concrete lining at the headrace tunnel of Moglice Hydropower Project.* [Master thesis]. NTNU.

Fulignati, P. (2020). Clay Minerals in Hydrothermal Systems. *Minerals*, *10*. https://doi.org/10.3390/min10100919

Goodman, R. E. (1993). *Engineering Geology: Rock in Engineering Construction*. Wiley.

Google Earth. (2021). *La Higura and La Confluencia, Chile* [Map]. https://earth.google.com/web/@-34.58992951,-71.42319929,149.22734439a,359120.9544079d,35y,0h,0t,0r

Graham, S. (2017). *Automated Mineralogy—The Past, Present and Future*. 20.

Graham, S., Brough, C., & Cropp, A. (2015, June 1). *An Introduction to ZEISS Mineralogic Mining and the correlation of light microscopy with automated mineralogy: A case study using BMS and PGM analysis of samples from a PGE-bearing chromitite prospect*. Precious Metals 2015.

Graham, S., & Keulen, N. (2019). Nanoscale Automated Quantitative Mineralogy: A 200-nm Quantitative Mineralogy Assessment of Fault Gouge Using Mineralogic. *Minerals*, *9*(11), 665. https://doi.org/10.3390/min9110665

He, J., & Barton, I. (2021). Hyperspectral remote sensing for detecting geotechnical problems at Ray mine. *Engineering Geology*, *292*. https://doi.org/10.1016/j.enggeo.2021.106261

Holder, C. F., & Schaak, R. E. (2019). Tutorial on Powder X-ray Diffraction for Characterizing Nanoscale Materials. *ACS Nano*, *13*(7), 7359–7365. https://doi.org/10.1021/acsnano.9b05157

Ikpe, A., Ebunilo, P., & Okovido, J. (2018). *Geotechnical Evaluation of Bentonite Clay for Municipal Solid Waste Landfill Lining Membrane*. *4*, 337–351.

ISRM. (1978a). Suggested methods for determining sound velocity. In *Commission on standardization of laboratory and field tests* (Vol. 15, pp. 53–58). Pergamon.

ISRM. (1978b). Suggested methods for the quantitative description of discontinuities in rock masses: International Society for Rock Mechanics. *International Journal of Rock Mechanics and Mining Sciences*, *15*, 319–368.

ISRM. (1978c). Suggested methods for determining tensile strength of rock materials. In *International Journal of Rock Mechanics and Mining Sciences & Geomechanics Abstracts* (Vol. 15, pp. 99–103). Pergamon.

ISRM. (1979a). Suggested Methods for Determining the Uniaxial Compressive Strength and Deformability of Rock Materials. In *Suggested Methods for Determining Compressive Strength and Deformability* (pp. 137–140).

ISRM. (1979b). Suggested methods for determining water content, porosity, density, absorption and related properties and swelling and slake durability index properties. *International Journal of Rock Mechanics and Mining Science*, *16*(2), 141–156.

ISRM. (1983). Characterization of swelling rock. In *Commission on Swelling Rocks*. International Society for Rock Mechanics.

Keulen, N., Malkki, S. N., & Graham, S. (2020). Automated Quantitative Mineralogy Applied to Metamorphic Rocks. *Minerals*, *10*(1), 47. https://doi.org/10.3390/min10010047

Koerting, F. M. (2021). *Hybrid imaging spectroscopy approaches for open pit mining: Applications for virtual mine face geology* [Doctoral thesis, Universität Potsdam]. https://doi.org/10.25932/publishup-49909

Kranz, R. L., Bish, D. L., & Blacic, J. D. (1989). Hydration and dehydration of Zeolitic Tuff from Yucca Mountain, Nevada. *Geophysical Research Letters*, *16*, 1113–1116. https://doi.org/10.1029/GL016i010p01113

Kurz, T. H., Buckley, S. J., & Becker, J. K. (2017). Hyperspectral imaging: A novel geological mapping technique for subsurface construction sites. *Proceedings of the World Tunnel Congress 2017–Surface Challenges–Underground Solutions, Bergen, Norway*.

Lanson, B., Sakharov, B. A., Claret, F., & Drits, V. A. (2009). Diagenetic smectite-to-illite transition in clay-rich sediments: A reappraisal of X-ray diffraction results using the multi-specimen method. *American Journal of Science*, *309*(6), 476–516. https://doi.org/10.2475/06.2009.03

Li, C. C. (2018). *Rock Mechanics (TGB4210)*. NTNU.

Madsen, F. T., & Müller-Vonmoos, M. (1989). The swelling behaviour of clays. *Applied Clay Science*, *4*(2), 143–156. https://doi.org/10.1016/0169-1317(89)90005-7

Malvern Panalytical. (2022). *WROXI - Certified Reference Materials | Malvern Panalytical*. https://www.malvernpanalytical.com/en/products/category/calibration-standards/elementalanalysisbyxrayfluorescence/wroxi

Mao, D., Nilsen, B., & Dahl, F. (2011). Laboratory Testing of Swelling Gouge from Weakness Zone—Principle and Recent Update. *SINTEF*. 45th US Rock Mechanics/Geomechanics Symposium, San Francisco, California.

Marinos, P., & Hoek, E. (2001). Estimating the geotechnical properties of heterogeneous rock masses such as flysch. *Bulletin of Engineering Geology and the Environment*, *60*(2), 85–92. https://doi.org/10.1007/s100640000090

Marinos, P., Hoek, E., & Marinos, V. (2006). Variability of the engineering properties of rock masses quantified by the geological strength index: The case of ophiolites with special emphasis on tunnelling. *Bulletin of Engineering Geology and the Environment*, *65*, 129–142. https://doi.org/10.1007/s10064-005-0018-x

Nelson, S. A. (2014). *Weathering and clay minerals*. Tulane University.

Nelson, S. A. (2015). *Phyllosilicates (Micas, Chlorite, Talc, & Serpentine)*. Tulane University.

NGU. (2020). *XRF | Norges geologiske undersøkelse*. https://www.ngu.no/fagomrade/xrf

Nieuwland, D. A., Oudmayer, B. C., & Valbona, U. (2001). The tectonic development of Albania: Explanation and prediction of structural styles. *Marine and Petroleum Geology*, *18*(1), 161–177. https://doi.org/10.1016/S0264-8172(00)00043-X

Nilsen, B. (2016). *Ingeniørgeologi—Berg, Grunnkurskompendium*. NTNU.

Panthi, K. K. (2006). *Analysis of Engineering Geological Uncertainties Related to Tunnelling in Himalayan Rock Mass Conditions* [Doctoral thesis]. NTNU.

Panthi, K. K. (2012). Probabilistic approach in assessing tunnel squeezing—A discussion based on tunnel projects from Nepal Himalaya. *46th US Rock Mechanics / Geomechanics Symposium 2012*, *1*, 476–482.

Panthi, K. K., & Nilsen, B. (2007). Predicted versus actual rock mass conditions: A review of four tunnel projects in Nepal Himalaya. *Tunnelling and Underground Space Technology*, *22*(2), 173–184. https://doi.org/10.1016/j.tust.2006.04.005

Panthi, K. K., & Shrestha, P. K. (2018). Estimating Tunnel Strain in the Weak and Schistose Rock Mass Influenced by Stress Anisotropy: An Evaluation Based on Three Tunnel Cases from Nepal. *Rock Mechanics and Rock Engineering*, *51*(6), 1823–1838. https://doi.org/10.1007/s00603-018-1448-7

Raith, M., Raase, P., & Reinhardt, J. (2012). *Guide to Thin Section Microscopy* (Vol. 2).

Rusi, M., & Hoxha, P. (2013). CSD correction as a tool for estimating 3d block size distribution. *Bulletin of the Geological Society of Greece*, *47*, 1854–1863. https://doi.org/10.12681/bgsg.11065

Sari, Q. (2018). *How do I difference the Muscovite and Illite Peak in XRD?* ResearchGate. https://www.researchgate.net/post/How_do_I_difference_the_Muscovite_and_Illite_Peak_in_XRD

Selen, L. (2017). *Study on material properties and testing of various rock types, development of investigation procedure and test methodology for future projects* [Master thesis]. NTNU.

Selen, L. (2020). *Assessment on the swelling and disintegration potential of weak and weathered rocks in water tunnels of hydropower projects—A contribution based on use of laboratory testing methods* [Doctoral thesis]. NTNU.

Selen, L., & Panthi, K. K. (2018). Influence of slaking and disintegration effect on the stability of water tunnels for hydropower. *1-11*. ARMS10 10th Asian Rock Mechanics Symposium, Singapore.

Selen, L., & Panthi, K. K. (2021). A review of the testing approaches in swelling rock conditions at three different institutions. *IOP Conference Series: Earth and Environmental Science*, *833*. https://doi.org/10.1088/1755-1315/833/1/012034

Selen, L., Panthi, K. K., Mørk, M. B. E., & Sørensen, B. E. (2021). Compositional Features and Swelling Potential of Two Weak Rock Types Affecting Their Slake Durability. *172-191*. https://doi.org/10.3390/geotechnics1010009

Selen, L., Panthi, K. K., Vergara, M. R., & Mørk, M. B. (2021). Investigation on the Effect of Cyclic Moisture Change on Rock Swelling in Hydropower Water Tunnels. *Rock Mechanics and Rock Engineering*, *54*(1), 463–476. https://doi.org/10.1007/s00603-020-02266-1

Selen, L., Panthi, K. K., & Vistnes, G. (2020). An analysis on the slaking and disintegration extent of weak rock mass of the water tunnels for hydropower project using modified slake durability test. *Bulletin of Engineering Geology and the Environment*, *79*(4), 1919–1937. https://doi.org/10.1007/s10064-019-01656-2

Selmer-Olsen, R., Palmström, A., & Strømme, B. (1989). *Tunnel collapses in swelling clay zones*. *21*, 49–51.

Skrede, S.-E. (2017). *Stability Assessment of Hydropower Tunnel in Swelling and Slaking Rock Mass* [Master thesis]. NTNU.

Statkraft. (2021a). *Devoll Hydropower Project*. https://www.statkraft.com/en-al/projects2/devoll-hydropower-project/

Statkraft. (2021b). *La Higuera vannkraftverk*. https://www.statkraft.com/om-statkraft/hvor-vi-har-virksomhet/chile/la-higuera-vannkraftverk/

Statkraft. (2021c). *Moglicë HPP*. Statkraft. https://www.statkraft.com/en-al/projects2/moglice-hpp/

Steele-MacInnis, M., & Manning, C. E. (2020). Hydrothermal Properties of Geologic Fluids. *Elements*, *V16*(N6). http://elementsmagazine.org/2020/12/01/hydrothermal-properties-of-geologic-fluids/

Stefanussen, W. (2017). Engineering geological experiences from international projects. In *TGB4190 Compendium 2021* (p. 14). NTNU.

Vivoda Prodan, M., & Arbanas, Ž. (2016). Weathering Influence on Properties of Siltstones from Istria, Croatia. *Advances in Materials Science and Engineering*, *2016*. https://doi.org/10.1155/2016/3073202

Wahlstrom, E. E. (1973). *Tunneling in Rock* (1st ed., Vol. 3). Elsevier.

Appendix

All appendices are located in a digital zip-file which is delivered along with the master thesis and can be found at NTNU Open. The zip-file contains the following appendices:

Appendix A – GSI Chart

Appendix B – Rock mechanical classification

Appendix C – Rock sample overview

Appendix D – Crushing overview

Appendix E – XRD results

Appendix F – XRF results

Appendix G – Thin section scans

Appendix H – AMS results for intact samples

Appendix I – AMS backscatter and mineral maps for intact samples

Appendix J – AMS results for powder samples

Appendix K – AMS backscatter and mineral map for powder samples

Appendix L – Hyperspectral image analysis, report

Appendix M – Swelling pressure charts

Appendix N – Rock mechanical results

Appendix O – Mineral chemical composition

Appendix P – XRD VS AMS mineral detection

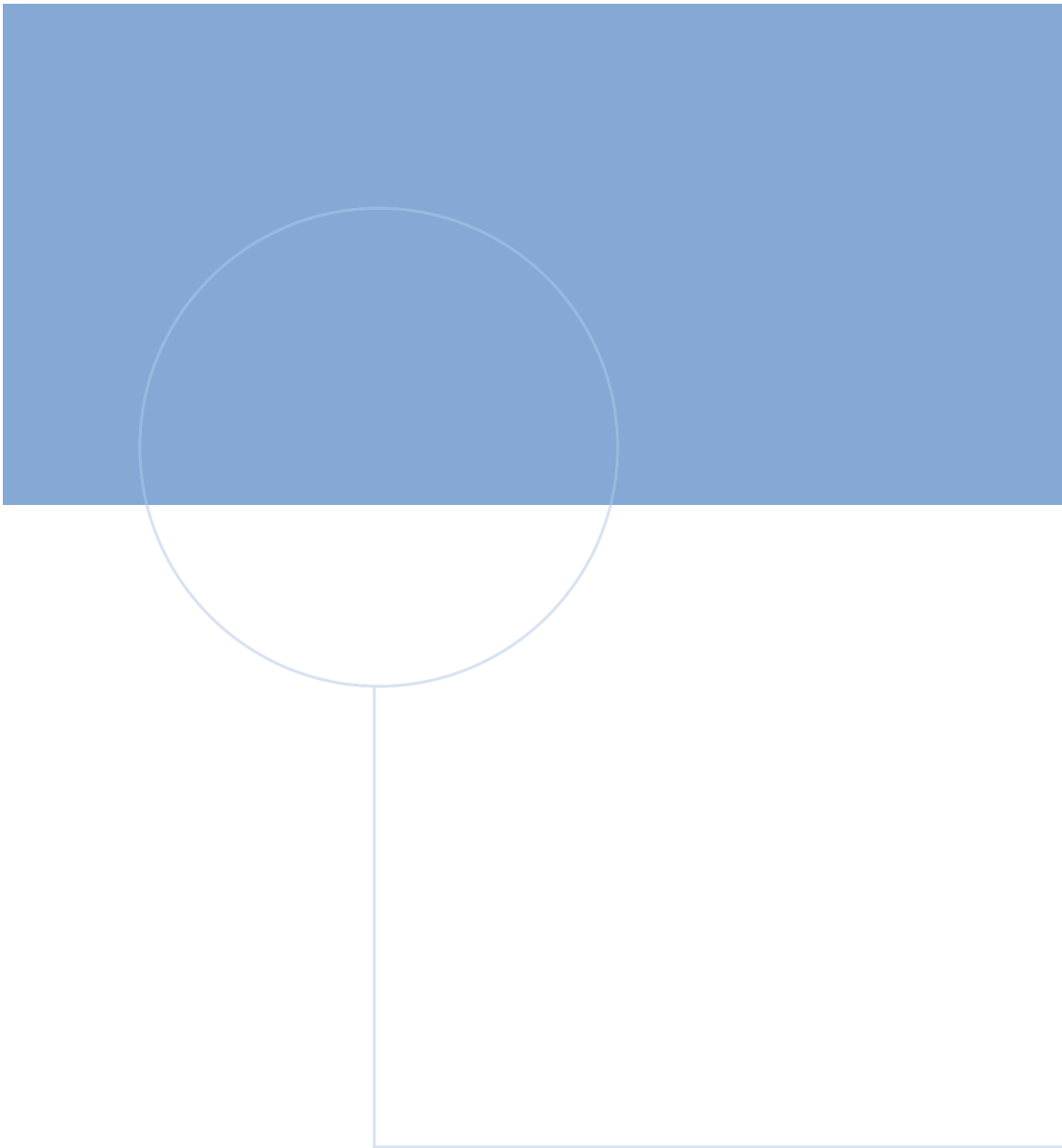

NTNU

Norwegian University of
Science and Technology